THE CHEMISORPTION OF CARBON MONOXIDE, OXYGEN AND NITRIC OXIDE ON THE RUTHENIUM (001) SURFACE

Thesis by

Glenn E. Thomas

In Partial Fulfillment of the Requirements
for the Degree of

Doctor of Philosophy

California Institute of Technology
Pasadena, California

1979

(Submitted September 25, 1978)

Acknowledgments

I would like to thank my advisor, W. Henry Weinberg, for his advice and assistance throughout this work. I am indebted also to Particia A. Thiel, John T. Yates, Jr. and Stephen P. Withrow for their contributions in the course of the instrument construction and surface experiments. I was supported, in part, by the National Science Foundation, through its Energy Trainee program, and by IBM, through its Predoctoral Fellowship program, during my graduate years.

ABSTRACT

The vibrational energies of small molecules adsorbed on the Ru(001) surface were studied by means of inelastic electron scattering. The instrument used to carry out this work is an electron spectrometer of the Kuyatt-Simpson type. The design and operation of this instrument, which is capable of carrying out a number of electron spectroscopies important in chemisorption research, is discussed in detail.

The vibrations of carbon monoxide, oxygen and nitric oxide chemisorbed on the basal plane of Ru provide insight into their chemical structures. Carbon monoxide exhibits the carbon-oxygen stretching frequency (1980 cm^{-1} - 2080 cm^{-1}) characteristic of a linear CO, with a single carbon-metal bond. This is true at all coverages, although at saturation coverage the low-energy electron diffraction pattern shows that the adsorbed CO overlayer is out of registry with the substrate. An interadsorbate interaction is proposed to explain the observed increase in the carbon-oxygen stretching frequency of 100 cm^{-1} with coverage.

Oxygen is adsorbed dissociatively on Ru(001) and exhibits a single coverage-dependent stretching frequency of approximately 570 cm^{-1}. The low frequency indicates that atomic oxygen is bonded in a bridged or threefold site. A study of chemisorbed oxygen over the temperature range, 100 K to 1000 K, shows the existence of energy gain peaks in the electron energy distribution.

Nitric oxide adsorbs molecularly at 130 K but dissociates at approximately 400 K, depending on coverage. Comparison with the stretching frequencies of metal nitrosyls suggests that NO is bound in a threefold

or bridged site at low coverage and as a linear NO with a single metal-nitrogen bond at high coverage. The vibrational spectrum of adsorbed NO changes irreversibly if the surface is heated to a temperature below the onset of desorption (depending on coverage). A mechanism is proposed for this in which the bridged NO dissociates at room temperature and the atomically bound nitrogen and oxygen atoms block further dissociation.

Table of Contents

Chapter I

Introduction

The primary motivation for studying the surface chemistry of molecules adsorbed on single crystals is the hope that the molecular structure and bonding geometry of the chemisorbed molecules can be determined. The determination of chemical structure and the relationship between structure and reactivity has been very productive in homogeneous chemistry, and it appears that this level of understanding will be extended to heterogeneous systems through the use of well-defined surfaces.

The work presented in this thesis concerns the vibrational energies of small molecules adsorbed on the Ru(001) crystal surface. This is the basal plane of the hexagonal close-packed Ru crystal. The vibrational energies of small molecules provide some of the most direct evidence of their structure. By using the very sensitive technique of inelastic electron scattering, it is possible to obtain this information about molecules adsorbed on single crystal metallic surfaces.

As an introduction to the vibrational measurements of adsorbates on the Ru(001) surface, some general background material concerning measurements of surface vibrations will be presented. The two principal techniques in this area, infrared adsorption spectroscopy and inelastic electron scattering, will be compared for sensitivity, energy resolution and the function of selection rules in interpreting the data.

Surface vibrations have been historically a topic of great interest among surface chemists (1,3). Eischens and coworkers pioneered the use of infrared absorption spectroscopy to study chemisorption and reaction on dispersed catalysts. In infrared absorption experiments, the catalyst

surface is typically several square meters in area, and the total number of molecules subject to measurement is on the order of 10^{16}, which provides adequate sensitivity (2,4). Catalytic studies of these systems face difficulties due to surface heterogeneity (variety of adsorption sites), to support effects and to reproducibility of samples.

An alternative, which circumvents these problems, is to study well characterized bulk metallic samples. Since saturation coverages are typically 10^{15} cm^{-2} for small molecules, achieving adequate sensitivity is quite difficult. At present, infrared reflectance spectroscopy and inelastic electron scattering are both used successfully to measure vibrations on single metallic surfaces, although each technique has its limitations.

Infrared reflectance measurements are carried out by reflecting the infrared beam off the metal surface of interest into an infrared detector(5). The monochromator may be placed in the beam path before or after reflection. In order to achieve greater sensitivity, multiple reflections are used occasionally, although a single reflection is more common. Because of the very small number of scatterers, delicate subtraction techniques are necessary to cancel the effects of gas adsorbed on the windows and otherwise in the beam path (6,7). These contamination problems cause experiments with hydrocarbons to be done normally with the deuterated species, and the very useful experiments depending on isotopic shifts are more difficult. Perhaps new infrared spectrometers which are totally in vacuum will overcome these problems.

Greenler has calculated that the absorption of infrared radiation

by a thin adsorbed layer is maximum when the light is incident on the surface at an angle of approximately 88^{o} from the normal and is reflected several times from the surface. This optimum depends primarily on the optical constants of the metal substrate (5,8). However, Yates and coworkers estimated that most of the intensity could be detected in a single reflection from the tungsten surface, and single-reflectance experiments are most common(9,10).

The dielectric constant of metals is large in the infrared, and the electric field of the grazingly incident light at the reflection plane is strictly normal to the surface. Therefore, the infrared reflectance experiment can detect only those vibrations which have transition dipole moments with a component normal to the surface(11). This is called the dipole-normal selection rule and has been considered also in connection with infrared adsorption measurements of finely divided metal samples(1,2).

Infrared reflectance measurements benefit from the inherently good energy resolution of optical techniques. Typically, the resolution of the infrared monochromator is degraded to 5 cm^{-1} (0.6 meV) in order to obtain sensitivities on the order of 4% of a monolayer in the case of chemisorbed carbon monoxide(10). Thus, it is possible to measure infrared lineshapes, which have been the subject of recent theoretical discussion(12). The measurements thus far appear to be limited to frequencies above 1000 cm^{-1} by the intensity of infrared sources and by the transmission characteristics of infrared windows commonly used in ultra-high vacuum cells.

Another way to measure surface vibrational energies is by inelastic

electron scattering. Low-energy electrons (~4 eV) can lose energy to the surface upon reflection, and the vibrational energies appear as peaks in the kinetic energy distribution of the scattered beam. Electron scattering is a sensitive technique; 0.1% of a monolayer of CO is detected readily. Tbe bandwidth of energy loss measurements is limited only by the energy-width of the peak due to elastically scattered electrons, and energy scans from 250 cm^{-1} to 4000 cm^{-1} are typical.

The chief limitation of inelastic electron scattering is its energy resolution, defined as the full-width at half-maximum of the elastic peak. The best resolved spectra reported to date show elastic peak widths of ~60 cm^{-1} (7 meV), and typical measurements are more poorly resolved (11). In addition, the use of the elastic peak width as the true resolution is not always justified because of the achromatic focusing properties of electrostatic lenses. Results of inelastic scattering measurements of CO adsorbed on Pt(111) suggested a natural width of approximately 40 cm^{-1} in the CO stretching frequency, whereas subsequent infrared reflectance measurements report an intrinsic broadening of 6 cm^{-1} (13,14). However, due to the good sensitivity, wide spectral range and general applicability of this technique, it is becoming increasingly popular in the study of simple molecules adsorbed on surfaces.

As discussed in Chapter 7, the issue of selection rules is more complicated in the case of electron scattering. Several authors have proposed a simple theoretical description in which the electron is treated as a plane wave reflecting from a barrier, and the surface molecule is treated as an oscillating dipole together with its image (15-17).

This model predicts that the inelastically scattered electrons are peaked sharply in the specular direction, and that only dipole-normal vibrations are excited. However, the frequency of the electron is more than an order of magnitude greater than infrared radiation and this "selection rule" can be violated even in a simple dipole model(17). Recent measurements of atomic hydrogen adsorbed on the W(100) surface suggest that the dipole-normal selection rule indeed can be violated in inelastic electron scattering (18), and a variety of scattering mechanisms have been suggested to explain this (19,20). This subject is reviewed in Chapter 7.

Carbon monoxide has been studied extensively in fundamental surface research. Aside from its convenience of use, the characterization of adsorbed CO is of potential importance in industrial catalysis through the understanding of CO oxidation (in pollution control systems), and of the water-gas shift and methanation reactions (in hydrogen and synthetic fuel production). Chemisorbed CO is a model system in the characterization of transition metal surfaces, and the vibrations of adsorbed CO are the subject of the work presented in Chapters 3 and 4. As an introduction to this material, we will summarize results of infrared and inelastic electron scattering measurements of CO adsorbed on tungsten, platinum and copper, three metals of notably different chemical behavior.

Carbon monoxide is adsorbed on W most strongly of the three metals. At 300 K, CO is adsorbed in a series of tightly bound states (β-CO) which may be adsorbed dissociatively, and a more weakly adsorbed form (α-CO) is found only at high coverage. The β-states desorb from the

W(100) surface at temperatures in the range 850 K to 1350 K, whereas the α states desorb near 500 K (18). On polycrystalline W as well as on the W(100) surface, two states of molecular CO (α_1,α_2) have been identified in thermal desorption mass spectra and by electron stimulated desorption (21,22). The α_1 state appears at saturation coverage, obtained with a constant background pressure of $\sim 10^{-6}$ torr CO (23,9).

It should be noted that the series of states of chemisorbed molecules is identified as features in the partial pressure of desorbing gas as a function of surface temperature. In general, the more strongly adsorbed molecules are desorbed at higher temperatures, and the development of different adsorption states can be monitored by measuring the thermal desorption spectra as a function of surface coverage. However, a contribution to the desorption energy can result from interactions between chemisorbed molecules, and multiple "states" in thermal desorption spectra may result from molecules in the same adsorption site (13).

The first vibrational study of CO on this subject was carried out by John Yates and coworkers (9,10). By infrared reflectance measurements of CO on polycrystalline W, the C-O stretching frequencies of α_2 and α_1 CO were found at 2090 cm^{-1} and 2128 cm^{-1}, respectively. By analogy to the infrared spectrum of $W(CO)_6$, the bands were assigned to a CO molecule with an s-p hybridized carbon bonded to the metal surface. The low frequencies due to the β-states were measured by Froitzheim and coworkers using inelastic electron scattering (13). Loss peaks at 548 and 629 cm^{-1} were attributed to the perpendicular stretching modes of atomic carbon and oxygen, adsorbed in separate sites. The assignment was supported by

separate energy loss measurements of carbon- and oxygen-covered surfaces. Subsequent measurements by Adnot and Carette, however, suggest that a relatively strong interaction between the neighboring C and O atoms in the β-CO states cannot be excluded (24). The C-O stretching mode of a β-CO complex, which would confirm this interaction, is assumed to be parallel to the surface and, therefore, to be undetectable. The metal-carbon stretching mode of α-CO is found at 347 cm^{-1} which is quite low compared to the metal-CO modes of linear CO on Pt and Ru. This indicates that the W surface, after adsorbing β-CO, takes on the characteristics of a less reactive metal. The role of surface passivation in reactions on W has been discussed by Madix (25).

Platinum is a more interesting metal catalytically than tungsten, in part because it is less reactive and, therefore, more likely to remain active under process conditions. A critical step in a heterogeneous catalytic reaction is the desorption of products, and the very reactive clean metal surfaces are frequently poor catalysts in this regard.

Carbon monoxide adsorption on dispersed Pt was studied by Eischens et al. on a variety of supports (1). Carbon-oxygen stretching frequencies at 1820 cm^{-1} and 2040 cm^{-1} were found for Pt supported on γ-alumina and were attributed to bridged and linear forms of adsorbed CO, respectively. The population of bridged CO molecules, in which the carbon is thought to be bonded to two metal atoms, is very sensitive to support effects (2).

A series of infrared reflectance studies of CO on the Pt(111) surface (either a single crystal or a recrystallized ribbon) failed to identify a CO stretching frequency below 1950 cm^{-1}, characteristic of

doubly coordinated CO (26,14). Inelastic electron scattering results of Froitzheim et al., however, confirmed the existence of CO bands at 1871 cm^{-1} and 2105 cm^{-1} at saturation coverage (13). Subsequent infrared reflectance measurements of Krebs and Lüth supported the electron scattering data (7). The bridging form of CO appears at high coverage, and a model proposed by Ertl in which CO occupies half linear and half bridge sites at saturation coverage is well supported (27).

The perpendicular metal-carbon stretching modes of linear and bridged CO on Pt(111) are found at 468 cm^{-1} and 363 cm^{-1}, respectively(13). The bending modes parallel to the surface have not been observed. Ibach et al. have proposed the rule that, in general, $\omega_{top} > \omega_{bridge}$ for metal-adsorbate modes on the grounds that the perpendicular vibration will have more bending character in the more highly coordinated site (11). This view has been supported in studies of oxygen chemisorption on W(100) as well(28).

Copper is the least reactive of these metals, and saturation coverages of chemisorbed CO are obtained only below room temperature. Early studies of high surface area Cu samples showed a variety of bands between 1990 cm^{-1} amd 2250 cm^{-1}(1,2). At 200 K, CO adsorbed on the silica support as well as on the Cu surface, and the strong band due to CO adsorbed on Cu was found at approximately 2100 cm^{-1}(2).

Pritchard and coworkers performed a thorough series of measurements of CO adsorption on Cu single crystal surfaces by infrared reflectance (29-31). Carbon-oxygen stretching frequencies between 2080 cm^{-1} and 2120 cm^{-1} are reported which are sensitive both to coverage and to

crystallographic orientation. Recent inelastic scattering data of CO adsorbed on the Cu(110) surface show a single carbon-oxygen stretching frequency of 2080 cm^{-1} at low coverage, shifting to 2097 cm^{-1} at saturation, in agreement with the infrared results (32).

CO adsorbed on Cu exhibits exclusively a vibrational spectrum which is characteristic of a terminal CO in metal carbonyl complexes, and in this respect Cu is similar to Ru. However, inspection of the low-energy electron diffraction patterns shows that compression structures exist on both Cu and Ru. As the coverage of CO approaches saturation, it appears that interadsorbate interactions frequently become a dominant effect in determining the adsorption site. In the case of Cu(110) the LEED pattern shows streaking indicating that CO is compressed out of registry with the substrate in the [001] direction, and on Cu(211), a hexagonal close-packed layer of CO is formed at high coverages (31). As discussed in detail in Chapter 3, one is forced to the conclusion that the characteristic terminal CO stretching frequency cannot be interpreted as an "on-top" CO in such cases.

The three metals, W, Pt, and Cu illustrate most of the characteristics of CO adsorption on transition metals. Both Ni and Pd surfaces result in both linear and bridged forms of CO, displaying a behavior somewhat similar to Pt (33,34). The use of vibrational spectroscopy to study chemisorption on single crystal surfaces is relatively new. Additional measurements of other crystal planes and more complicated adsorbates will contribute futher to a fundamental understanding of chemisorption.

The chapters which follow are manuscripts which have been submitted separately for publication. The figure, equation and reference numbers are therefore local to each chapter. In Chapter 2, the instrument used to carry out this work is described. Chapters 3, 4, and 5 report studies of CO and oxygen adsorption on the Ru(001) surface. Chapter 6 concerns the vibrational spectrum of adsorbed NO. Chapter 7 is a model calculation proposing a mechanism for the diffuse scattering of electrons by vibrational modes parallel to the surface. Following the conclusions are several appendices which describe the mechanical design and operation of the electron spectrometer.

References

1. R. P. Eischens and W. A. Pliskin, Advan. Catal. 10, 1 (1958).
2. M. L. Hair, Infrared Spectroscopy in Surface Chemistry, Marcel Dekker, New York, 1967.
3. L. H. Little, Infrared Spectroscopy of Adsorbed Species, Academic Press, London, 1966.
4. J. T. Yates, Jr. and C. W. Garland, J. Phys. Chem. 65, 617 (1961).
5. R. G. Greenler, J. Chem. Phys. 44, 310 (1966).
6. A. M. Bradshaw and F. M. Hoffman, Surface Sci. 68, 539 (1978).
7. H. J. Krebs and H. Lüth, Appl. Phys. 14, 337 (1977).
8. R. G. Greenler, J. Vac. Sci. Technol. 12, 1410 (1975).
9. J. T. Yates, Jr. and D. A. King, Surface Sci. 32, 231 (1972).
10. J. T. Yates, Jr., R. G. Greenler, I. Ratajczykowa and D. A. King, Surface Sci. 36, 739 (1973).
11. H. Ibach, H. Hopster and B. Sexton, Appl. Surface Sci. 1, 1 (1977).
12. H. Metiu, J. Chem. Phys. 68, 1453 (1978).
13. H. Froitzheim, H. Ibach and S. Lehwald, Surface Sci. 63, 56 (1977).
14. A. Crossley and D. A. King, Surface Sci. 68, 528 (1977).
15. E. Evans and D. L. Mills, Phys. Rev. B5, 4126 (1972).
16. D. M. Newns, Phys. Letters 60A, 461 (1977).
17. D. Šokčević, Z. Lenac and R. Brako, Z. Physik B28, 273 (1977).
18. W. Ho, R. F. Willis and E. W. Plummer, Phys. Rev. Letters 40, 1463 (1978).
19. J. W. Davenport, W. Ho and J. R. Schrieffer, Phys. Rev. B17, 3115 (1978).
20. R. F. Willis, W. Ho and E. W. Plummer, Surface Sci., to be published.
21. T. E. Madey and J. T. Yates, Jr., J. Vac. Sci. Technol. 8, 63 (1971).

22. J. T. Yates, Jr. and D. A. King, Surface. 32, 479 (1972).

23. T. E. Madey, J. T. Yates, Jr. and R. C. Stern, J. Chem. Phys. 42, 1372 (1965).

24. A. Adnot and J. D. Carette, Surface Sci. 74, 109 (1978).

25. R. J. Madix, Proceedings, First European Conference on Surface Science, to be published.

26. R. A. Shigeishi and D. A. King, Surface Sci. 58, 379 (1976).

27. G. Ertl, M. Neumann and K. M. Streit, Surface Sci. 64, 393 (1977).

28. H. Froitzheim, H. Ibach and S. Lehwald, Phys. Rev. B14, 1362 (1976).

29. M. A. Chesters, J. Pritchard and M. L. Sims, Adsorption-Desorption Phenomena, Ed., F. Ricca, Academic Press, London, 1972, p. 277.

30. K. Horn and J. Pritchard, Surface Sci. 55, 701 (1976).

31. K. Horn, M. Hussain and J. Pritchard, Surface Sci. 63, 244 (1977).

32. J. Wendelken, to be published.

33. S. Andersson, Solid State Commun. 21, 75 (1977).

34. J. C. Bertolini, G. Dalmai-Imelik and J. Rousseau, Surface Sci. 68, 539 (1977).

Chapter II

A Versatile Electron Spectrometer for Surface Studies

Abstract

An electron spectrometer is described which is designed to carry out a variety of electron spectroscopies of solid surfaces in ultra-high vacuum. The instrument is capable of the high energy resolution (10-15 meV) required for inelastic electron scattering from surface vibrations. It has also been designed to carry out angle-resolved photoemission measurements, Auger electron spectroscopy and energy-loss measurements of electronic excitations. The performance of the instrument in these modes of operation is discussed.

1. Introduction

Much of the recent progress in the study of well characterized surfaces has been due to advances in various kinds of electron spectroscopy. Among the most promising techniques in chemisorption research are Electron Energy Loss Spectroscopy (EELS) for the study of surface vibrations, Angle-Resolved Ultraviolet Photoelectron Spectroscopy (ARUPS), and Auger Electron Spectroscopy. The purpose of this work is to describe an electron spectrometer which combines these techniques in a mechanically simple and economical fashion.

Electrostatic electron energy analyzers and monochromators for high resolution spectroscopy are commonly in use for electron scattering from gas molecules[1-3]. Recently, interest in vibrational energy loss measurements has motivated the construction of spectrometers optimized for very low energy electrons which are compatible with the ultrahigh vacuum requirements of chemisorption studies[4]. An electron scattering system with a rotating analyzer which is capable of the very high energy resolution necessary for vibrational energy loss measurements can also be employed for other analytic electron spectroscopies, provided that the optics and electronics are sufficiently versatile. In Section 2 of this paper, such a system is discussed, followed by a brief illustration of its performance in Section 3.

2. The Electron Spectrometer

The electron spectrometer is of the Kuyatt-Simpson type with hemispherical energy dispersing elements and electron optics consisting of

cylindrical tube lenses. Although cylindrical energy dispersing elements have been very successful in high resolution electron scattering[5,6], hemispherical elements were chosen because of their property of second-order angle focusing[1,7]. In addition, the hemispherical system is used most easily with circular apertures rather than the rectangular slits used frequently in cylindrical systems. The scattering intensity, in the case of a circular beam, is interpreted more conveniently in terms of a partially integrated cross-section than is the scattering intensity of a rectangular beam.

The scattering system was designed to be used without any appreciable translation of the crystal. The electron optics, ultraviolet discharge lamp[8], ion gun, and gas doser[9] are all directed at the sample at the center of the stainless steel bell jar so that a minimum of alignment difficulties are encountered in the course of an experiment. The sample is positioned at the scattering center with a Varian precision manipulator mounted on a side port of the bell jar. The manipulator allows the sample to move through two angles (θ,ϕ), which are not strictly orthogonal, and to be translated in three orthogonal directions in the scattering region. The ultraviolet light source, the ion gun, and the gas doser are mounted on side ports which face the sample at various angles. The electron spectrometer is attached to a 35.6 cm ID Wheeler flange which serves to close off the top of the bell jar. The spectrometer consists of a fixed electron monochromator and a rotating energy analyzer. The angle of incidence of the gun may be changed by rotating and resealing the top of the bell jar or by rotating the crystal through the angles (θ,ϕ).

The scattering system is lined with conetic shielding which serves to reduce the magnetic field to <30 mgauss throughout the region occupied by the electron spectrometer. The relatively high magnetic field is quite compatible with high resolution electron spectroscopy, although commonly used design criteria would suggest otherwise[10].

The flange which supports the spectrometer contains the feedthroughs necessary for the electrical and mechanical connections to the spectrometer. The axis of rotation of the analyzer (Fig. 1.b.) is the center line of the bell jar and is defined by two Cu-Be bearings in the spectrometer frame. The shaft which holds the analyzer in these bearings is hollow to accommodate the multiplier collection lead and supports a 15.2 cm diameter spur gear parallel to the flange face. Angle markings, engraved in 2^{o} increments on the gear face, are visible through a window on the top wheeler flange. This allows the angular position to be measured ($\pm 0.2^{o}$) without consideration of the backlash in the rotary feedthrough and off-axis spur gear which turns the energy analyzer.

The electron optics are supported by a stainless steel frame which is suspended from the top flange. The electrical connections were made to the rotating analyzer with flexible shielded cables from Ceramaseal, to avoid the noise associated with sliding contacts.

The electron optics are machined from Cu-Be alloy with the exception of the cathode and anode which are Mo. The Cu-Be pieces were treated with a thin nonmagnetic nickel plate followed by a layer of plated gold. Although the reflectivity of gold is thought to be undesirably high for use in electron spectrometers[11], we were seeking a treatment that would

provide chemical stability in a wide range of experiments and that would not be degraded with use at high electron energies. This appears to have been successful in practice.

The hemispheres of the monochromator define a central trajectory 5.08 cm in diameter. The hemispheres of the energy analyzer define a central path 7.62 cm in diameter. The monochromator hemispheres are small because of the difficulty of space-charge spreading[1] imposed by the low pass energy and relatively high beam currents in this region.

The two sets of hemispheres were machined to within 0.001 cm of true hemispheres and positioned with sapphire balls on mounting plates. The hemispheres and other optics were positioned with dowel pins and alignment grooves during machining and further alignment was not necessary. Deflector plates positioned throughout the optics proved superfluous.

The cathode optics of this instrument are similar to several reported previously[1,2]. A metal oxide dispenser cathode obviates the necessity of accurate filament placement for high resolution work. The current for the indirect heater is delivered through four wires arranged in four holes of an alumina rod in such a way that both the dipole and quadrupole parts of the magnetic field set up by the current cancel sufficiently far from the rod.

The beam-defining apertures of the spectrometer were chosen to satisfy the resolution requirements of vibrational energy loss measurements. The beam-defining apertures of the gun (element 4, Fig. 1.a.) are approximately 0.03 cm in diameter. Two additional apertures at the analyzer entrance are 0.05 cm in diameter and define an acceptance cone from the surface

which subtends a full-angle of 4.5^{o}, independent of electron energy.

The Spiraltron electron multiplier is positioned after the energy defining aperture of the analyzer in such a way that the fixed collector can lie on the axis of rotation of the analyzer. The pulse from the electron multiplier travels a short path (25 cm) through a high-voltage feedthrough and decoupling capacitor before reaching the amplifier-discriminator, thus minimizing losses and reflections.

An outline of the spectrometer electronics is given in Fig. 2. The system is under the control of a minicomputer (PDP 11/10) which is supervised by a software package designed for data acquisition and reduction[12]. The software system controls the spectrometer by interpreting a string of statements once during each clock period of 16 msec. The relatively slow clock reduces the machine overhead to the point where time-sharing is possible.

The kinetic energy of the electrons which are counted is selected by a power supply which is programmed by a 12-bit digital-to-analog converter. The low-noise requirements of high-resolution measurements were satisfied by Kepco PCX supplies. A separate set of high voltage supplies is used for analyzer operation to 1000 eV and for beam energies up to 2 kV, chiefly for Auger Electron Spectroscopy. The lens potentials are set with potentiometers. The focusing error encountered in retardation does not appear to be serious in the vibrational energy loss experiments, presumably because of the narrow energy range involved. Two additional D/A channels and power supplies were provided for non-linear corrections to the field lens and zoom lens of the energy analyzer.

Pulses from the amplifier-discriminator are accumulated in a 16-bit counter which is read and cleared by the computer every 16 msec. This allows for a maximum count rate of 4 MHz. The maximum rate encountered in energy loss experiments is about 2×10^6 counts/sec. The amplifier-discriminator (PAR 1120) has a 10 nsec dead time, and the first stages of the counting string are Schottky-clamped flip-flops, so good counting statistics should obtain even at high rates. The spectrometer electronics are isolated completely from the computer with optical isolators.

3. Performance

Examples will be given of the various capabilities of the spectrometer. The most demanding application is certainly the measurement of vibrational energy-loss spectra. An example from a series of measurements of CO on the Ru(001) surface is given in Fig. 3. The energy resolution (full-width at half-maximum of the elastic peak) in these measurements ranges from 11-15 meV, where the variation is presumably due to the changing condition of the spectrometer surfaces during the measurements. A resolution of 9 meV has been obtained under favorable conditions. Typical electrode potentials employed in the electron energy-loss measurements are listed in Table I. Some care in tuning is required to eliminate spurious peaks, similar to those described previously[13]. The vibrational energy-loss data are accumulated typically in 20 min. using incident currents of 100-300 pamp. The count rate in the elastic channel in the specular direction from the clean surface is typically 3×10^5 cps.

Electron energy-loss measurements can be used also to study the larger energy losses due to plasmon excitations and electronic transitions. Fig. 4 shows energy-loss spectra obtained in the specular direction at primary energies of 60 and 90 eV from the clean surface and at a primary energy of 60 eV after CO adsorption. These results were obtained with the analyzer positioned 6^{o} out of the specular direction in order to reduce the intensity of the elastic peak. The surface and bulk plasmons are found at 9.6 eV and 22 eV, respectively the fact that the bulk plasmon is considerably higher in energy than $\sqrt{2}$ times the surface plasma frequency reflects the deviation of Ru from free-electron-like behavior[14]. Energy-loss spectra which were obtained at 300 and 900 eV show the bulk plasmon excitation as the dominant feature. An additional energy-loss feature at 28 eV (Fig. 4.b.) may be due to an interband transition[14]. After CO chemisorption (Fig. 4.c.), a new feature is visible at 14 eV; the peak at 7.6 eV may be composed of a CO loss feature between 5 and 6 eV and an attenuated surface plasmon[15]. It has been proposed that these losses are related to the electronic excitations of CO[15].

The addition of an ultraviolet light source has made possible angle-resolved photoemission in the same system. Fig. 5.a. shows the energy distribution curve for photoelectrons emitted normal to the surface obtained with an energy resolution of approximately 0.25 eV. The 21.2 eV light is incident on the surface at 52^{o} from the normal. The energy distribution curve normal to the Ru(001) surface shows three very prominent features in the d-band, which are observed to a lesser extent in angle-averaged spectra[16]. In Fig. 5.b., the difference spectrum obtained from the surface saturated with CO is shown. The two peaks in this spectrum

are due to the ionization of the 4σ, 1π, and 5σ molecular orbitals of chemisorbed CO. It appears that ultimately ARUPS may resolve the 5σ and 1π peaks as it has for CO chemisorbed on Ni[17].

Finally, the electron spectrometer was designed to permit angle-resolved Auger spectroscopy. Recent theoretical work suggests that anisotropies in the Auger election angular distribution are primarily due to final state effects, and are not so sensitive to initial state symmetry as angle-resolved photoemission[18]. Nevertheless, because of the convenience of carrying out AES in the same instrument, and the possibility of comparing techniques, the spectrometer was adapted also to operation at intermediate electron energies (0-1000 eV).

The aperture size at the analyzer entrance was chosen to satisfy the high-resolution requirements of vibrational energy-loss measurements rather than to maximize the étendue[19]. Nevertheless, Auger spectroscopy is possible by degrading the analyzer resolution to approximately 0.6 eV and by increasing the monochrometer pass energy to the point where the energy resolution of the gun is determined by the thermal width of the cathode. In Fig. 6.a., an Auger spectrum [N(E)] of clean Ru(001) for normal emission obtained with a gun current of 1.5 μamp at 2kV is shown. The count rate at the 273 eV Ru ($M_5N_{4,5}N_{4,5}$) peak is approximately 5×10^5 cps with a signal/background ratio of unity. The differential spectrum was obtained digitally after smoothing the N(E) curve with a five-point cubic fit[12]. The spectrum agrees well with others reported for clean Ru obtained with angle-integrating analyzers[9].

Thus, a wide range of techniques important in chemisorption research

have been combined in a single instrument. The utility of these various electron spectroscopies has been demonstrated explicitly.

Acknowledgment

The support of this research by the National Science Foundation (Grant No. ChE77-16314) is gratefully acknowledged. We thank also Seichi Nakawatase for his careful machining of the instrument, and Patricia A. Thiel for valuable assistance during assembly.

References

1. C. E. Kuyatt and J. A. Simpson, Rev. Sci. Instrum. 38, 103 (1967).
2. A. Chutjian, J. Chem. Phys. 61, 4279 (1974).
3. A. J. Williams and J. P. Doering, J. Chem. Phys. 51, 2859 (1969).
4. H. Froitzheim, Electron Spectroscopy for Surface Analysis, H. Ibach, ed., Springer-Verlag, Berlin, 1977, p. 205.
5. H. Ibach, H. Froitzheim and B. Sexton, Appl. Surface Sci. 1, 1 (1977).
6. J. F. Wendelken and F. M. Propst, Rev. Sci. Instrum. 47, 1069 (1976).
7. D. Roy and J. D. Carette, Electron Spectroscopy for Surface Analysis, H. Ibach, ed., Springer-Verlag, Berlin, 1977, p. 13.
8. P. A. Thiel, Ph.D. Thesis, California Institute of Technology (in preparation).
9. D. W. Goodman, T. E. Madey, M. Ono and J. T. Yates, Jr., J. Catal. 50, 279 (1977).
10. D. Roy, A. Delage and J. D. Carette, J. Phys. E 8, 109 (1975).
11. P. Marmet and L. Kerwin, Can. J. Phys. 38, 787 (1960).
12. J. L. Taylor, Ph.D. Thesis, California Institute of Technology, 1978.
13. H. Froitzheim, H. Hopster, H. Ibach and S. Lehwald, Appl. Phys. 13, 147 (1977).
14. H. Raether, Springer Tracts in Modern Physics 38, 84 (1965).
15. G. W. Rubloff, Solid State Comm. 26, 523 (1978).
16. K. A. Kress and G. J. Lapeyre, Phys. Rev. B2, 2532 (1970).
17. C. L. Allyn, T. Gustafsson and E. W. Plummer, Chem. Phys. Letters 47, 127 (1977).
18. J. W. Gadzuk, Surface Sci. 60, 76 (1976).

19. D. W. O. Heddle, J. Phys. E 4, 589 (1971).

Table I

Voltages Used for High Resolution Energy Loss Spectroscopy

(See Fig. 1)

Electrode	Potential (volts)	Electrode	Potential (volts)
1	-5.9	13	34.2
2	16.2	14	22.7
3	125.0	15	18.5
4	-1.1	16	68.5
5	-3.9	17	22.7
6	-3.6	18	-3.3
7	-4.1	19	-3.0
8	-1.1	20	-3.6
9	0.5	21	-3.3
10	6.7	22	5.1
11	48.9	23	150
12	14.2		

Figure Captions

Fig. 1. (a) Schematic drawing of electron monochromator showing the function of the various optical stages. The diameter of the central trajectory between the hemispheres is 5.1 cm.

(b) Electron energy analyzer. The average diameter of the hemispherical electrodes is 7.6 cm.

Fig. 2. Outline of the spectrometer electronics and the data acquisition system.

Fig. 3. Energy-loss spectrum of CO on the Ru(001) surface. The angle of incidence is 62^{o} from the surface normal; the analyzer is centered on the specularly reflected beam. The incident energy is approximately 4.5 eV.

Fig. 4. Energy-loss spectra at different impact energies, E_{o}, of the clean and CO-covered Ru(001) surface.

Fig. 5. (a) Photoemission spectrum of the clean Ru(001) surface with 21.2 eV radiation incident at 52^{o} from the normal.

(b) Difference spectrum of a saturated CO layer.

Fig. 6. Auger spectrum of clean Ru(001) collected normal to the surface displayed

(a) as acquired, and

(b) after smoothing and differentiation.

(a)

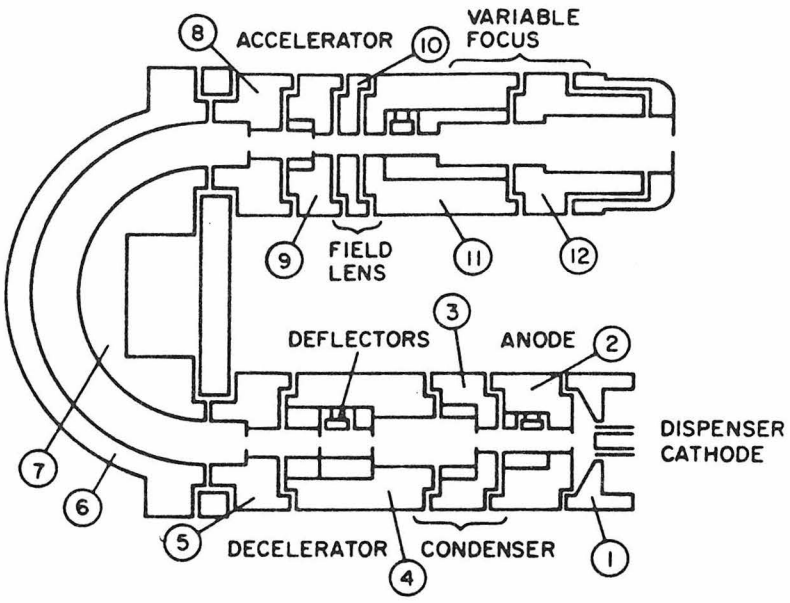
ELECTRON MONOCHROMATOR
8
ACCELERATOR
10
VARIABLE FOCUS
9
FIELD LENS
11
12
3
DEFLECTORS
ANODE
2
DISPENSER CATHODE
7
6
5
DECELERATOR
4
CONDENSER
1

(b)

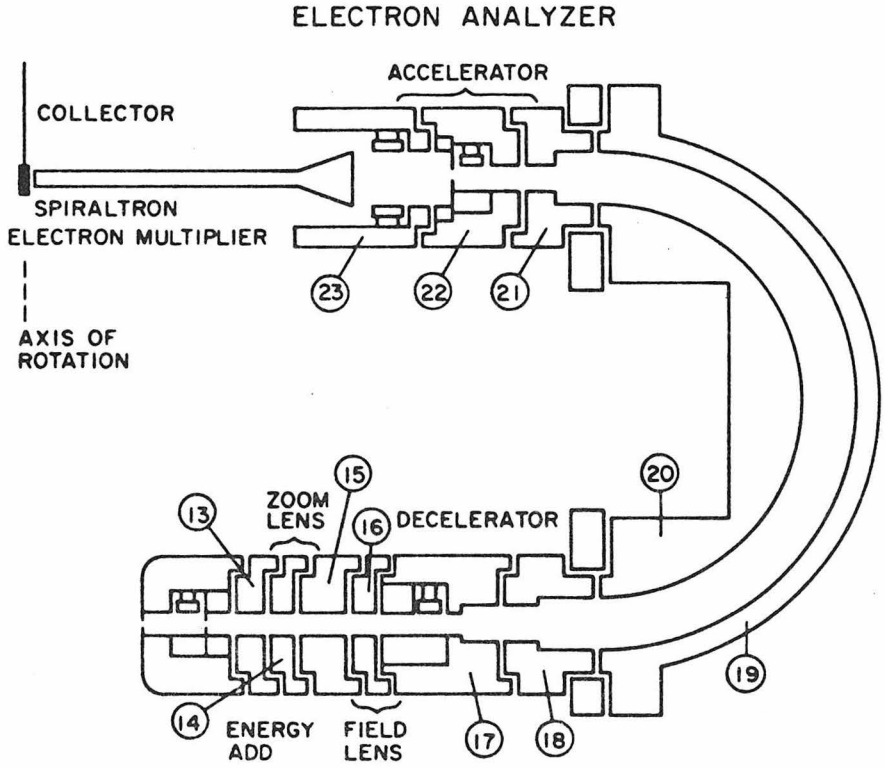
ELECTRON ANALYZER
ACCELERATOR
COLLECTOR
SPIRALTRON ELECTRON MULTIPLIER
AXIS OF ROTATION
23
22
21
15
20
13
ZOOM LENS
16
DECELERATOR
19
14
ENERGY ADD
FIELD LENS
17
18

Fig. 1

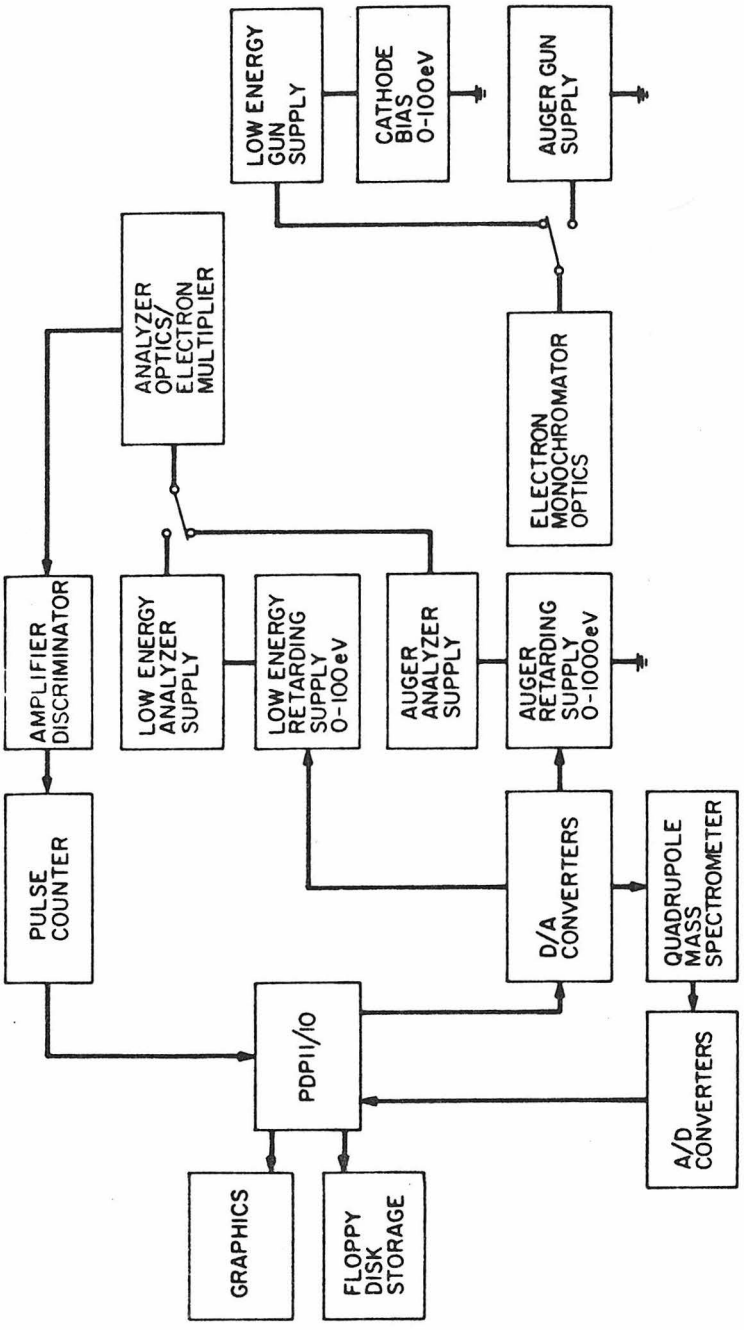
LOW ENERGY GUN SUPPLY
CATHODE BIAS 0-100eV
AUGER GUN SUPPLY
ANALYZER OPTICS/ ELECTRON MULTIPLIER
ELECTRON MONOCHROMATOR OPTICS
AMPLIFIER DISCRIMINATOR
LOW ENERGY ANALYZER SUPPLY
LOW ENERGY RETARDING SUPPLY 0-100eV
AUGER ANALYZER SUPPLY
AUGER RETARDING SUPPLY 0-1000eV
PULSE COUNTER
D/A CONVERTERS
QUADRUPOLE MASS SPECTROMETER
PDP11/10
A/D CONVERTERS
GRAPHICS
FLOPPY DISK STORAGE

Fig. 2

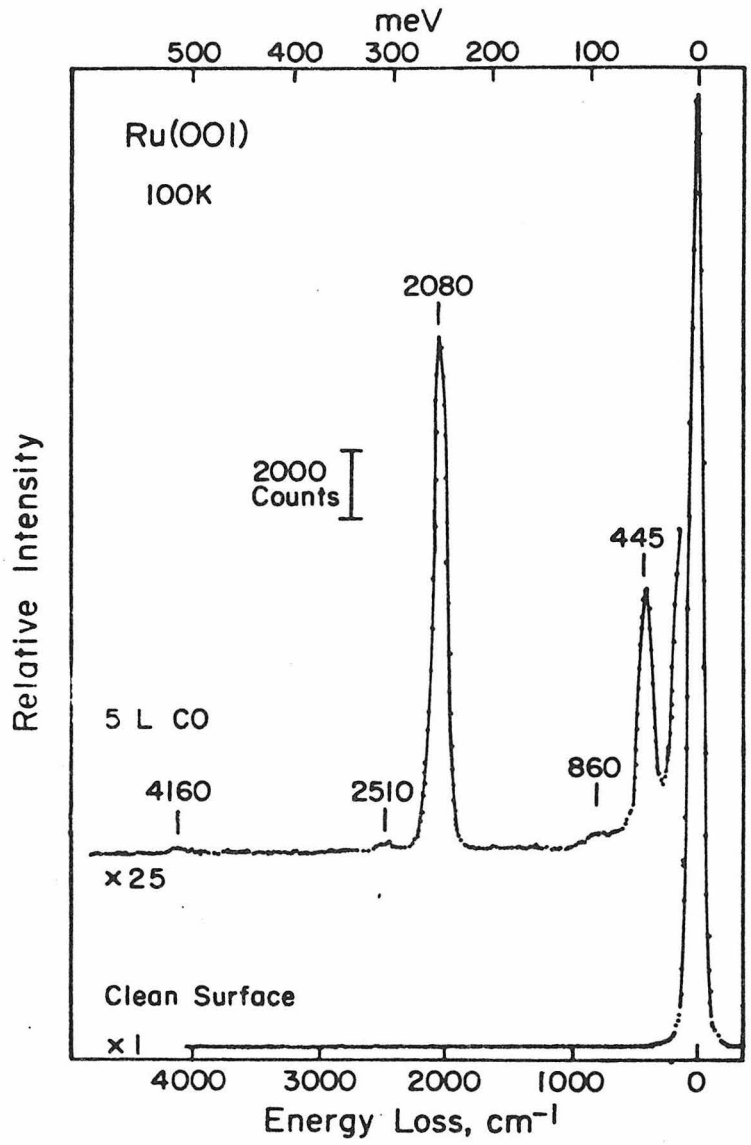
meV
500
400
300
200
100
0
Ru(001)
100K
2080
2000
Counts
445
5 L CO
860
4160
2510
×25
Clean Surface
×1
4000
3000
2000
1000
0
Energy Loss, cm⁻¹
Relative Intensity

Fig. 3

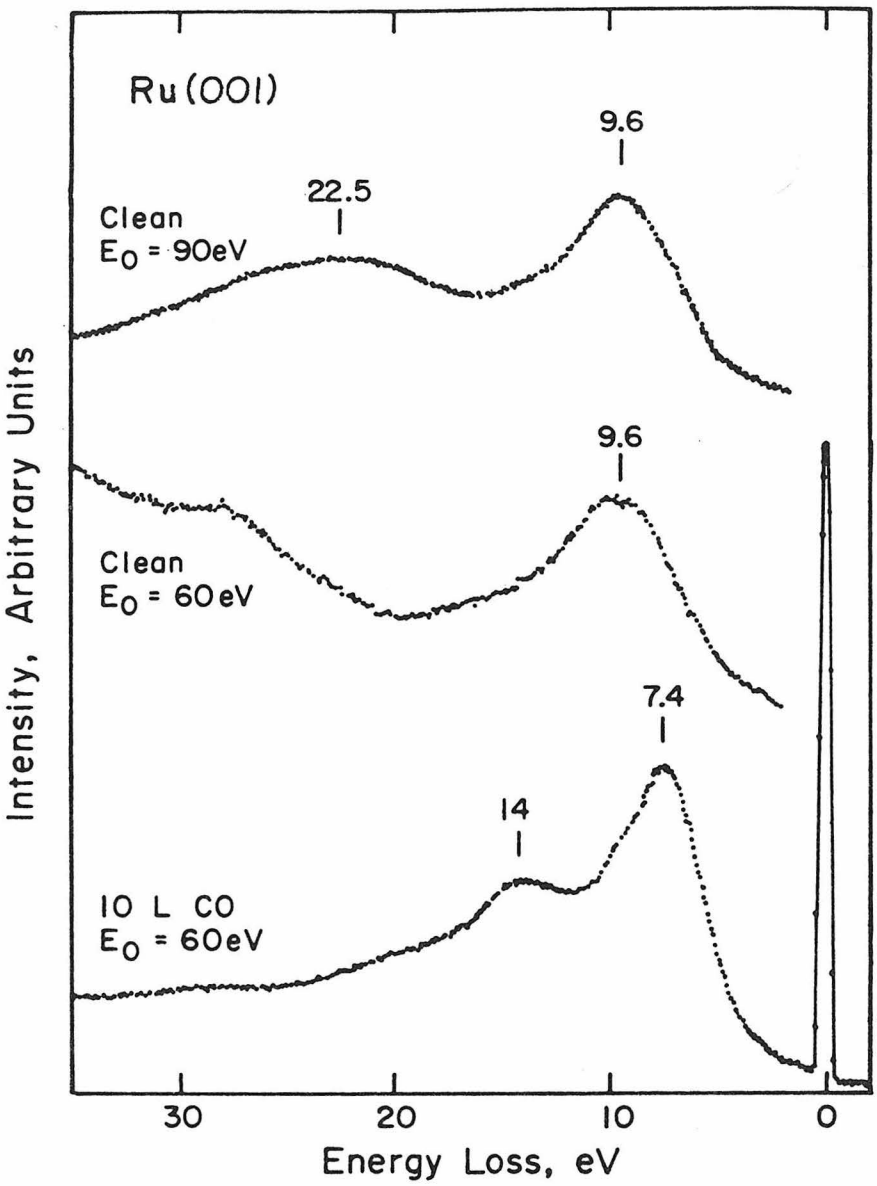
Ru(001)
9.6
22.5
Clean
E_0 = 90eV
9.6
Clean
E_0 = 60eV
7.4
14
10 L CO
E_0 = 60eV
Intensity, Arbitrary Units
30
20
10
0
Energy Loss, eV

Fig. 4

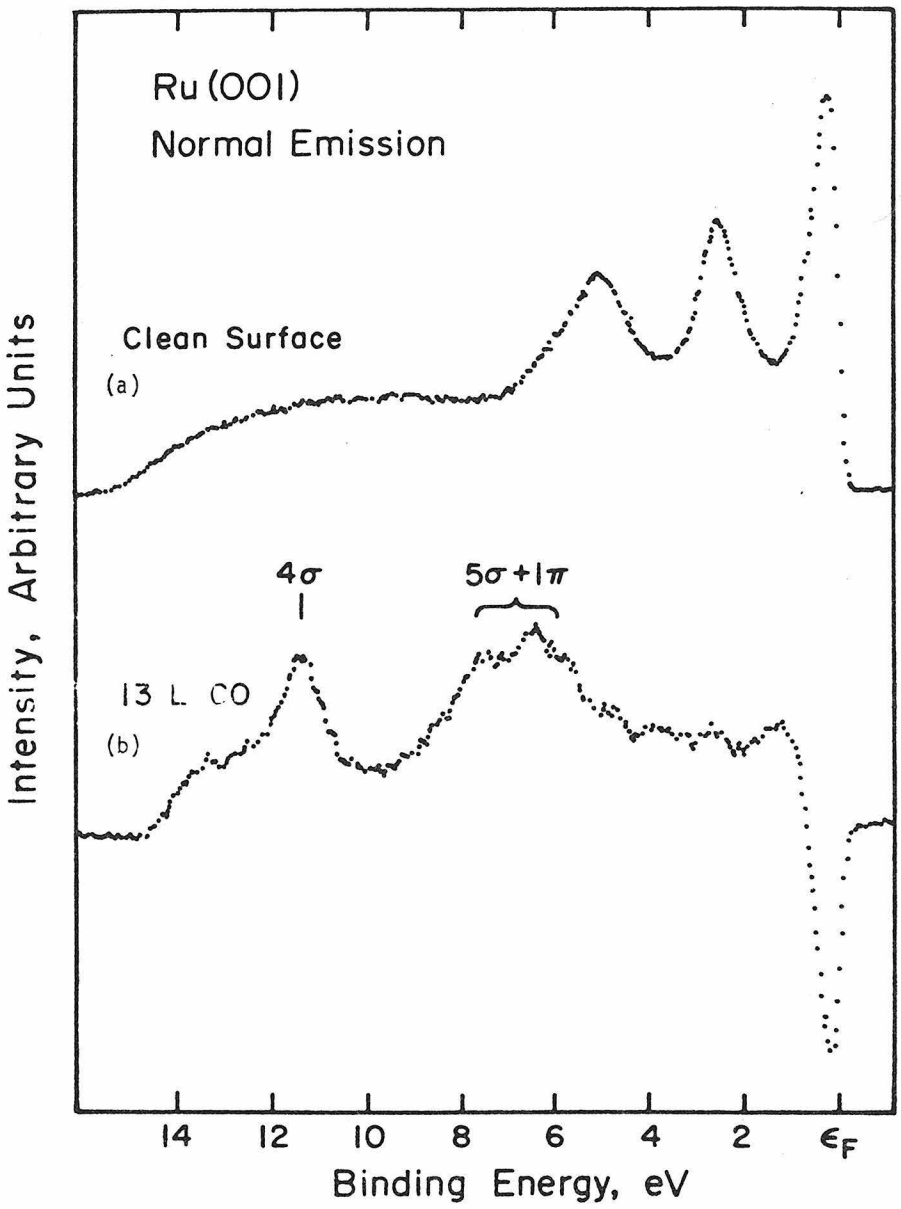
Ru (001)
Normal Emission
Clean Surface
(a)
4σ
5σ+1π
13 L CO
(b)
Intensity, Arbitrary Units
14
12
10
8
6
4
2
ϵ_F
Binding Energy, eV

Fig. 5

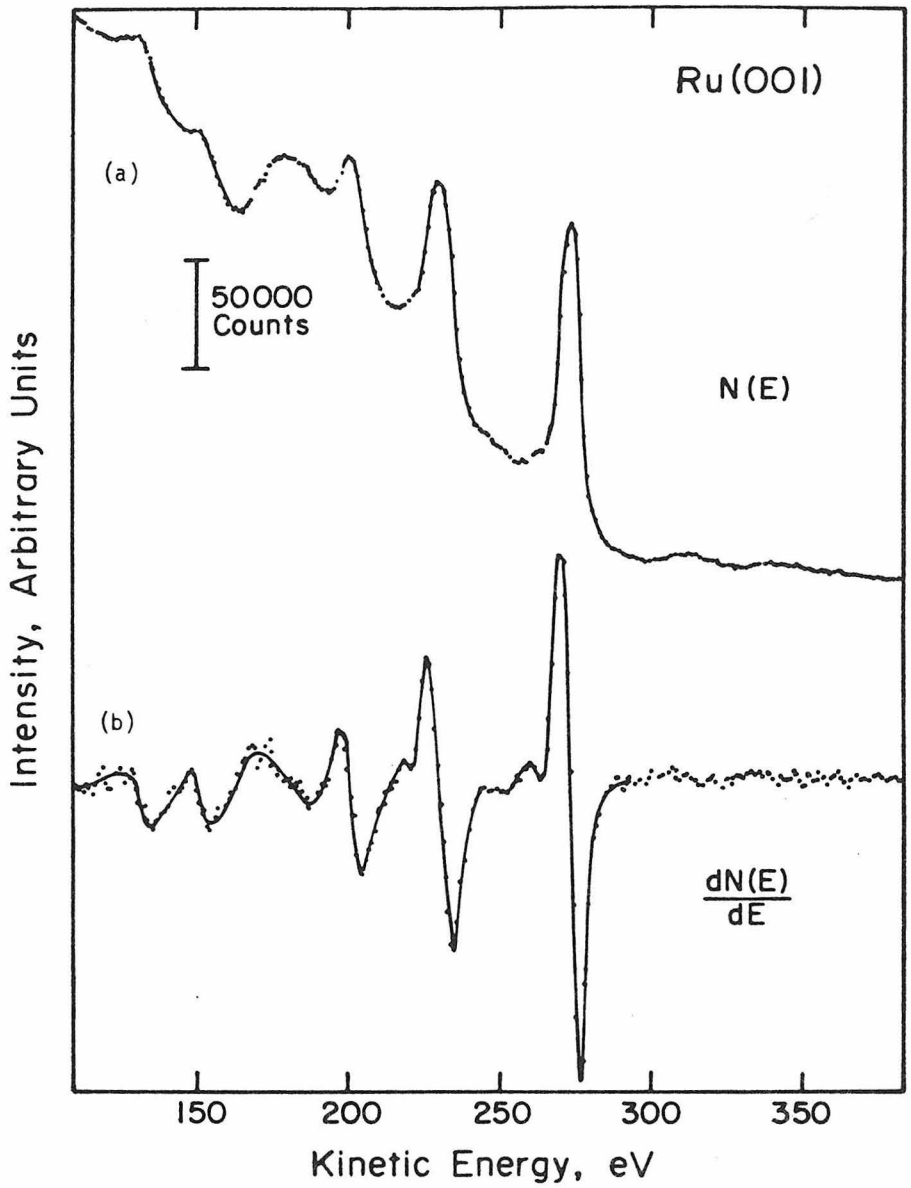
Ru(001)
(a)
50000
Counts
N(E)
(b)
dN(E)
dE
Intensity, Arbitrary Units
150
200
250
300
350
Kinetic Energy, eV

Fig. 6

Chapter III

The Vibrational Spectrum and Adsorption Site of CO on the Ru(001) Surface

Abstract

Vibrational spectra and LEED structures of CO on the Ru(001) surface were measured as a function of coverage at 100 K. The LEED patterns indicate that CO occupies a variety of asymmetric sites at high coverage, while the vibrational spectra show a single Ru-C stretching frequency (445 cm^{-1}) and a single C-O stretching frequency (1980 - 2080 cm^{-1}) at all coverages. This shows that on this surface the CO adsorption site at high coverages is determined by interadsorbate interactions, and that the carbon-oxygen stretching frequency is not site-sensitive within the resolution of electron scattering measurements.

1. Introduction

The vibrational structure of adsorbed CO has been studied on a variety of transition metals by electron energy loss spectroscopy (EELS) and by infrared reflectance spectroscopy. Vibrational studies of adsorbed CO are especially popular since CO possesses a large transition dipole moment and since the spectra are thought to be readily interpretable in terms of the adsorption site of the CO molecule. However, the EELS measurements reported here of CO adsorbed on the Ru(001) surface show that the binding site of CO on this surface cannot be determined from the vibrational data alone.

By analogy to CO stretching frequencies found in inorganic metal carbonyl compounds, CO is usually assumed to be in an on-top site if the carbon-oxygen stretching frequency is above 1990 cm^{-1}, and that it is in a bridged site (two-fold, or of higher coordination) if the frequency is lower. For example, on Ni(111) (1,2), Pt(111)(3,4) and Pd(111)(5), two carbon-oxygen stretching frequencies are observed at saturation coverage. A band in the range 1800 cm^{-1} to 1920 cm^{-1} is attributed to a bridged CO. The frequency of this band increases with coverage by 100 cm^{-1} on the Ni(111) and Pd(111) surfaces, an effect which has been ascribed either to a change in bridge sites or to direct CO-CO interactions. An additional band above 2000 cm^{-1} is assigned to CO occupying an on-top site.

Of course, the structures assigned to CO must be compatible with LEED patterns observed under the same conditions. On Pd(111)(5), Ni(111)(6) and Pt(111)(7), the low temperature LEED pattern is a $(\sqrt{3} \times \sqrt{3})R30^{o}$ up to a fractional coverage of a third of a monolayer,

followed by a continuous compression to a c(4x2) structure. On Ni and Pt, additional compression structures are observed, corresponding to a coverage of approximately 0.6 monolayer (based on the number of substrate atoms). The continuous compression and the existence of ordered overlayers indicates that the CO adsorption site at high coverages is determined largely by interadsorbate interactions. In general, the LEED structures can be reconciled with the vibrational frequencies with only minor adjustments of CO position within the unit cell, since both "linear" and "bridged" frequencies appear in the vibrational spectra. This is not the case for CO on the Ru(001) surface, and the contradiction of the LEED structural information with the vibrational frequencies shows that on this close-packed surface a linear CO molecule is not necessarily in an on-top site.

2. Experimental

Vibrational energy loss measurements were performed in a scattering system equipped with a hemispherical electron monochromator and electron energy analyzer (8). The analyzer was positioned in the specular direction and accepted electrons in a cone of full angle 4.5^{o}. The incident beam had a kinetic energy of approximately 4.5 eV. The Ru crystal was oriented within 1^{o} of the (001) plane, and was cut and polished using standard techniques (9). The sample was mounted in an ultrahigh vacuum system with a base pressure $< 5 \times 10^{-11}$ torr. It was positioned with a Varian precision manipulator equipped with a liquid nitrogen cooling reservoir. The surface was cleaned by heating repeatedly to 1370 K in 5×10^{-8} torr O_2, and subsequent annealing in vacuum at 1570 K.

LEED measurements were made in a separate ultrahigh vacuum system using a different Ru(001) sample cut from the same boule. Surface cleanliness was verified by Auger electron spectroscopy using a cylindrical mirror analyzer.

3. Results and Discussion

Representative spectra for low and high coverages of CO on the Ru(001) surface at 100 K are shown in Fig. 1. The 5L exposure (1L ≡ 1 Langmuir ≡ 10^{-6} torr-sec) produces essentially saturation coverage. Two fundamental vibrations are observed in the spectra, a metal-carbon stretch at 445 cm^{-1} (55 meV), and a carbon-oxygen stretch which varies from 1984 cm^{-1} (246 meV) for a 0.1L exposure to 2080 cm^{-1} (258 meV) at saturation. In addition, at high coverage the overtones and combination frequency of these two bands are observable. These frequencies are in good agreement with those of the corresponding modes in the $Ru_3(CO)_{12}$ complex in which CO is linearly bonded to the Ru atoms (10). It appears that CO is upright on the Ru(001) surface and that there is a single carbon-metal bond. Measurements of the electron stimulated desorption ion angular distributions of CO^+ and O^+ from this surface also indicate an upright geometry (11). The two bending modes of this structure are not observed, presumably because they are parallel to the surface and have weak dipole transition moments.

The most significant aspect of the vibrational spectra is that the carbon-oxygen stretching frequency is found exclusively in the range usually associated with an "on-top" CO at all coverages. The carbon-oxygen stretching region is shown in detail in Fig. 2; within the instrumental resolution (11-15 meV full-width at half-maximum of the elastic peak), there is a single symmetric peak at all coverages. The carbon-metal frequency is constant, 445 cm^{-1} $\pm$ 8 cm^{-1}, at all coverages.

As reported previously by Madey and Menzel, at fractional coverages less than 1/3 on this surface, CO forms a $(\sqrt{3} \times \sqrt{3})R30^{o}$ LEED structure (12,13). The CO molecules may reside in

on-top sites (Fig. 3a), as is suggested by the vibrational spectrum. At higher coverages, the fractional order LEED beams split and move to form a $(2\sqrt{3} \times 2\sqrt{3})R30^{o}$ pattern (12, 13). A structure may be assigned to this pattern by assuming that the most intense non-substrate beams result from first order diffraction from a CO superlattice. The primitive vectors of the superlattice are indicated in Fig. 3b as b_1 and b_2. The unit cell of the superlattice has been placed at an arbitrary origin on the substrate.

At saturation coverages at 100 K a new LEED pattern appears, a $(5\sqrt{3} \times 5\sqrt{3})R30^{o}$, which is due to a hexagonally close-packed layer of CO with a lattice spacing of 3.33Å (13). Coverages, as determined from the areas under thermal desorption peaks, agree with these LEED structural observations. It is not possible to shift all the CO molecules to on-top sites at high coverage, unless an unreasonably small CO-CO spacing of 2.71Å and an extremely complex ordering mechanism are assumed. Therefore, an inspection of the LEED patterns requires that the interpretation of the vibrational frequencies in terms of exclusively on-top CO be rejected.

4. Conclusions

The vibrational spectra of CO on the Ru(001) surface indicate that CO is "linearly" bound to the surface at all coverages, and that a bridged form is not present. LEED studies indicate that CO is found in a variety of asymmetric sites at high coverage. Consequently, the linear CO may not be assumed to be in on-top sites exclusively. Evidently, the carbon-oxygen stretching frequency is sensitive to the hybridization of the bonding orbitals of adsorbed CO but not necessarily sensitive to its position with respect to the substrate. This suggests that

in regard to CO adsorption, the Ru(001) surface is electronically, as well as geometrically, homogeneous, and that the adsorption site is not of primary chemical importance.

Acknowledgment

We would like to thank Ellen D. Williams who observed and interpreted the LEED patterns discussed here.

References

1. J. C. Bertolini, G. Dalmai-Imelik and J. Rousseau, Surface Sci. 68, 539 (1977).
2. W. Erley, H. Ibach and H. Wagner, Nederlands Tijdschrift voor Vacuum-technick 2/3/4, 154 (1978).
3. H. Froitzheim, H. Hopster, H. Ibach and S. Lehwald, Appl. Phys. 13, 147 (1977).
4. H. J. Krebs and H. Lüth, Appl. Phys. 14, 337 (1977).
5. A. M. Bradshaw and F. M. Hoffman, Surface Sci. 72, 513 (1978).
6. H. Conrad, G. Ertl, J. Küppers and E. E. Latta, Surface Sci. 57, 475 (1976).
7. G. Ertl, M. Neumann and K. M. Streit, Surface Sci. 64, 393 (1977).
8. C. E. Kuyatt and J. A. Simpson, Rev. Sci. Instrum. 38, 103 (1967).
9. C. M. Comrie and W. H. Weinberg, J. Chem. Phys. 64, 250 (1976).
10. C. O. Quicksall and T. G. Spiro, Inorg. Chem. 7, 2365 (1968).
11. T. E. Madey, private communication.
12. T. E. Madey and D. Menzel, Japan. J. Appl. Phys., Suppl. 2, Pt. 2, 229 (1974).
13. E. D. Williams and W. H. Weinberg, Surface Sci., submitted.

Figure Captions

Figure 1. Vibrational spectra of CO on the Ru(001) surface at low and high coverages measured by electron energy loss spectroscopy.

Figure 2. Detail of carbon-oxygen stretching region as a function of CO exposure.

Figure 3. Structures assigned to the low temperature LEED patterns of CO on the Ru(001) surface at coverages of 1/3 and 7/12 of a monolayer. The large open circles represent substrate atoms, and the shaded circles denote CO adsorption sites.

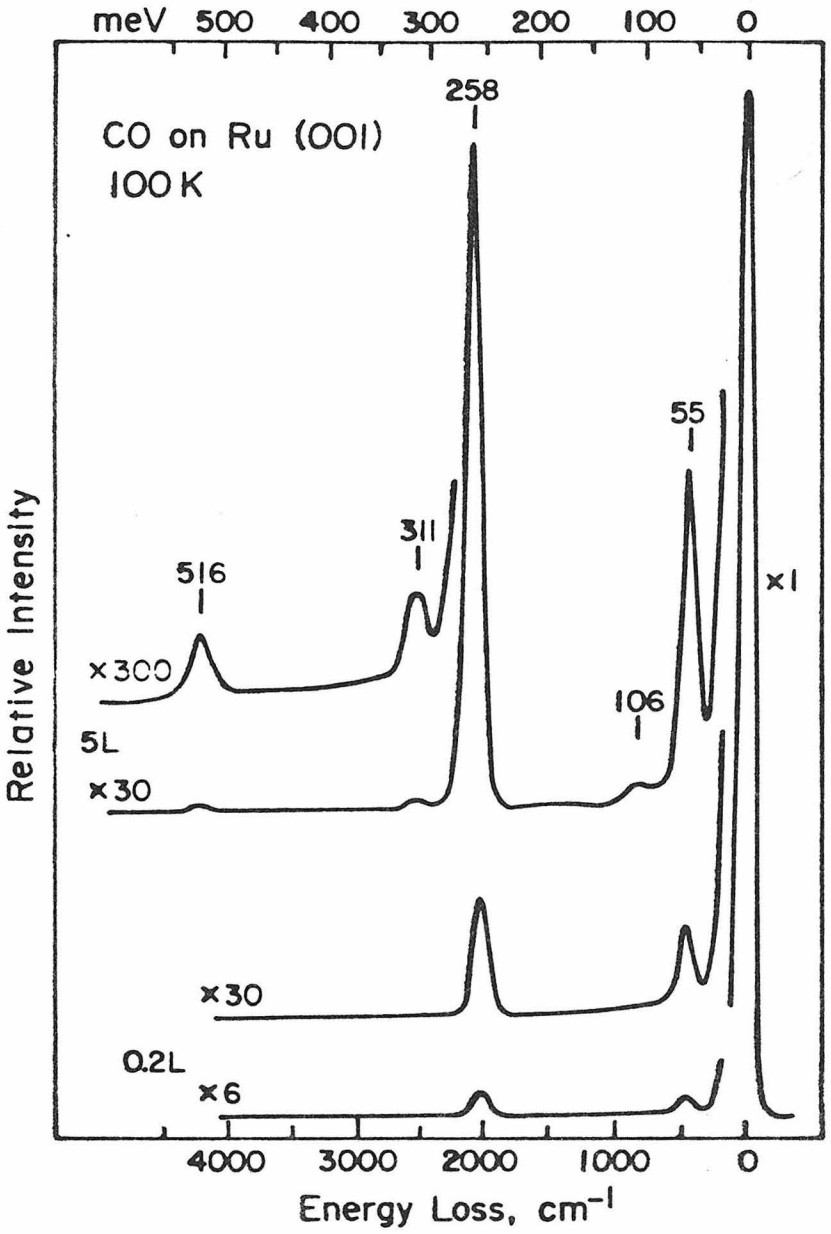
meV 500 400 300 200 100 0
CO on Ru (001)
100 K
258
311
516
55
106
×300
5L
×30
×1
×30
0.2L
×6
Relative Intensity
4000 3000 2000 1000 0
Energy Loss, cm⁻¹

Fig. 1

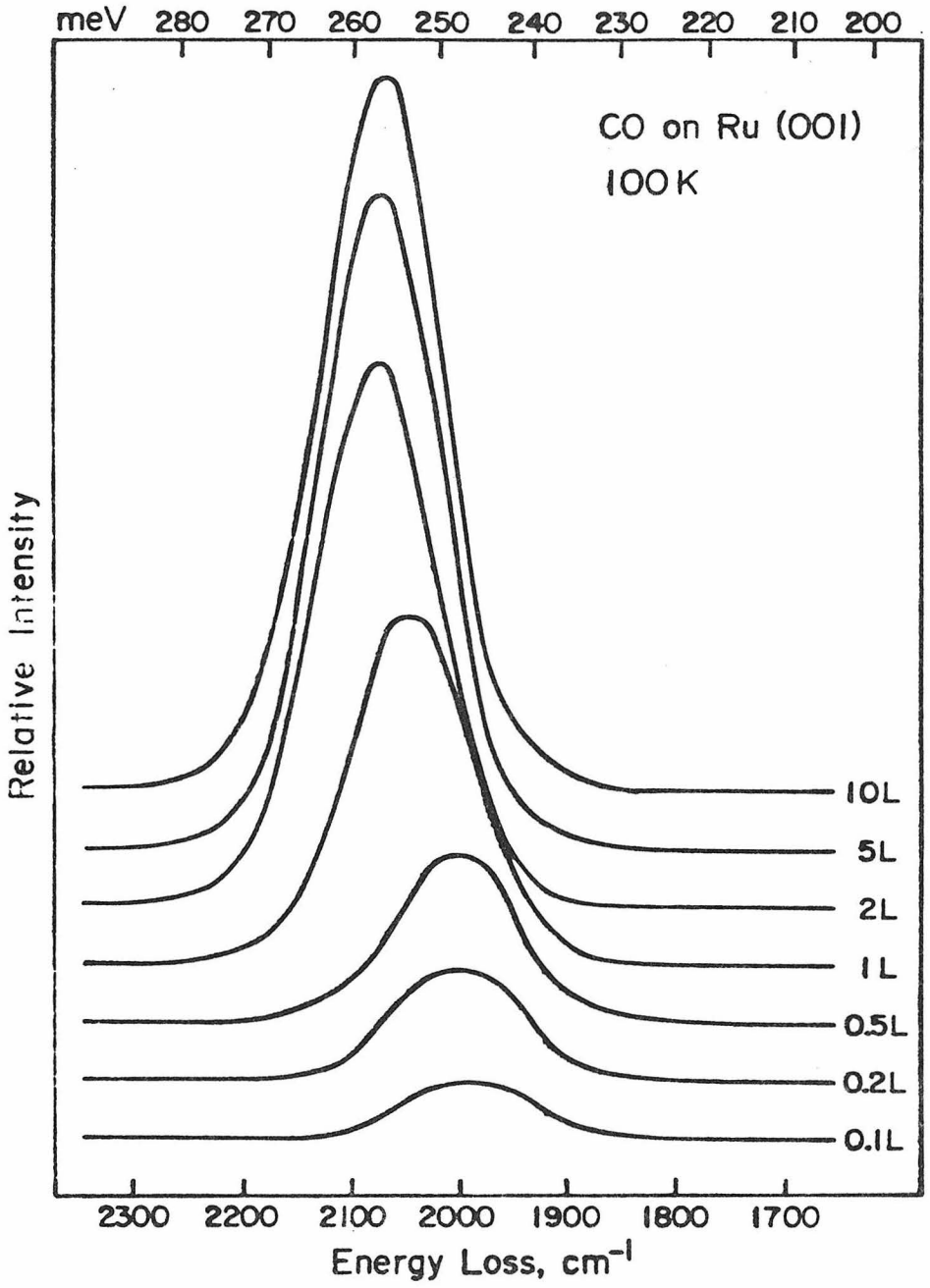
meV 280 270 260 250 240 230 220 210 200
CO on Ru (001)
100 K
Relative Intensity
10L
5L
2L
1L
0.5L
0.2L
0.1L
2300 2200 2100 2000 1900 1800 1700
Energy Loss, cm⁻¹

Fig. 2

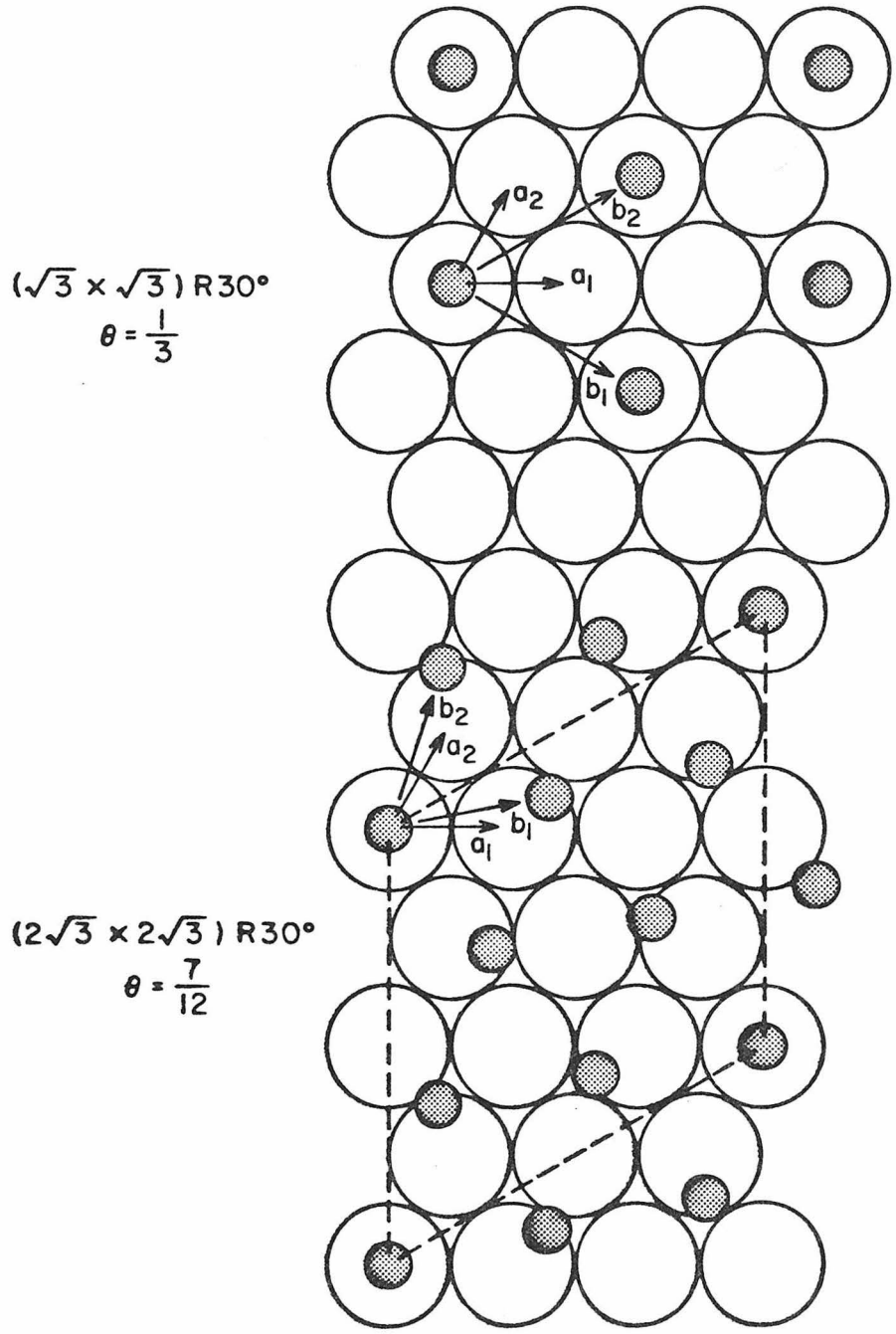
$(\sqrt{3} \times \sqrt{3})R30°$
$\theta = \frac{1}{3}$
a_2
b_2
a_1
b_1
$(2\sqrt{3} \times 2\sqrt{3})R30°$
$\theta = \frac{7}{12}$
b_2
a_2
b_1
a_1

Fig. 3

Chapter IV

High Resolution Electron Energy Loss Spectroscopy of Carbon Monoxide and Oxygen on the Ru(001) Surface

ABSTRACT

The adsorption of CO and O_2 on the Ru(001) surface and the interaction between CO and chemisorbed oxygen on this surface have been studied by measuring the vibrational energies of the adsorbed layer with electron energy loss spectroscopy. Adsorbed CO shows two vibrational energies which are assigned to the metal-carbon and carbon-oxygen stretching frequencies of an upright CO with a single metal-carbon bond. Oxygen adsorbed on Ru(001) has a single vibrational energy which can be attributed to a mode of atomic oxygen perpendicular to the surface. The variation of the frequency spectrum of CO with CO coverage and with the coverage of oxygen in coadsorption experiments is discussed in terms of direct interadsorbate interactions and indirect through-bond interactions. A simple force-constant model for the CO-CO interaction is proposed.

1. INTRODUCTION

The chemisorption of CO and O_2 and the oxidation of CO has been studied on a variety of single crystal surfaces (1-3). In this work we have applied the technique of electron energy loss spectroscopy (EELS) to study the vibrational structure of this model chemisorption system on Ru(001).

The vibrational energies of adsorbed molecules provide perhaps the most direct information about adsorbate chemistry in those cases in which the energies can be used to calculate the force constants of the individual bonds. Correlations between force constants and bond order and between bond order and reactivity have been essential in homogeneous chemistry for the prediction of reaction pathways. There is some hope that this endeavor can be extended to well characterized heterogeneous systems using EELS or infrared reflectance spectroscopy to measure the vibrational frequencies of the adsorbed layer. Determining the force constants from the vibrational frequencies in the heterogeneous system is, however, more difficult in two respects. Vibrations of which the normal coordinate is parallel to the surface are usually not observed, so that the number of frequencies measured is insufficient to determine uniquely the force constants of an assumed geometry. In addition, the closely spaced chemisorbed molecules may interact with one another, requiring the consideration of additional forces in the proper calculation of the intramolecular force constants. Both of these issues will be addressed in this work.

The vibrational measurements of CO and O_2 adsorbed on the Ru(001) surface can serve to characterize the importance of interadsorbate

interactions on the vibrational frequencies and to compare this effect with a through-bond or chemical effect. The carbon-oxygen stretching frequency, ν_1, of adsorbed CO has been found to shift upward with CO coverage on a variety of surfaces. On Ni(111) (4), Pd(111) (5) and Pt(111) (6-8), there are two carbon-oxygen stretching frequencies which are usually attributed to CO in bridged ($1800\ cm^{-1} \lesssim \omega_{CO} \lesssim 2000\ cm^{-1}$) and linear ($\omega_{CO} \gtrsim 2000\ cm^{-1}$) sites, although this interpretation is not appropriate in the case of CO adsorbed on Ru(001) (9). The most intense vibrational band at low coverage is due to bridged CO on Pd(111) and Ni(111) and to linear CO on Pt(111). On Ni(111) and Pd(111), the frequency, ν_1, increases by 100 cm^{-1} as a function of increasing CO coverage (4,5). On Pt(111), the primary ν_1 band increases by 37 cm^{-1} with CO coverage, from 2063 cm^{-1} to 2100 cm^{-1} (8).

The observation of an increasing carbon-oxygen stretching frequency with coverage appears to be quite general. In addition to occurring on a variety of metals for different CO hybridizations, it has been observed by infrared transmission spectroscopy on dispersed catalysts (10), and we have also observed a similar effect for the N-O stretching vibration of NO adsorbed molecularly on Ru(001) (11). To understand this frequency shift is crucial for the interpretation of vibrational spectra. This shift may be ascribed to dipole-dipole interactions between adsorbed CO molecules (8,10), to local site effects (5), and to through-bond or chemical interactions. The dipole-dipole interaction has been shown recently to be inadequate to explain the total frequency shift (12). However, as will be shown in this work, additional direct interadsorbate interactions of a chemical nature can be proposed, which can cause a frequency shift of

the correct magnitude. The force constants calculated for adsorbed CO at high coverage will depend on which of these interpretations is selected.

The chemisorption of CO and O_2 on Ru(001) can serve as a model system to illustrate the importance of through-bond and direct interadsorbate interactions in interpreting vibrational spectra in adsorbed layers. In Sec. 2, the experimental methods of this work will be described. The experimental results are presented in Sec. 3, followed by a discussion of their implications in Sec. 4. A brief synopsis is presented in Sec. 5.

2. EXPERIMENTAL

The electron energy loss spectra were obtained with an electron spectrometer which has hemispherical energy-dispersing elements (13). The monochromator delivers a beam with an energy of approximately 4 eV to the surface at 62^{o} from the normal. The rotatable energy analyzer was positioned in the specular direction for these measurements. The analyzer accepts electrons reflected from the surface in a cone of half-angle, 2.7^{o}. The energy resolution (full width at half maximum of the elastic peak) obtained in these measurements was in the range of 11 to 15 meV (1 meV = 8.066 cm^{-1}), although a resolution of 9 meV has been obtained in this scattering system. This complete experimental system will be described in detail elsewhere (14).

Two Ru(001) samples were prepared from a randomly oriented single crystal from Materials Research Corp. The crystal was oriented to within $\pm 0.5^{o}$ with a back-reflection Laue camera, and cut with a rotating wire saw. The rough crystal slices were mounted on a polishing goniometer (15) and reoriented on each face before using standard mechanical polishing techniques. The samples were treated for 30 seconds in boiling aqua-regia

before mounting on Varian precision manipulators equipped with liquid nitrogen cooling. The Ru(001) surfaces were then placed in separate ultra-high vacuum systems (base pressure $\lesssim 5 \times 10^{-11}$ torr).

One system was equipped with LEED optics, a single-pass cylindrical mirror energy analyzer for Auger electron spectroscopy, and a quadrupole mass spectrometer. The other sample was placed in the electron scattering system, also equipped with a quadrupole mass spectrometer.

The Ru crystal was cleaned chemically as suggested by previous authors (16). The crystal was heated repeatedly to 1370 K in 5×10^{-8} torr O_2, followed by several minutes of annealing in vacuum at 1570 K. Repeated oxidation and annealing cycles were found to eliminate an Auger peak at 92 eV which was attributed to a Si impurity in the original material. The final Auger spectrum was identical to that reported previously for clean Ru (17), and the clean surface exhibited a sharp (1x1) LEED pattern. This cleaning procedure was also followed in the electron scattering system, and the clean surface was evidenced by a featureless vibrational energy loss spectrum.

Exposures are reported using uncorrected ion gauge readings. The crystal temperature was monitored using a W-5%Re/W-26%Re thermocouple. CO exposures were made after cooling the crystal to 110 K; oxygen exposures were made between 120 K and 130 K when a disordered oxygen layer was desired (1). Vibrational energy loss measurements could then be obtained from the surface at $\sim$ 100 K. The liquid nitrogen reservoir of the manipulator was connected to the sample mounting blocks with copper straps to provide a high-conduction cooling path. With this arrangement, the experimental temperature could be attained within ten minutes after a heating cycle above 700 K.

3. RESULTS

A. CO on Clean Ru(001)

Representative vibrational energy loss spectra for low and high coverages of CO are shown in Fig. 1. The loss spectrum for a 0.2L (1L ≡ 1 Langmuir ≡ 10^{-6} torr-sec) exposure of CO shows peaks at 1980 cm^{-1} (245 meV) and 445 cm^{-1} (55 meV). These modes are labeled ν_1 and ν_2, respectively. A 5L exposure of CO at 110 K produces an essentially saturated surface. The frequency, ν_1, of the saturated CO layer is approximately 100 cm^{-1} higher than at low coverages. The softer mode, ν_2, is unchanged within ±1 meV.

In addition, the overtones and combination frequency are clearly visible. The overtones occur at approximately $2\nu_1$ and $2\nu_2$, the harmonic frequencies. The peak intensities are of the right order of magnitude for a two-step scattering mechanism (18,19), in which case the harmonic values are expected.

The frequency, ν_1, is shown as a function of exposure in Fig. 2. The corresponding coverages were determined by normalizing the peak areas of thermal desorption spectra to a coverage of 1×10^{15} cm^{-2}. This saturation coverage was determined by interpreting the compression LEED structure as a simple CO superlattice (9,20). Because of the variable pumping by the liquid nitrogen cooling system, these coverage determinations are accurate to only ±20%.

The ν_1 peak, which is shown to shift smoothly from low coverage to saturation, is symmetric and of constant width at all coverages (±2 meV, in agreement with the variation in elastic peak width). There is nothing

in the electron energy loss data to suggest that CO is bound in more than one kind of "site" at any coverage.

B. O_2 on Clean Ru(001)

Previous work has shown that at 100 K O_2 is adsorbed in a disordered form, whereas at room temperature it forms an ordered (2x2) pattern which may result from a true (2x2) structure or from three degenerate domains of a (2x1) structure (1). Accordingly, vibrational spectra were recorded for the disordered surface after adsorption at 110 K and again after an annealing cycle at 340 K.

The vibrational spectra of the disordered and ordered surfaces were essentially the same. Typical spectra obtained for adsorbed oxygen after ordering are shown in Fig. 3. A single vibrational frequency, ν_0, is observed which varies from 516 cm^{-1} (64 meV) at low coverage to 596 cm^{-1} (74 meV) at saturation. Since oxygen is dissociatively adsorbed on this surface, this vibration must be due to a metal-oxygen stretching mode. Before ordering, the peak position was found within 16 cm^{-1} (2 meV) of the position after ordering, and the intensity of the loss peak relative to the elastic peak remained the same (±10%). The effect of ordering was clearly visible, however, in an increase in the absolute intensity of both the elastic peak and the loss peak. This is because the specularly reflected beam is more sharply defined in angle.

C. Coadsorption of CO and O_2

Coadsorption studies were carried out first by preparing an ordered overlayer of oxygen at 340 K and, subsequently, cooling the surface to 110 K

before adsorbing CO. Spectra obtained in this way are shown in Fig. 4 for low and high exposures of CO to surfaces prepared with either low-coverage or saturated overlayers of oxygen. Measurements carried out with intermediate exposures of both CO and oxygen provided results intermediate to those presented here.

The three peaks observed for the individual spectra can be identified in Fig. 4, although the ν_0 mode of adsorbed oxygen is obscured by the ν_2 vibration of CO for the 0.4L exposures of O_2. The frequency, ν_0, after a 5L exposure of O_2 [Fig. 4 (a) and (b)] is clearly visible at 589 cm^{-1}, just where it would appear on the clean surface. The metal-oxygen vibration is unaffected by the subsequent adsorption of CO. In the case of the pre-exposure of 0.4L O_2 [Fig. 4 (c) and (d)] the low-frequency peak can be described as the sum of an unshifted ν_0 peak at $\sim$520 cm^{-1} and a ν_2 vibration of CO at $\sim$430 cm^{-1}. These values are obtained by assuming that for high coverages of CO the low-frequency peak is dominated by the ν_2 vibration of CO, and that the ν_0 vibration of oxygen is unchanged from the clean surface value. This was found to be the case for all spectra in which the oxygen vibration was resolved fully.

The preadsorption of O_2 has a strong effect on the vibrational energies of adsorbed CO. The surface oxygen shifts ν_1 to a higher frequency and ν_2 to a lower frequency relative to the clean surface. In these measurements, this appears to be a uniform shift; it is not possible to separate CO which is affected by oxygen from CO which is not.

If the CO coverage is varied on a surface with a given coverage of oxygen, the frequency, ν_1, shifts upward as for CO adsorbed on the clean surface. Again, within the experimental resolution, ν_2 is constant.

The preadsorption of O_2 also changes the binding energy of CO on the Ru(001) surface. Thermal desorption spectra obtained for the same conditions as the vibrational spectra given in Fig. 4 are shown in Fig. 5. A heating rate of approximately 25 K sec^{-1} was employed. Carbon monoxide which desorbs from the surface prepared with 0.4L exposure to O_2 is essentially the same as for desorption from the clean surface (16), with desorption maxima at 382 K and 470 K. If the surface is treated with 5L O_2 the second state disappears, and the maximum is shifted to 375 K.

4. DISCUSSION

A. CO Adsorption

The interpretation of the vibrational modes, ν_1 and ν_2, (Fig. 1) is quite straightforward by reference to the vibrational energies of the corresponding metal carbonyl complex, $Ru_3(CO)_{12}$ (21). As shown in Fig. 6 (a), this molecule consists of a triangle of Ru atoms with an interatomic distance of 2.88Å, six radial carbonyls in the plane of the ring and six axial carbonyls perpendicular to the ring. It belongs to the D_{3h} point group. The frequencies observed for the four general types of vibrational modes of the carbonyl groups of $Ru_3(CO)_{12}$ [Fig. 6(b)] are listed in Table 1. By comparison it is clear that the ν_1 and ν_2 vibrations of adsorbed CO represent the carbon-oxygen and the metal-carbon stretching modes, respectively, of CO bound to the metal surface as shown in Fig. 6(b). Measurements of electron-stimulated desorption ion angular distributions (ESDIAD) support the conclusion that CO is bound perpendicularly to the Ru(001) surface (22). The ν_1 vibration is in the range generally found for CO bound to a single metal atom in metal carbonyl complexes, as it is in

$Ru_3(CO)_{12}$. If this force constant is used in a bond energy bond order (BEBO) correlation, a carbon-oxygen bond energy of 250 kcal/mole is obtained as opposed to 256 kcal/mole in the gas phase, suggesting that the CO molecule is only slightly perturbed upon chemisorption.

It is quite common in vibrational studies of CO chemisorption to carry the analogy to the metal carbonyl spectra somewhat further and to determine the adsorption site of CO from the ν_1 frequency. However, a study of the LEED patterns at 100 K has shown that CO is not adsorbed in an on-top site on Ru(001) at high coverages, and, in fact, that it must be found in a variety of low symmetry sites (9). In keeping with this observation, CO adsorption on Ru(001) will be discussed in terms of a model which is not sensitive to the registry of CO with respect to the substrate. That is, CO may be thought to be adsorbed on a uniform substrate with a single carbon-metal bond. This structure has the two stretching modes and two sets of degenerate bending modes indicated in Fig. 6(b).

The modes ν_3 and ν_4, are not observed in the electron energy loss spectra. The explanation of this requires a discussion of the so-called "dipole normal selection rule." In a simple dipole scattering theory, the transition probability for a vibrational excitation is proportional to the square of the component of the dynamic effective charge tensor normal to the surface multiplied by the normal coordinate of the vibration (23). That is, taking the z-axis as the surface normal,

$$W \propto \sum_{\kappa,\alpha} e^*_{z\alpha}(\kappa)\xi_\alpha(\kappa) \qquad (1)$$

where W is the transition probability, and $e^*_{z\alpha}$ is the derivative of the z-component of the dipole moment with respect to the displacement of the

atom, κ, in the α direction. The α-component of the normal coordinate is $\xi_\alpha(\kappa)$. If the dynamic effective charge tensor is diagonal, then only vibrations for which the normal coordinate of the vibration has a z-component will appear in the electron energy loss spectra.

The intensity predicted by Eq. (1) can be expected to obtain only when the electron scatters from the long-range part of the electric field created by the surface vibration. Recent work suggests that for scattering out of the specular direction the electron may interact with the short-range part of the potential, perhaps through a temporary negative ion state (24,25). The results of scattering in the specular direction, however, suggest that for such measurements the "selection rule" given in Eq. (1) is operative.

The LEED patterns of CO on Ru(001) at low temperature indicate that CO is found in a hexagonal lattice on the substrate (9). The assumption of a six-fold axis of symmetry perpendicular to the surface requires that the tensor, $e^*_{\beta\alpha}$, be diagonal (23). Hence, from Eq. (1), it is required that for a vibration to be detected in the electron energy loss spectrum the eigenvector of the vibration must have a component perpendicular to the surface. Therefore, it is not surprising that in the case of CO adsorbed perpendicularly to the Ru(001) surface,the modes, ν_3 and ν_4 [Fig. 6(b)], are not observed. In the absence of such a symmetry requirement, however, vibrational modes which are strictly parallel to the surface might still be dipole-active. The normal coordinates of the vibration do not define, by themselves, the conditions of dipole-activity.

Of special interest in the study of the vibrations of adsorbed CO is the large shift in ν_1 with coverage (Fig. 2). As discussed above, the dipole-dipole interaction in the adsorbed layer is not sufficient to explain this shift.

Another possible view of the shift in ν_1 is that the chemisorptive bond of CO is modified as the coverage is increased. As the chemisorption becomes weaker, the carbon-oxygen stretching frequency shifts toward the gas-phase value [allowing for the mechanical effect of adsorption on this frequency (26)]. This is not a satisfactory explanation in the case of CO on Ru(001), since the metal-carbon stretching frequency, ν_2, is constant with coverage. Earlier work, as well, suggests that the chemisorptive bond of CO on Ru(001) is essentially uniform over the full range of coverage and that the change with coverage in the heat of desorption results purely from direct interadsorbate interactions (16). The shift in the ν_1 vibration must also be due to interadsorbate interactions. We shall develop a simple model to illustrate the consequences of such a conclusion.

The frequencies, ν_1 and ν_2, are calculated easily assuming a force constant model for the CO overlayer. In keeping with the LEED results, we assume a hexagonal lattice of CO molecules and allow a single nearest neighbor interaction between the oxygen of one CO and the carbon of the neighbors [Fig. 6(c)]. The assumption of a central force between nearest neighbors is quite arbitrary and is intended only to model a direct chemical interaction; it is not to be taken literally as resulting from a chemical bond between nearest neighbor carbon and oxygen atoms. Only vibrations perpendicular to the surface are of interest in interpreting the energy-loss data. The relevant force constants are [employing the notation of

Maradudin et al. (27)]

$$k_1 = - \Phi_{zz}(\vec{\ell}\,0;\vec{\ell}\,C)$$

$$k_2 = - \Phi_{zz}(\vec{\ell}\,C;\vec{\ell}\,Ru) \qquad (2)$$

$$k_3 = - \Phi_{zz}(\vec{\ell}\,0;\vec{\ell}\pm\vec{a}\,C)$$

where

$$\Phi_{\alpha\beta}(\vec{\ell}\,\kappa;\vec{\ell}\,'\kappa') = \frac{\partial\Phi}{\partial u_\alpha(\ell\kappa)\partial u_\beta(\ell'\kappa')} \qquad (3)$$

Here Φ is the potential, and $\Phi_{\alpha\beta}$ is the derivative of the total potential with respect to the displacements, $u_\alpha(\vec{\ell}\,\kappa)$. The subscript, α, identifies the Cartesian component, and the quantity, $(\vec{\ell}\,\kappa)$, labels the atom, κ, in the unit cell, $\vec{\ell}$. The vector $\vec{a}$ is a primitive lattice vector of the CO lattice. The secular equation is:

$$\omega^4 - \omega^2\left(\frac{k_1+6k_3}{m_o} + \frac{k_1+k_2+6k_3}{m_c}\right) - \frac{(k_1+k_3\xi)^2-(k_1+6k_3)(k_1+k_2+6k_3)}{m_o m_c} = 0 \qquad (4)$$

where m_c and m_o are the masses of carbon and oxygen, respectively. The energy of the vibration is $\hbar\omega$. The quantity, ξ, is defined by

$$\xi \equiv \sum_j e^{i\vec{q}_{||}\cdot\vec{a}_j} \qquad (5)$$

where $\vec{q}_{||}$ is the wavevector of the surface vibration, and the sum is over nearest neighbor sites. The vibrational energies measured by inelastic electron scattering in the specular direction are associated with $\vec{q}_{||} = 0$ modes, the vibrations in which the CO molecules are moving in phase (23). For these modes, $\xi = 6$.

The coverage dependence of the frequency shift is contained in the dependence of the total potential on the nearest neighbor spacing, a, and therefore appears in the model through k_3. Clearly, a potential can be chosen which will fit any function, $\nu_1(\theta)$ where θ is the coverage of CO. Rather than pursuing the detailed nature of the potential, we will evaluate Eq. (4) in the limits of low and high coverage for $\vec{q}_{||} = 0$ to determine the force constants, k_1, k_2 and k_3. The predictions of this model for other wavevectors can then be examined.

The constants, k_1 and k_2, were calculated from the low-coverage limit ($k_3 = 0$) of Eq. (4). These constants are given in Table 2(a). The constant, k_2, is found to be about 25% greater than the corresponding constant in the $Ru_3(CO)_{12}$ complex, which is due in part to our assumption that the metal surface is rigid. This supports our conclusion that the Ru-C bond has a bond order of one. The shift in the frequency, ν_1, of 100 cm^{-1} from the low coverage to saturation is fit properly if $k_3 = 2.65 \times 10^4$ dyne-cm^{-1}. The vibrational energies calculated from this model are given in Fig. 7 for $\vec{q}_{||}$ along the Γ-K direction in the Surface Brillouin Zone. Since the force giving rise to k_3 interacts only between the carbon and oxygen atoms of neighboring CO molecules [Fig. 6(c)], it has no effect on the ν_2 vibration for $\vec{q}_{||} = 0$, in agreement with the experimental data. The value chosen for k_3 is reasonable for a very weak chemical interaction.

Of special interest in this picture is the prediction of dispersion. Although the electron energy loss measurements in the specular direction are limited to the $\vec{q}_{||} = 0$ modes, there is the possibility that a short-

range interaction between the electron and the adsorbed molecule could excite all phonon modes (25). In this case, the wavevector of the electron need no longer be conserved within $\vec{q}_{||}$, and a substantial broadening and shifting of the vibrational peak, particularly ν_2, should be observed.

The dispersion predicted for the ν_1 vibration corresponds closely to the splitting of the ν_1 vibration of the axial CO ligands of $Ru_3(CO)_{12}$. In the case of the metal carbonyls, the in-phase vibrations, which can be compared to the $\vec{q}_{||} = 0$ surface wave, are those belonging to the A representations. The axial CO groups are parallel and only 2.88Å apart and can be expected to interact as the parallel CO molecules on the surface. That this is the case can be seen in the similar "dispersion" in the $Ru_3(CO)_{12}$ complex. The three-fold symmetric vibrations, A_1' and A_2'', appear at 2127 cm^{-1} and 2062 cm^{-1}, to be compared with the 2080 cm^{-1} stretching frequency for the $\vec{q}_{||} = 0$ vibration of CO on Ru(001) at saturation. The E" and E' modes, which are not symmetric with respect to the C_3 axis, show a ν_1 frequency of 2034 cm^{-1} and 2028 cm^{-1}, respectively, to be compared with 2014 cm^{-1} for the zone-edge vibration calculated above. The radial CO ligands of this complex are more widely spaced than the axial groups and are not parallel. Since they interact less strongly, these modes are not split so much as the ν_1 modes of the axial ligands. The ν_1 modes of the radial groups range from 1989 cm^{-1} to 2011 cm^{-1}, which can be compared with the $k_3 = 0$ limit of the ν_1 vibration of chemisorbed CO, which is 1980 cm^{-1}.

Another prediction of this model is very strong dispersion of the ν_2 vibration, which shifts from 445 cm^{-1} at the zone center to 692 cm^{-1} at

the zone edge. The modes between 350 cm^{-1} and 650 cm^{-1} of $Ru_3(CO)_{12}$ have not been assigned definitively and may include high energy Ru-C stretching modes, although it is suggested that the ν_2 modes are found primarily below 500 cm^{-1}.

The analogy between $Ru_3(CO)_{12}$ and chemisorbed CO provides convincing evidence that the shift in ν_1 with coverage is due to direct CO-CO interactions. Differences between the two systems are obvious. The CO-CO spacing in $Ru_3(CO)_{12}$ is 2.88Å as opposed to 3.33Å for the CO superlattice at saturation on Ru(001) (9). In the metal carbonyl, the axial CO groups have only two nearest neighbors as opposed to six on the Ru(001) surface. These effects may cancel to some extent.

It is not expected that this model will explain completely the vibrational behavior of CO on the surface. In particular, additional forces may have to be considered to fit the behavior of ν_2 at large wavevectors. Nevertheless, this model illustrates that the addition of a weak chemical interaction between nearest neighbors can explain the coverage-dependence of the vibrational spectrum of adsorbed CO. The close parallel with the modes of $Ru_3(CO)_{12}$ shows that such an interaction exists.

B. Oxygen Adsorption

The interpretation of the energy loss feature, ν_0, of adsorbed oxygen is less conclusive than in the case of CO. According to the "selection rule" of Eq. (1), we can assume that the single frequency in the range of 576 cm^{-1} to 596 cm^{-1} is due to the vibrational mode of atomic oxygen normal to the surface.

The vibrational spectra of multinuclear oxy-complexes have been studied in some detail (28-30), but the general lack of a metal-metal bond in the complexes studied means that the bond angles for atomic oxygen in the bridged and three-fold positions are substantially different than for the metal surface. Since these frequencies cannot be compared directly it is possible only to eliminate the on-top site, for which a Ru=O stretching frequency of 800 cm^{-1} to 950 cm^{-1} would be expected (28).

Atomic oxygen has been found from dynamic LEED calculations to reside in three-fold sites on Ni(111) (31). The low vibrational frequency observed for oxygen on Ru(001) is consistent with a highly coordinated site with the oxygen close to the surface. In this case, the mode perpendicular to the surface is expected to have a significant bending character and to appear at a lower frequency than the perpendicular stretch of an on-top oxygen (32).

Although oxygen exhibits complex order-disorder phenomena on this surface (1), the vibrational spectrum is quite simple. Our results indicate that the oxygen occupies the same, or very similar, sites at all coverages on the ordered and the disordered surfaces. The shift in frequency with coverage is conceivably due to direct interactions as it is for CO. However, since oxygen is chemisorbed quite strongly on Ru(001) ($E_d \simeq 80$ kcal/mole)(1), strong chemical effects can be expected also through the substrate (33). The data do not allow a separation of these effects as they do for adsorbed CO.

C. CO and Oxygen Coadsorption

The influence of preadsorbed oxygen on CO chemisorption can be seen most clearly in Table 2, where the CO force constants, k_1 and k_2 are given for several pretreatments of oxygen. In the cases for which the ν_2 vibration of adsorbed CO could not be separated from the ν_0 vibration of the surface oxygen, the constants were calculated assuming that ν_2 does not shift with CO coverage. Adsorbed oxygen causes CO to be bound less tightly to the surface, giving rise to a lower k_2 and a higher k_1 than for CO on the clean surface. Since k_1 and k_2 change in sympathy, it appears that the frequency shift is due to a modification of the electronic properties of the substrate introduced by the oxygen. A similar phenomenon is observed as a substituent effect in metal carbonyl complexes (34). The addition of an electronegative ligand reduces the ability of the metal to donate electrons into the $2\pi^*$ orbital of the CO ligands, thereby increasing k_1.

This effect is seen also in the thermal desorption spectra of Fig. 5. Redhead's expression can be used to estimate the desorption energies (E_d) of these spectra assuming a pre-exponential factor of 10^{13} sec^{-1} (35). The higher temperature desorption peak of CO from the clean surface and from the surfaces prepared with 0.4L O_2 corresponds to an E_d of 28 kcal/mole. The CO that is adsorbed on the saturated oxygen overlayer desorbs in a single state at a lower temperature which corresponds to E_d = 22 kcal/mole.

The direct CO-CO interaction which is so important on the clean surface remains significant in the presence of oxygen. The ν_1 frequency of CO increases with CO coverage on all of the surfaces examined.

5. CONCLUSIONS

The study of CO and oxygen adsorption on the Ru(001) surface has proved to be very fruitful in illustrating the importance of interadsorbate and through-bond interactions on the vibrational frequencies of adsorbed overlayers. The existence of a direct CO-CO interaction was demonstrated by showing that the force constant assumed for the interaction is of a reasonable magnitude in view of the known CO-CO interaction in the $Ru_3(CO)_{12}$ complex. The effect of surface oxygen on CO chemisorption is to change both the CO force constants. Chemisorbed oxygen causes CO to bond less strongly to the Ru(001) surface and provides an example of a through-bond interaction.

The vibrational spectra show CO to be upright on the surface with a single carbon-metal bond at all coverages, although LEED work indicates that CO cannot be placed exclusively in on-top sites at high coverage. The atomically bound oxygen exhibits a soft vibration characteristic of a bridged or three-fold site.

Vibrational spectroscopy will continue to provide uniquely useful information in the study of chemisorbed overlayers. In some cases, particularly at high coverages, a careful consideration of the relevant force constants may be necessary to exploit this technique fully.

ACKNOWLEDGMENT

The support of this research by the National Science Foundation (Grant No. CHE77-16314) is gratefully acknowledged.

References

1. T. E. Madey, H. A. Engelhardt and D. Menzel, Surface Sci. 48, 304 (1975).

2. G. Ertl and M. Neumann, Z. Phys. Chem. NF 90, 127 (1974).

3. P. A. Zhdan, G. K. Boreskov, W. F. Egelhoff, Jr. and W. H. Weinberg, Surface Sci. 61, 377 (1976).

4. J. C. Bertolini, G. Dalmai-Imelik and J. Rousseau, Surface Sci. 68, 539 (1977).

5. A. M. Bradshaw and F. M. Hoffmann, Surface Sci. 72, 573 (1978).

6. H. Froitzheim, H. Hopster, H. Ibach and S. Lehwald, Appl. Phys. 13, 147 (1977).

7. H. J. Krebs and H. Lüth, Appl. Phys. 14, 337 (1977).

8. A. Crossley and D. A. King, Surface Sci. 68, 528 (1977).

9. G. E. Thomas and W. H. Weinberg, Phys. Rev. Letters (submitted).

10. R. M. Hammaker, S. A. Francis and R. P. Eischens, Spectro Chimica Acta 21, 1295 (1965).

11. G. E. Thomas, P. A. Thiel, J. T. Yates, Jr. and W. H. Weinberg, to be published.

12. G. D. Mahan and A. A. Lucas, J. Chem. Phys. 68, 1344 (1978).

13. C. E. Kuyatt and J. A. Simpson, Rev. Sci. Instrum. 38, 103 (1967).

14. G. E. Thomas and W. H. Weinberg, to be published.

15. J. F. Wendelken, S. P. Withrow and C. A. Foster, Rev. Sci. Instrum. 9, 1215 (1977).

16. T. E. Madey and D. Menzel, Japan. J. Appl. Phys., Suppl. 2, Pt. 2, 229 (1974).

17. D. W. Goodman, T. E. Madey, M. Ono and J. T. Yates, Jr., J. Catal. 50, 279 (1977).

18. E. Evans and D. L. Mills, Phys. Rev. B7, 853 (1973).

19. A. Lucas and M. Sunjic, Phys. Rev. Letters 26, 229 (1971).

20. E. D. Williams and W. H. Weinberg, to be published.

21. C. O. Quicksall and T. G. Spiro, Inorg. Chem. 7, 2365 (1968).

22. T. E. Madey, Surface Sci. (submitted, 1978).

23. E. Evans and D. L. Mills, Phys. Rev. B5, 4126 (1972).

24. J. W. Davenport, W. Ho and J. R. Schrieffer, Phys. Rev. B17, 3115 (1978).

25. W. Ho, R. F. Willis and E. W. Plummer, Phys. Rev. Letters 40, 1463 (1978).

26. If the force constant of the carbon-oxygen bond were unchanged from the gas phase value the frequency, ν_1, would increase by $\sim$60 cm^{-1} upon adsorption, assuming $k_2 = 3 \times 10^5$ dyne-cm^{-1}.

27. A. A. Maradudin, E. W. Montroll, G. H. Weiss and I. P. Ipatova, Theory of Lattice Dynamics in the Harmonic Approximation, Academic Press, N.Y., 1971.

28. W. P. Griffith, J. Chem. Soc. (A) 211 (1969).

29. W. P. Griffith and T. D. Wickins, J. Chem. Soc. (A) 400 (1968).

30. W. P. Griffith, J. Chem. Soc. (A) 2270 (1969).

31. P. M. Marcus, J. E. Demuth and D. W. Jepsen, Surface Sci. 53, 501 (1975).

32. H. Froitzheim, H. Ibach and S. Lehwald, Phys. Rev. B14, 1369 (1976).

33. T. L. Einstein and J. R. Schrieffer, Phys. Rev. B7, 3629 (1973); T. B. Grimley and M. Torrini, J. Phys. C6, 868 (1973).

34. T. L. Brown and D. J. Darensbourg, Inorg. Chem. 6, 971 (1967).

35. P. A. Redhead, Vacuum 12, 203 (1962).

Table 1. Frequencies of CO Vibrations in $Ru_3(CO)_{12}$ in cm^{-1} from Ref. 21.

ν_1 - axial	2028(E´) - 2127(A_1')	
ν_1 - radial	1989(A_2') - 2011(A_1')	
ν_2	350 - 500	Approximate
ν_3	500 - 650	Assignment
ν_4	<200	

Table 2. Force Constants Calculated for CO Adsorbed on Ru(001) as a Function of Pre-exposure to Oxygen.

	ε_{O_2}, L	ν_1, cm^{-1}	ν_2, cm^{-1}	k_1, dyne/cm x 10^{-6}	k_2, dyne/cm x 10^{-6}
(a)	0	1980	445	1.46	0.35
(b)	0.4	2000	∿430	1.51	0.32
(c)	1.0	2032	∿420	1.57	0.31
(d)	5.0	2048	387	1.61	0.26

FIGURE CAPTIONS

Fig. 1. Electron energy loss spectra for two coverages of CO on the Ru(001) surface. The loss features are the carbon-oxygen stretching frequency, ν_1, the ruthenuim-carbon stretching frequency, ν_2, and their overtones and combination frequency.

Fig. 2. Carbon-oxygen stretching frequency, ν_1, as a function of CO exposure. O-obtained for separate exposures. Δ-obtained from measurements in a constant background of CO.

Fig. 3. Electron energy loss spectra for several coverages of oxygen on Ru(001). Intensities are normalized to the elastic peak height.

Fig. 4. Electron energy loss spectra of CO adsorbed at 110 K on a surface pre-exposed to O_2 at 340 K. Intensities are normalized to the elastic peak height.

Fig. 5. Thermal desorption spectra of CO obtained under the same conditions as the energy loss spectra of Fig. 4.

Fig. 6. (a) Structure of $Ru_3(CO)_{12}$ (21).
(b) Vibrational modes of a linear CO adsorbed on a flat surface.
(c) Force constant model used to calculate the frequencies given in Fig. 7.

Fig. 7. The vibrational frequencies, ν_1 and ν_2, of adsorbed CO predicted by the force constant model (see text). The frequencies are given for surface wavevectors along the Γ-K direction, which is defined in the diagram of the irreducible 1/12 th of the two-dimensional Surface Brillouin Zone.

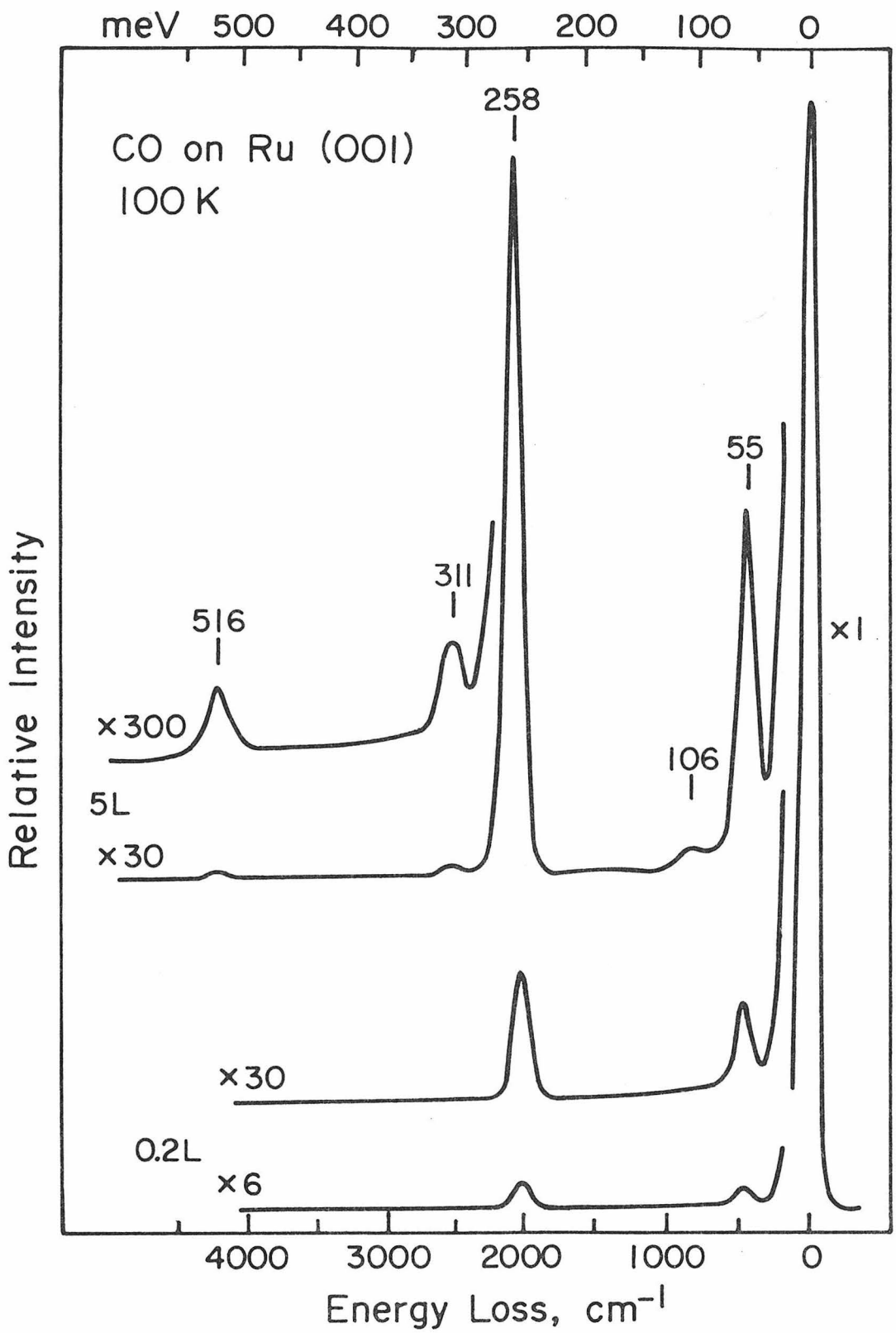
meV 500 400 300 200 100 0
CO on Ru (001)
100 K
258
55
311
516
106
×300
5L
×30
×1
×30
0.2L
×6
Relative Intensity
4000 3000 2000 1000 0
Energy Loss, cm⁻¹

Fig. 1

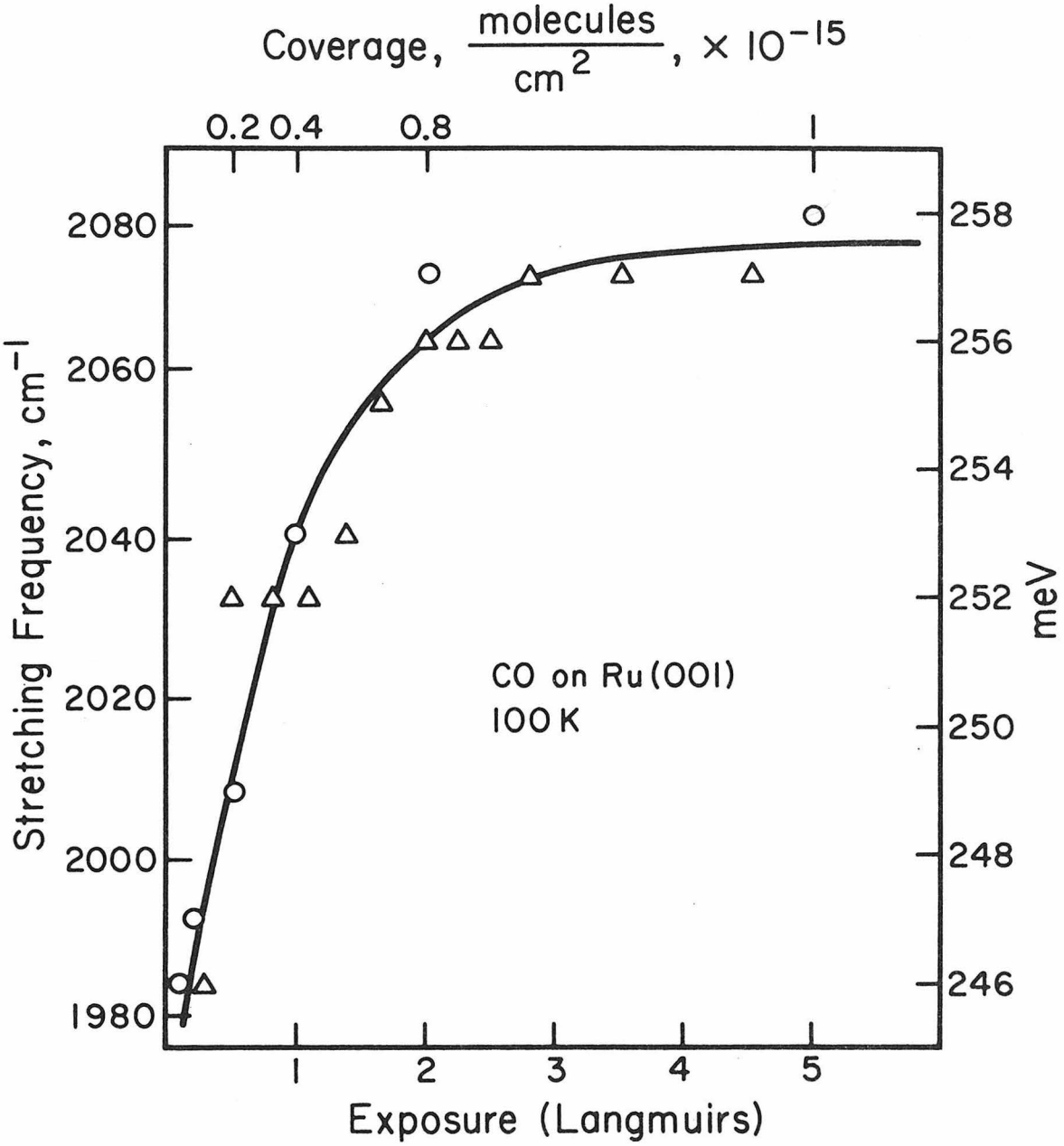
Coverage, molecules/cm², × 10⁻¹⁵
0.2
0.4
0.8
1
Stretching Frequency, cm⁻¹
2080
2060
2040
2020
2000
1980
meV
258
256
254
252
250
248
246
CO on Ru(001)
100 K
1
2
3
4
5
Exposure (Langmuirs)

Fig. 2

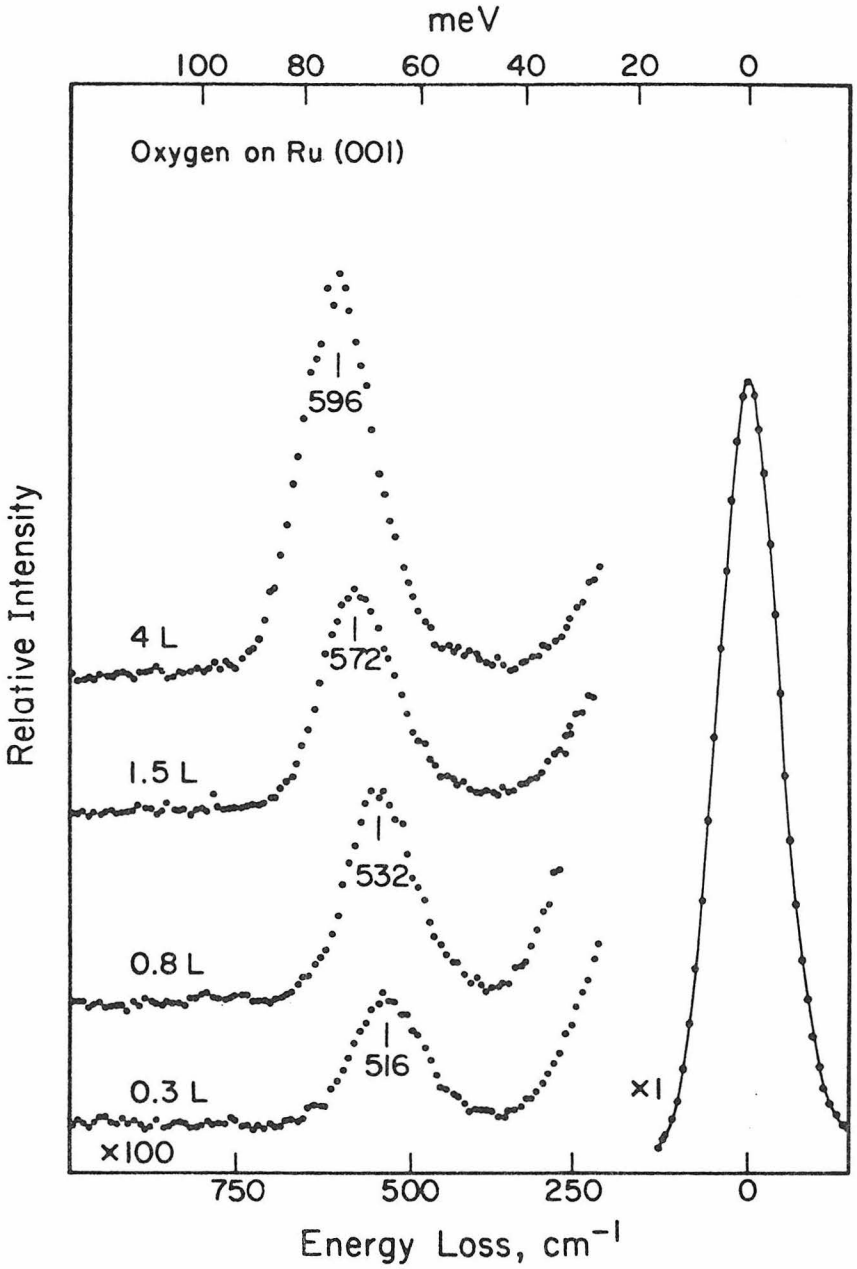
meV
100
80
60
40
20
0
Oxygen on Ru (001)
596
572
532
516
4 L
1.5 L
0.8 L
0.3 L
×100
×1
Relative Intensity
750
500
250
0
Energy Loss, cm⁻¹

Fig. 3

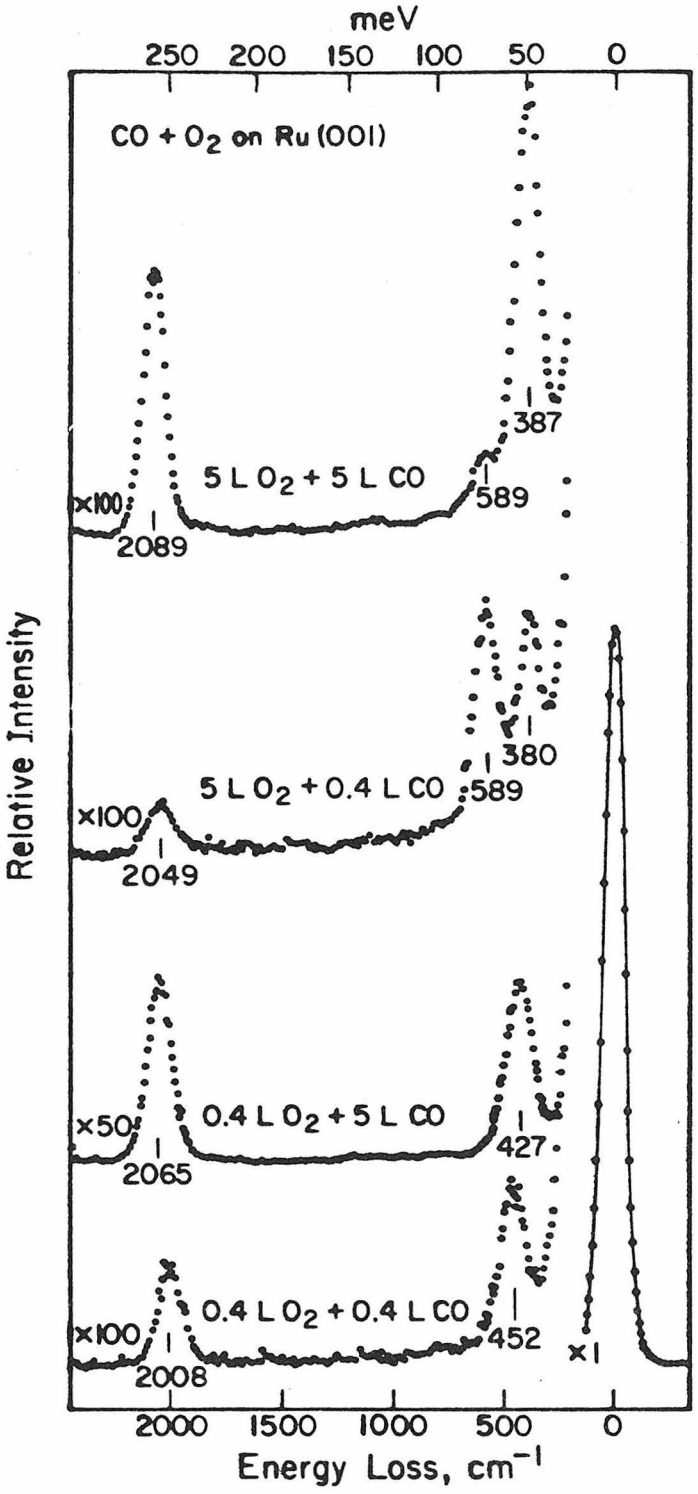
meV
250 200 150 100 50 0
CO + O2 on Ru(001)
5 L O2 + 5 L CO
×100
2089
387
589
5 L O2 + 0.4 L CO
×100
2049
380
589
0.4 L O2 + 5 L CO
×50
2065
427
0.4 L O2 + 0.4 L CO
×100
2008
452
×1
Relative Intensity
2000 1500 1000 500 0
Energy Loss, cm-1

Fig. 4

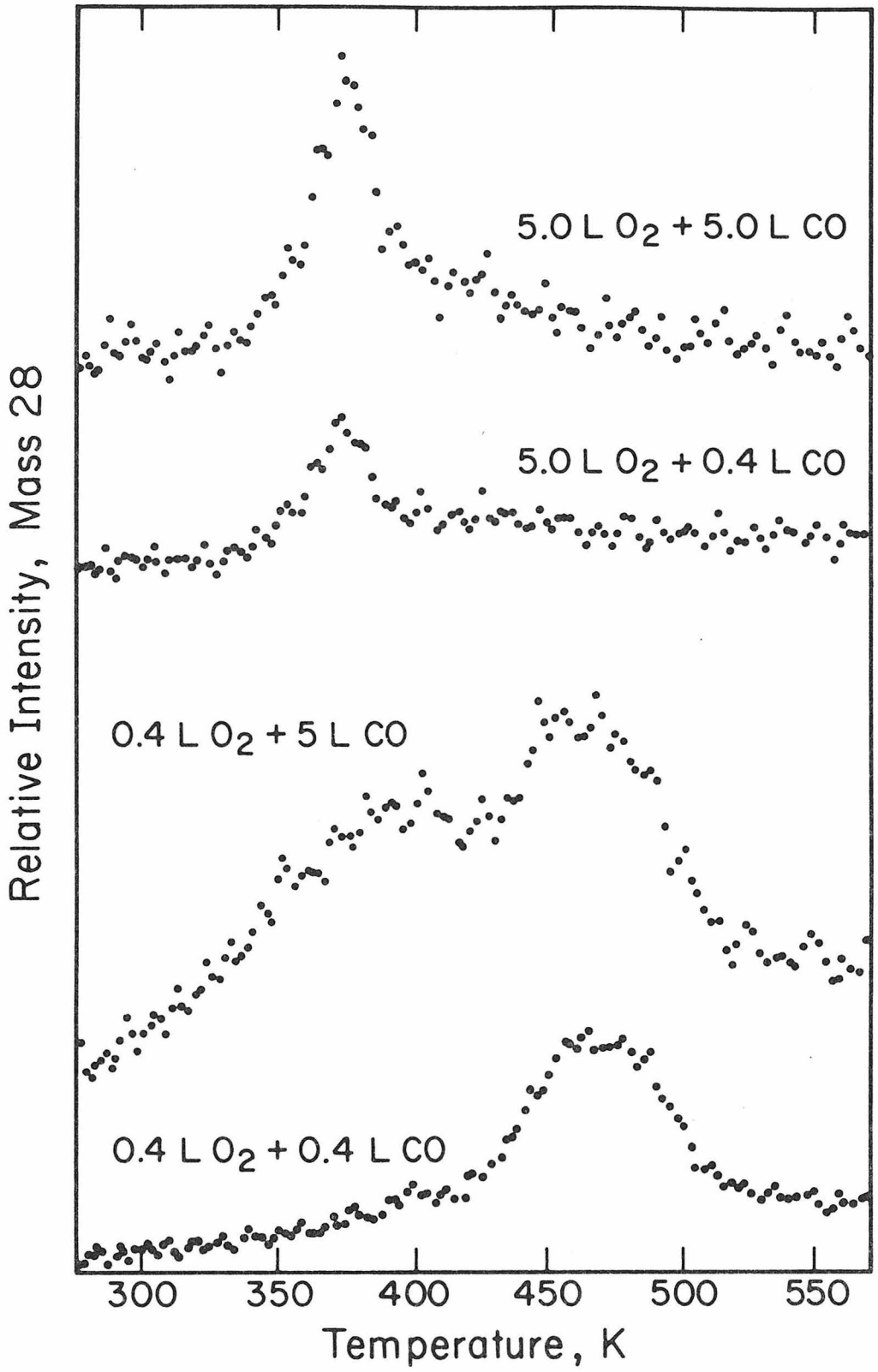
5.0 L O2 + 5.0 L CO
5.0 L O2 + 0.4 L CO
0.4 L O2 + 5 L CO
0.4 L O2 + 0.4 L CO
Relative Intensity, Mass 28
300
350
400
450
500
550
Temperature, K

Fig. 5

(a)

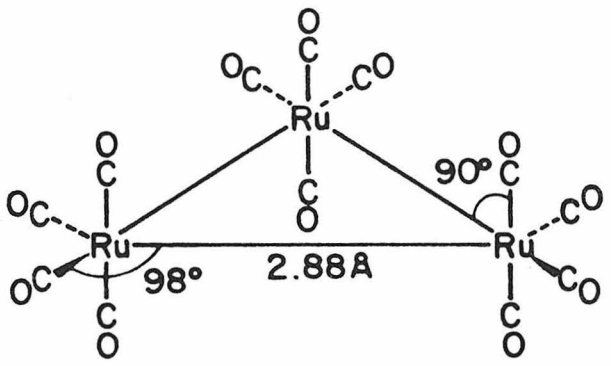

(b)

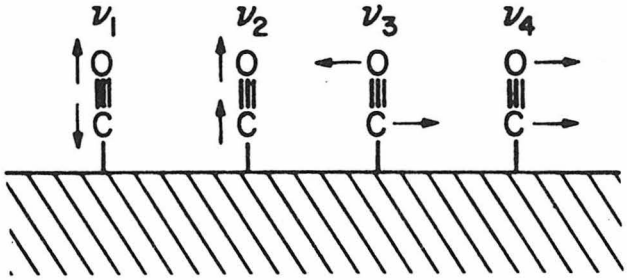

(c)

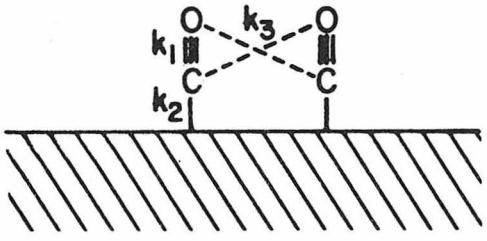

Fig. 6

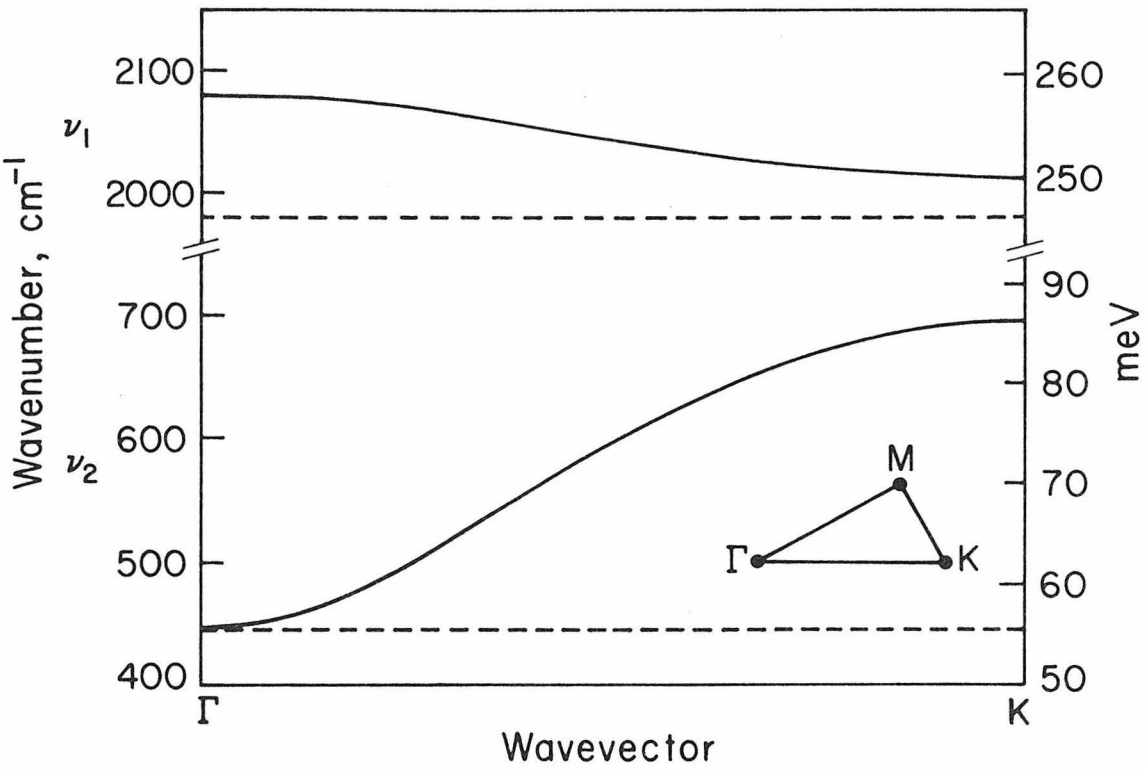
2100
2000
700
600
500
400
ν_1
ν_2
Wavenumber, cm^{-1}
260
250
90
80
70
60
50
meV
M
Γ
K
Γ
K
Wavevector

Fig. 7

Chapter V

High Resolution Electron Scattering from Chemisorbed Oxygen on the Ru(001) Surface

Abstract

Inelastic electron scattering spectroscopy has been used to measure energy-gain as well as energy-loss transitions of oxygen chemisorbed on the Ru(001) surface. The relative intensity of the energy-gain to the energy-loss transition was found to follow the expected Boltzmann distribution. The intensities of the inelastic peaks relative to the elastic peak were observed to increase with temperature. The temperature dependence and sources of experimental error are explained within the context of an approximate theory for the scattering of electrons from adsorbates on metal surfaces.

Electron energy loss spectroscopy is becoming increasingly popular as a probe of surface vibrations of adsorbed layers on metal surfaces. At temperatures for which $k_B T \gtrsim h\omega_o$, where ω_o is the oscillator frequency, slow electrons also may be used to observe the emission of vibrational energy from adsorbed layers. Similar observations for surface phonons in bulk metal oxides were first made by Ibach (1) and recently by Dalmai-Imelik et al. (2).

In this work, we present measurements of emission intensities from oxygen chemisorbed on the Ru(001) surface over a wide temperature range, and the first observations of energy-gain scattering from a chemisorbed layer. The intensity measurements are sensitive to the scattering angle and surface condition. To explain these effects and the observed temperature dependence, the results are interpreted in terms of a dipolar scattering theory (3,4,5).

The electron energy distribution curves were obtained with a scattering system of the Kuyatt-Simpson type (6) contained in an ultra-high vacuum system of which the base pressure is 4×10^{-11} torr. An electron beam with a kinetic energy of 4 eV was incident on the crystal at an angle of 62^o with respect to the surface normal. The scattered beam was detected by a rotatable analyzer which was positioned approximately ($< \pm 1^o$) in the direction of the specularly reflected beam, and which accepted electrons in a cone subtending a half-angle (θ_c) of 2.2^o from that direction. The specularly-reflected beam has a full angular width at half maximum of approximately 2^o, as measured by rotating the analyzer.

The Ru sample was cut and polished within 1^o of the (001) plane using standard techniques (7). It was spot welded to Ta support wires and

mounted on a Varian precision manipulator which had been modified to allow for resistive heating. The temperature of the crystal was monitored with a W-5%Re/W-26%Re thermocouple spot welded to its side. The crystal temperature was controlled using a programmable current source for resistive heating. A variable voltage reference was compared to the thermocouple voltage to provide the temperature control (8). Since the current required to heat the crystal is on the order of 20 amps, and a coaxial wiring arrangement is not practical, unacceptably high magnetic fields prohibit the simultaneous operation of the temperature controller and the electron spectrometer. Hence, the temperature controller was placed under the control of the computer (PDP 11/10) also used to control the spectrometer. The heater could be disabled momentarily under program control to permit operation of the energy analyzer and then re-enabled to allow the crystal temperature to recover. At the highest temperatures employed here (1000 K), it was necessary to heat two seconds for each second of data acquisition, and the sample cooled about 30 K during the one second of spectrometer operation. Better temperature control could be obtained at higher switching rates although this was not necessary in the results reported here.

Energy distribution curves have been obtained for saturation coverages of oxygen in the range 100 K to 1000 K (9). In this work, the Ru surface was exposed to 10 Langmuirs (1L $\equiv 10^{-6}$ torr-sec) of oxygen at 300 K and then heated to 1200 K. The resulting surface exhibited a single stretching frequency of 69 meV (range 67.5 to 70.5 meV), presumably due to a stretching mode of atomically bound oxygen. This variation in peak position is slightly more than the usual experimental scatter ($< \pm$ 1 meV)

and is due to the changing coverage of oxygen resulting from its diffusion into the bulk (10). The metal-oxygen stretching frequency varies from 64 meV at low coverage to 74 meV at saturation (9). The error in frequency is not significant to these results, and coverage effects are eliminated when the peak ratios are taken. The fact that only one stretching frequency was observed for oxygen on the Ru(001) surface (possibly due to the "dipole-normal selection rule") (3).means that the atomic position of oxygen cannot be deduced from the energy loss measurements in the specular direction. Since oxygen resides in three-fold coordinated sites on the (111) surface of Ni (11), this may also obtain on the Ru(001) surface. Dynamic low-energy electron diffraction calculations in our laboratory will decide this question unequivocally.

Representative spectra obtained at two temperatures are shown in Fig. 1. Between measurements at different temperatures, the oxygen-covered surface was heated to above 1000 K to remove all adsorbed gases except oxygen. The vibrational energy gain peak was clearly observable at temperatures above 400 K. The areas of the inelastic peaks were obtained after subtracting the background intensity due to their proximity to the elastic peak. The intensity of the inelastic features relative to the intensity of the elastic peak is approximately 2% of that obtained on bulk metal oxides (1,2). This is expected due to the much larger relative inelastic cross section calculated for scattering from the surface phonon of an ionic material (1,3,5). The logarithm of the ratio of the inelastic intensities is plotted in Fig. 2 as a function of reciprocal temperature. The data are in good agreement with the theoretical line with a slope of 0.069 eV divided by the Boltzmann constant (k_B) and with an intercept of

zero.

The cross section for inelastic electron scattering from surface vibrations in the forward direction has been calculated both semi-classically (4) and quantum mechanically in the Born approximation (3). If temperature effects are considered, both calculations predict a cross section of the form

$$\frac{d\sigma}{d\Omega} = \frac{2C}{M\hbar\omega v^2}(n+\gamma)\left(\frac{d\mu}{dz}\right)^2 \frac{(\theta\cos\alpha\cos\phi - \theta_o\sin\alpha)^2 + \theta^2\sin^2\phi}{(\theta^2+\theta_o^2)^2\cos\alpha} \qquad (1)$$

in the approximation, $\theta \ll 1$ and $\theta_o \ll 1$.

Here θ and ϕ are polar and azimuthal angles in a spherical coordinate system in which the specular direction lies along the z-axis. M is the reduced mass of the oscillator, which together with its image has a dynamic dipole moment, $\frac{d\mu}{dz}$, perpendicular to the surface and a frequency, ω. The electron is incident on the surface at the angle, α, from the surface normal with velocity, v. n is the occupation number at the temperature of interest, given by the Planck distribution, $\left[\exp(\frac{\hbar\omega}{k_B T})-1\right]^{-1}$, and γ is one for energy loss and zero for energy gain. θ_o is $\pm\frac{\hbar\omega}{mv^2}$, where m is the mass of the electron; θ_o is positive for energy gain and negative for energy loss. The understood dependence on dipole density and surface reflectivity is included in the constant C, which is equal to $e^2 n_o |R|^2$, where e is the electronic charge, n_o is the surface unit cell density and $|R|^2$ is the surface reflectivity. The simplifications leading to Eq. (1) do not allow for interadsorbate interactions (12), or scattering of the electron from the short-range part of the molecular potential (13), but it is probably a reasonable form to use to examine the effects of temperature and angle on

scattering near the specular direction.

The denominator of Eq. (1) is a strong function of θ, but it is independent of the sign of θ_o and therefore has the same value for energy gain or energy loss. We see at once that the ratio of the energy gain intensity (I_{+1}) to the energy loss intensity (I_{-1}) is relatively insensitive to small errors in alignment. This is not true of the ratio of the inelastic to elastic peak intensities $\left(\frac{I_{+1}}{I_o}\right)$. Since the inelastically scattered electrons are spread more in angle than the elastically scattered electrons, the ratio I_{+1}/I_o will increase as the analyzer is moved out of the specular direction. If the acceptance cone of the electron analyzer is assumed to be centered on the specular direction, Eq. (1) can be compared directly with the experiment by integrating over ϕ from 0 to 2π and over θ from 0 to the experimental cutoff angle θ_c [2.2^o in this work] (3,4). The result is

$$\sigma = \frac{\pi C\left(\frac{d\mu}{dz}\right)^2}{M\hbar\omega_o v^2} \cos\alpha \left[\frac{(\tan^2\alpha - 2)\theta_c^2}{\theta_c^2 + \theta_o^2} + (\tan^2\alpha + 2)\ln\left(1 + \frac{\theta_c^2}{\theta_o^2}\right)\right](n + \gamma). \quad (2)$$

This expression does not depend on the sign of θ_o, so the ratio, I_{+1}/I_{-1}, is predicted to be

$$\frac{I_{+1}}{I_{-1}} = \frac{n}{n+1} = e^{-\hbar\omega/k_B T} \quad (3)$$

in agreement with the experimental results shown in Fig. 2. If the energy analyzer is not positioned exactly in the specular direction this ratio will, in addition, depend weakly on scattering angle. It would appear that movement of the Ru crystal on its support wires due to heating effects

can explain the scatter in the data shown in Fig. 2.

Eq. (1) also predicts that the ratios I_{+1}/I_o and I_{-1}/I_o will depend on temperature, and that they will be much more sensitive to alignment errors than the ratio I_{+1}/I_{-1}. Certainly, the data support qualitatively the conclusion that the inelastic intensity increases with temperature. However, the more severe alignment requirements for the accurate measurement of $\frac{I_{\pm 1}}{I_o}$ prohibit a quantitative comparison. An additional, more fundamental, source of error in measuring the ratios, $I_{\pm 1}/I_o$, at elevated temperatures is that the oxygen surface coverage may change. There is recent evidence that surface oxygen on Rh(111) and Ru(001) may diffuse into the bulk far below the desorption temperature (10,14).

In conclusion, vibrational scattering spectra have been measured for chemisorbed oxygen on Ru(001) over a wide range of surface temperature. The peak intensities are in agreement with the expected distribution functions. The sources of error in these intensity measurements have been outlined in terms of the recent theories of electron scattering from vibrations in adsorbed layers (3,4).

References

1. H. Ibach, Festokörperprobleme 11, 135 (1971).
2. G. Dalmai-Imelik, J. C. Bertolini and J. Rousseau, Surface Sci. 63, 67 (1977).
3. E. Evans and D. L. Mills, Phys. Rev. B5, 4126 (1972).
4. D. M. Newns, Phys. Letters 60A, 461 (1977).
5. H. Froitzheim, Electron Spectroscopy for Surface Analysis, H. Ibach, Ed., Springer-Verlag, Berlin, 1977, p. 205.
6. C. E. Kuyatt and J. A. Simpson, Rev. Sci. Instrum. 38, 103 (1967).
7. C. M. Comrie and W. H. Weinberg, J. Chem. Phys. 64, 250 (1976).
8. G. E. Thomas and W. H. Weinberg (to be published).
9. G. E. Thomas and W. H. Weinberg (to be published).
10. E. Williams, private communication, March 1978.
11. P. M. Marcus, J. E. Demuth and D. W. Jepsen, Surface Sci. 53, 501 (1975).
12. A. Crossley and D. A. King, Surface Sci. 68, 528 (1977).
13. J. W. Davenport, W. Ho and J. R. Schrieffer, Phys. Rev. B17, 3115 (1978).
14. P. Thiel, J. T. Yates, Jr. and W. H. Weinberg (to be published).

Figure Captions

Fig. 1. Electron energy distribution curves obtained at 545 K and 1000 K normalized to the elastic peak height.

Fig. 2. The logarithm of ratio of the energy gain to energy loss peak areas as a function of reciprocal temperature. The solid line is the theoretical dependence.

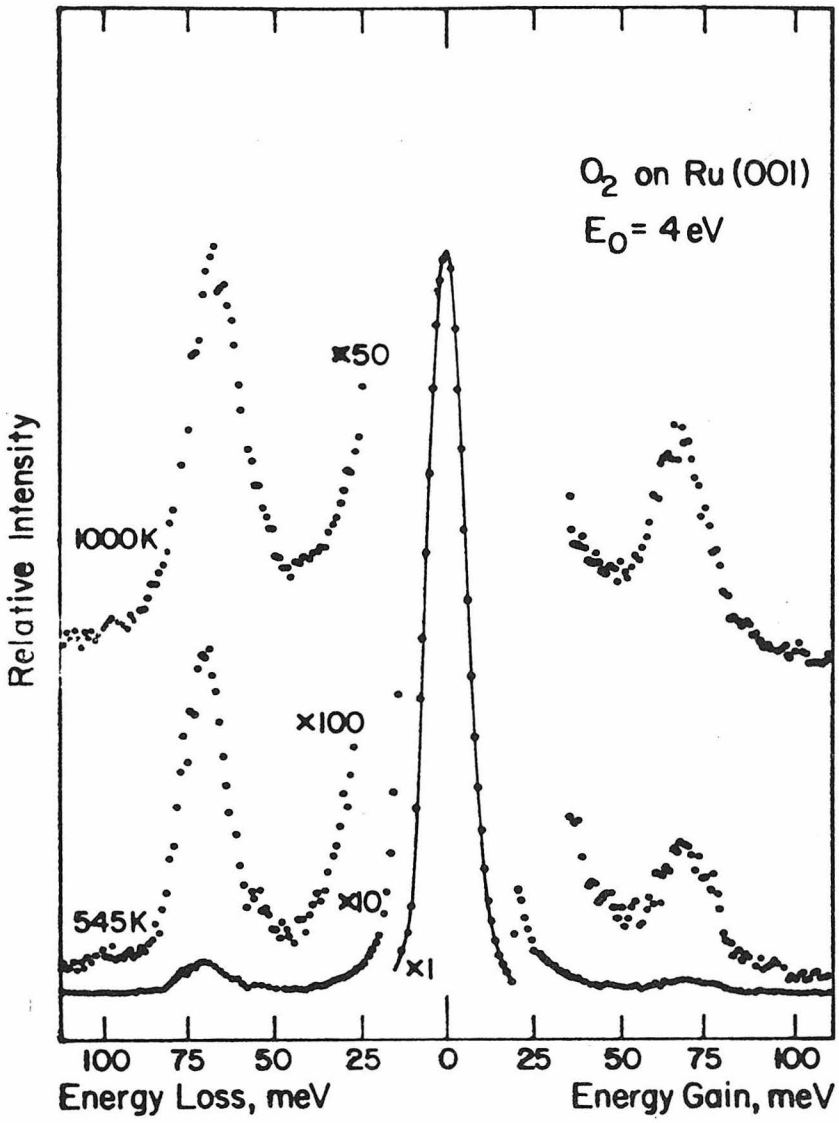
O_2 on Ru(001)
E_0 = 4 eV
Relative Intensity
1000K
545K
×50
×100
×10
×1
100 75 50 25 0 25 50 75 100
Energy Loss, meV
Energy Gain, meV

Fig. 1

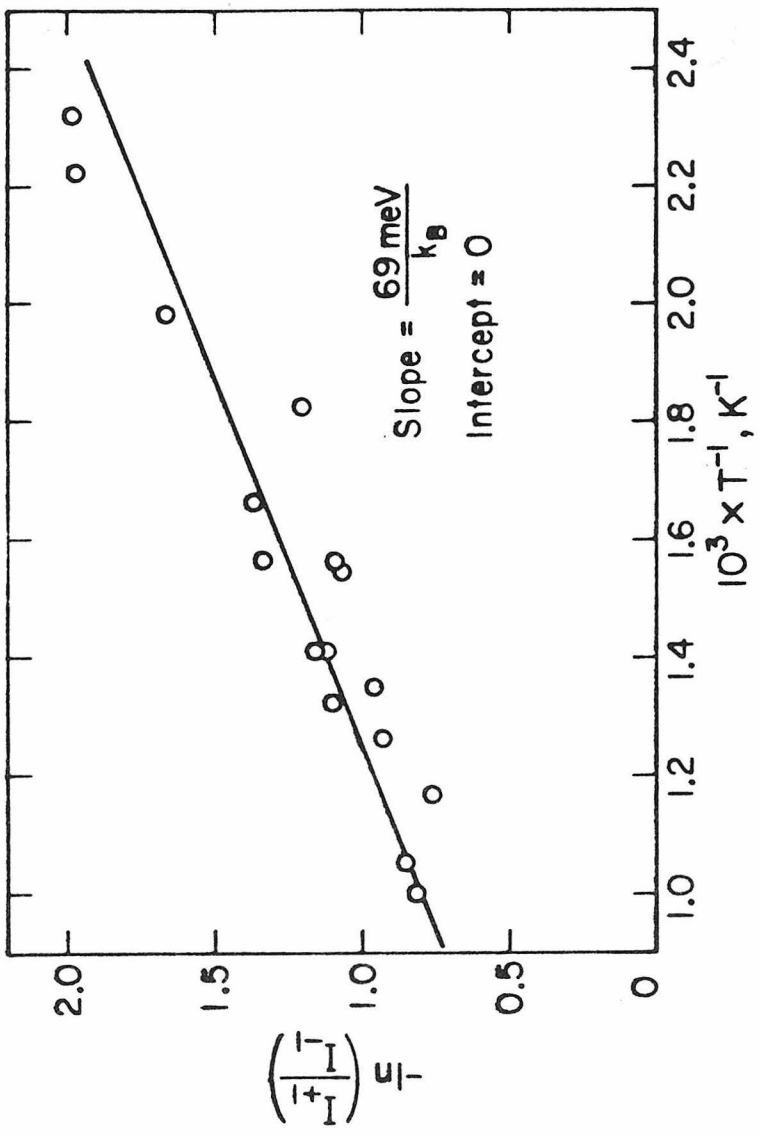
Slope = 69 meV / k_B
Intercept = 0
$10^3 \times T^{-1}$, K^{-1}
$-\ln\left(\frac{I_{+1}}{I_{-1}}\right)$
0
0.5
1.0
1.5
2.0
1.0
1.2
1.4
1.6
1.8
2.0
2.2
2.4

Fig. 2

Chapter VI

The Adsorption and Dissociation of Nitric Oxide on the Ru(001) Surface

ABSTRACT

The adsorption of nitric oxide and its dissociation on the Ru(001) surface have been studied through the vibrational energies of the adsorbed layer. The inelastic electron scattering measurements show that two distinct states of molecular NO are adsorbed at 130 K. For coverages less than one-third of saturation, a single nitrogen-oxygen stretching frequency is found which is attributed to a triply coordinated or bridge bonded NO. At higher coverages, an additional frequency appears which is characteristic of a linear NO. Both forms are thought to be perpendicular to the surface. The dissociation of bridged NO is complete at 316 K, whereas the linear form remains on the surface until 500 K. This is explained by a difference in activation energies for dissociation of NO and by the blocking of sites by nitrogen and oxygen adatoms.

The adsorption and reaction of NO on metal surfaces is a subject of obvious interest in surface chemistry. In addition to the industrial importance of the catalytic reduction of NO, the wide variety of NO complexes in metal-nitrosyls suggests that the surface chemistry of NO will be a fertile area of research (1). In this work, we report the first vibrational measurements of NO on the Ru(001) surface and direct evidence of two forms of adsorbed NO with differing activation energies for dissociation.

Previous studies have been made of NO chemisorbed on the Ru(101) and Ru(100) surfaces as well as on a Ru field emission tip (2 - 6). The photoemission measurements of NO adsorbed on the Ru(100) surface by Bonzel and Fischer were carried out well above room temperature and indicated molecular adsorption only at the highest coverages (2). Reed et al. present chemical evidence that NO is primarily adsorbed associatively on Ru(101) at 300 K and suggest that the dissociation reaction may be sensitive to the surface crystallography (4). Madey has reported measurements of the angular distribution of the ion beams desorbed by electron bombardment (ESDIAD) of NO adsorbed on the Ru(001) surface at 90 K (7). The results indicate that NO is bound molecularly to the surface.

The inelastic electron scattering measurements presented here show the molecular adsorption and dissociation of NO on the basal plane of Ru as a function of surface temperature. The electron spectrometer employed in the electron energy loss spectra has been described in detail elsewhere (8). The Ru sample was cut and polished within 1^{o} of the (001) direction using standard techniques. It was mounted on a manipulator equipped with liquid nitrogen cooling and cleaned with oxidation and

reduction cycles in situ (9). The cleaning procedure has been found to yield both a sharp (1x1) LEED pattern and the characteristic Auger spectrum of a clean surface (10). Depending on the history of the sample, prolonged annealing above 1600 K was occasionally necessary to remove the surface oxygen, as measured by the vibrational energy loss feature at 530 cm^{-1}. The crystal was exposed to NO through a gas doser, and the coverages were established relative to saturation using the integrated peaks of thermal desorption spectra (12).

The intensity of the elastically scattered electron beam varied by a factor of ten depending on the NO exposure and treatment, indicating that order-disorder phenomena were affecting the angular spread of the specular beam. In order to assure a good signal/noise ratio throughout, the electron spectrometer was tuned so that 2 x 10^6cps appeared in the elastic channel of the beam reflected specularly from the clean surface. The full-width at half-maximum of the elastic peak was approximately 18 meV during these measurements to attain this counting rate. The primary energy of the electron beam was 4 eV. Due to the large variation in the elastic intensity in the spectra presented here, the intensities relative to the elastic intensity cannot be compared directly from spectrum to spectrum. The role of ordering phenomena in the inelastic scattering intensity has been discussed by Ibach (13).

The vibrational spectra of chemisorbed NO are shown as a function of coverage in Fig. 1. The temperature of exposure was between 120 K and 150 K. Two nitrogen-oxygen stretching frequencies are observed, in the ranges 1411 - 1508 cm^{-1} and 1806 - 1831 cm^{-1}, where both frequencies

increase with increasing surface coverage. The higher frequency, which is characteristic of a linear NO in metal nitrosyls, appears only at fractional coverages above 0.35. In addition, a very weak feature at approximately 1145 cm^{-1} appeared in some spectra and disappeared within a few minutes even below 140 K. This peak may be due to other oxides of nitrogen present in the NO supply or to a temporary complex formed in adsorption. It could not be characterized further in these measurements. A third vibrational loss between 532 cm^{-1} and 548 cm^{-1} is found at higher coverages. This is in the range of the vibrational mode of atomic oxygen on the Ru(001) surface studied previously (14) and shows that some dissociation of NO occurs at 130 K. The Ru-NO vibration of a variety of metal nitrosyls has been found to vary between 572 cm^{-1} and 638 cm^{-1} depending on the other substituents of the complex (15). Neither this mode nor a Ru-N stretching mode of dissociated NO could be resolved from the single low frequency peak which is attributed to the metal-oxygen vibration. This is presumably due to a small dynamic effective charge associated with these vibrational modes.

The chemistry of metal nitrosyls has been reviewed by Eisenberg and Meyer (16). In general, a nitrogen-oxygen stretching frequency (ν_{NO}) above 1800 cm^{-1} is associated with a linear NO. Frequencies in the range between 1620 cm^{-1} and 1750 cm^{-1} are due to bent nitrosyls with M-N-O bond angles between 124^{o} and 177^{o}. This correlation is not exact, since electronic effects due to other ligands are quite important in the N-O bond of metal-nitrosyls (17). However, the ν_{NO} peak which appears at 1831 cm^{-1} at high coverages is interpreted most reasonably as a linear NO bound to the surface through the nitrogen atom.

The first adsorption state on this surface exhibits a stretching frequency too low to be due either to a linear or to a bent nitrosyl complex. Bridging nitrosyls, however, exhibit lower stretching frequencies. The nitrosyls in $Ru_3(CO)_{10}(NO)_2$ are bonded to two Ru atoms and have stretching frequencies of 1517 cm^{-1} and 1500 cm^{-1} (17); in the compound, $(C_5H_5)_3Co_3(NO)_2$, the nitrosyls are both bonded to the three cobalt atoms, and the most intense N-O stretching band appears at 1405 cm^{-1} (18). The lower frequency vibration, indicated in Fig. 1, then, is due to a more highly coordinated nitrosyl. The Ru(001) surface is three-fold symmetric, and the analogy with the μ_3-nitrosyl tricobalt structure suggests that the first adsorption state of NO at 130 K is in a three-fold site. The increase in both N-O stretching frequencies with coverage may result from direct interactions or from changes in the chemisorptive bond. The same phenomenon is seen frequently in the CO stretching frequency as a function of CO coverage and has been the subject of recent discussion (19). The analogy with the metal nitrosyl complexes suggests that NO is perpendicular to the surface in both states.

In order to illustrate the steps involved in the dissociation of NO, a series of experiments was performed in which the surface prepared with molecularly adsorbed NO was heated briefly at approximately 5^{o}/sec and allowed to cool. The maximum temperature was maintained for approximately one second. The surface cooled below 140 K during the recording of the vibrational spectrum, so that only irreversible changes in the adsorbed layer could be observed. The vibrational spectrum is shown as a function of temperature treatment in Fig. 2 and Fig. 3 for surfaces prepared with NO coverages of 0.35 and 0.8, respectively.

In Fig. 2(b) and (c), spectra are shown which illustrate the irreversible change in the adsorbed layer as the surface is heated to room temperature. The low frequency N-O stretching mode disappears well before complete dissociation occurs, although the appearance of the peak at 538 cm^{-1} indicates that some dissociation has taken place. After this surface is heated to 407 K, dissociation is complete. The intermediate state of the surface [Fig. 2(c)] is characterized by a single N-O stretching frequency at approximately 1782 cm^{-1} and a low frequency mode at 538 cm^{-1}, depending upon coverage.

One explanation for the change in the vibrational spectrum is that the bridged NO begins to dissociate near room temperature, and that the N and O atoms displace the remaining NO from the three-fold or bridged sites. The linear form of NO is less reactive and does not dissociate until higher temperature. The metal-oxygen stretching frequency is consistent with its occupying a three-fold or bridge site (14).

The mechanism of site blocking also explains results obtained for an NO coverage of 0.8 (Fig. 3). Here, the disappearance of the more highly coordinated NO is nearly complete only at 406 K, after complete dissociation would have occurred for an NO coverage of 0.35; and the linear NO is not removed until 500 K. The final transformation of the saturated surface is accompanied by the rapid evolution of NO and the beginning of N_2 desorption. The dissociation of the linear NO is prevented at high coverage by the lack of sites for the reaction products. The transformations observed in these experiments are most likely limited kinetically in the brief heating cycles. The temperatures of reaction and corresponding vibrational spectra given here characterize the activation energies for dissociation qualitatively.

Thus, a relatively simple scheme is proposed in which the two forms of NO adsorbed on the Ru(001) surface have different activation energies for dissociation. The dissociative reaction is poisoned by the reaction products below their temperature of desorption.

We thank Patricia Thiel and Dr. John Yates for their assistance and helpful suggestions in this work. We have benefited also from useful discussions with Professors John Bercaw and Robert Grubbs.

References

1. R. L. Klimisch and J. G. Larson, Eds., Catalytic Chemistry of Nitrogen Oxides, Plenum Press, New York, 1975.
2. H. P. Bonzel and T. E. Fischer, Surface Sci. 51, 213 (1975).
3. R. Ku, N. A. Gjostein and H. P. Bonzel, Surface Sci. 64, 465 (1977).
4. P. D. Reed, C. M. Comrie and R. M. Lambert, Surface Sci. 72, 423 (1978).
5. T. W. Orient and R. S. Hansen, Surface Sci. 67, 325 (1977).
6. R. Klein and A. Shih, Surface Sci. 69, 403 (1977).
7. T. E. Madey, Surface Sci. (submitted).
8. G. E. Thomas and W. H. Weinberg, Rev. Sci. Instrum.(submitted).
9. T. E. Madey and D. Menzel, Japan. J. Appl. Phys., Suppl. 2, Pt. 2, 229 (1974).
10. E. D. Williams and W. H. Weinberg, Surface Sci. (submitted).
11. G. E. Thomas and W. H. Weinberg, J. Chem. Phys. (submitted).
12. P. A. Thiel, G. E. Thomas, W. H. Weinberg and J. T. Yates, Jr., in preparation.
13. H. Ibach, Surface Sci. 66, 56 (1977).
14. G. E. Thomas and W. H. Weinberg, J. Chem. Phys., October 15, 1978.
15. E. E. Mercer, W. A. McAllister and J. R. Durig, Inorg. Chem. 5, 1881 (1966).
16. R. Eisenberg and C. D. Meyer, Accounts Chem. Res. 8, 26 (1975).
17. K. Nakamoto, Infrared and Raman Spectra of Inorganic and Coordination Compounds, 3rd ed., John Wiley, New York, 1978.
18. J. Müller and S. Schmitt, J. Organometal. Chem. 97, C54 (1975).
19. G. D. Mahan and A. A. Lucas, J. Chem. Phys. 68, 1344 (1978).

Figure Captions

Fig. 1. Vibrational spectrum of NO adsorbed on the Ru(001) surface below 150 K as a function of coverage. The coverages relative to saturation are (a) 0.12, (b) 0.35, (c) 0.55, (d) 0.67 and (e) 0.82.

Fig. 2. Effect of heating the surface with an NO coverage of 0.35. (a) After exposure at 147 K. (b) After heating to 290 K. (c) After heating to 316 K. (c) After heating to 407 K.

Fib. 3. Effect of heating the surface with an NO coverage of 0.8. (a) After exposure at 158 K. (b) After heating to 406 K. (c) After heating to 500 K.

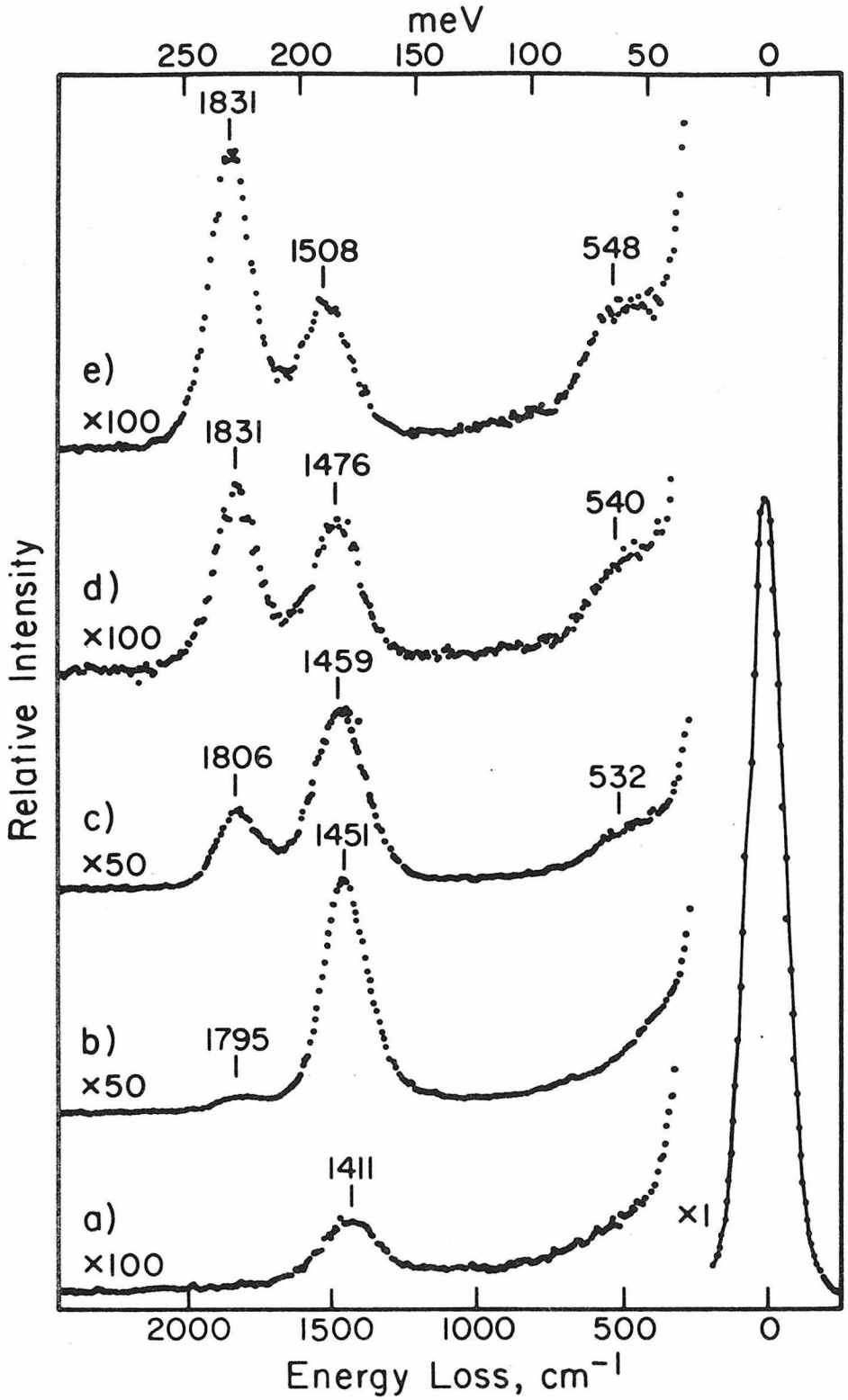
meV
250
200
150
100
50
0
1831
1508
548
e)
×100
1831
1476
540
d)
×100
1459
1806
532
c)
×50
1451
b)
1795
×50
1411
a)
×100
×1
Relative Intensity
2000
1500
1000
500
0
Energy Loss, cm⁻¹

Fig. 1

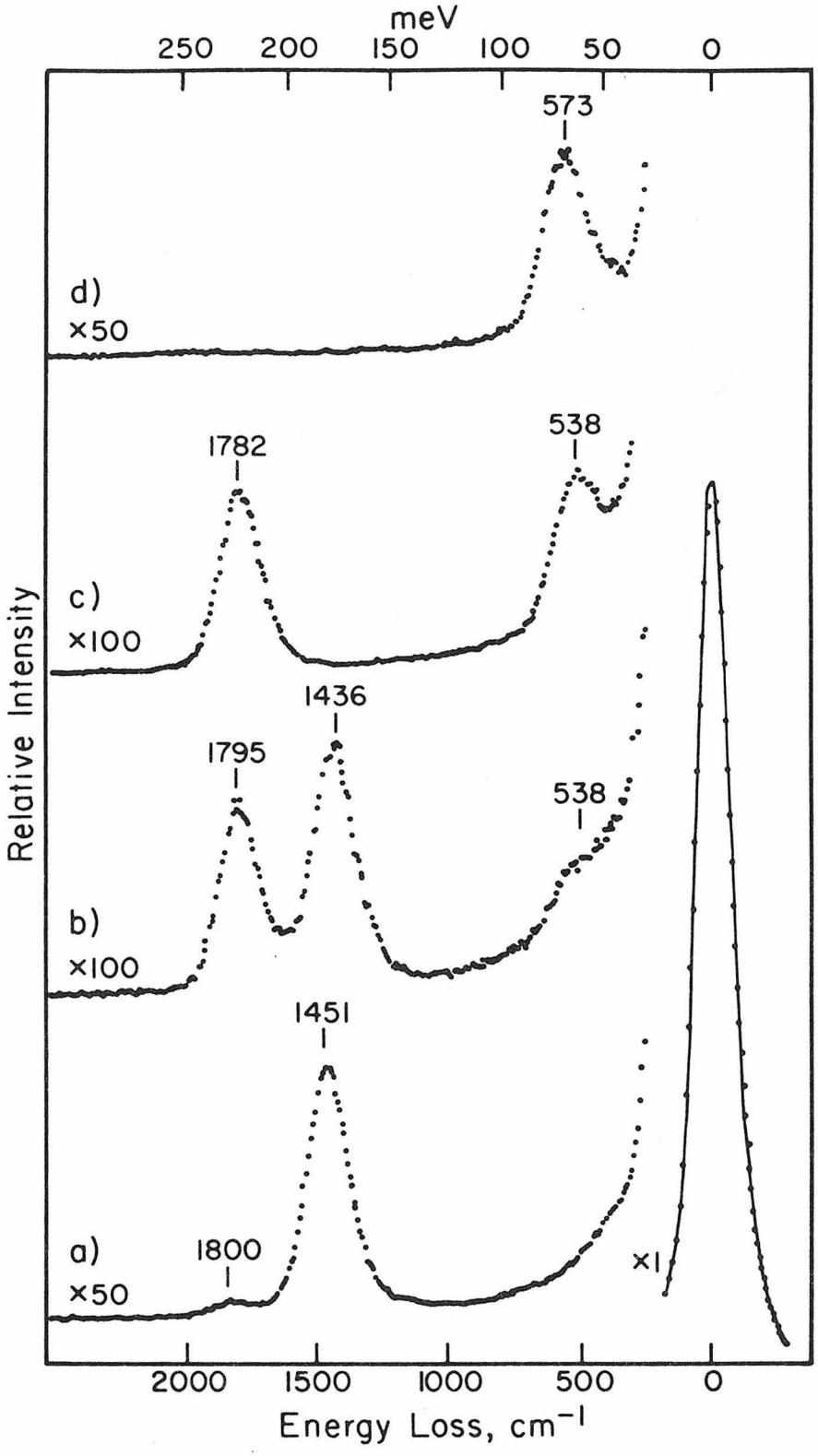
meV
250
200
150
100
50
0
573
d)
×50
1782
538
c)
×100
1436
1795
538
b)
×100
1451
a)
1800
×50
×1
Relative Intensity
2000
1500
1000
500
0
Energy Loss, cm⁻¹

Fig. 2

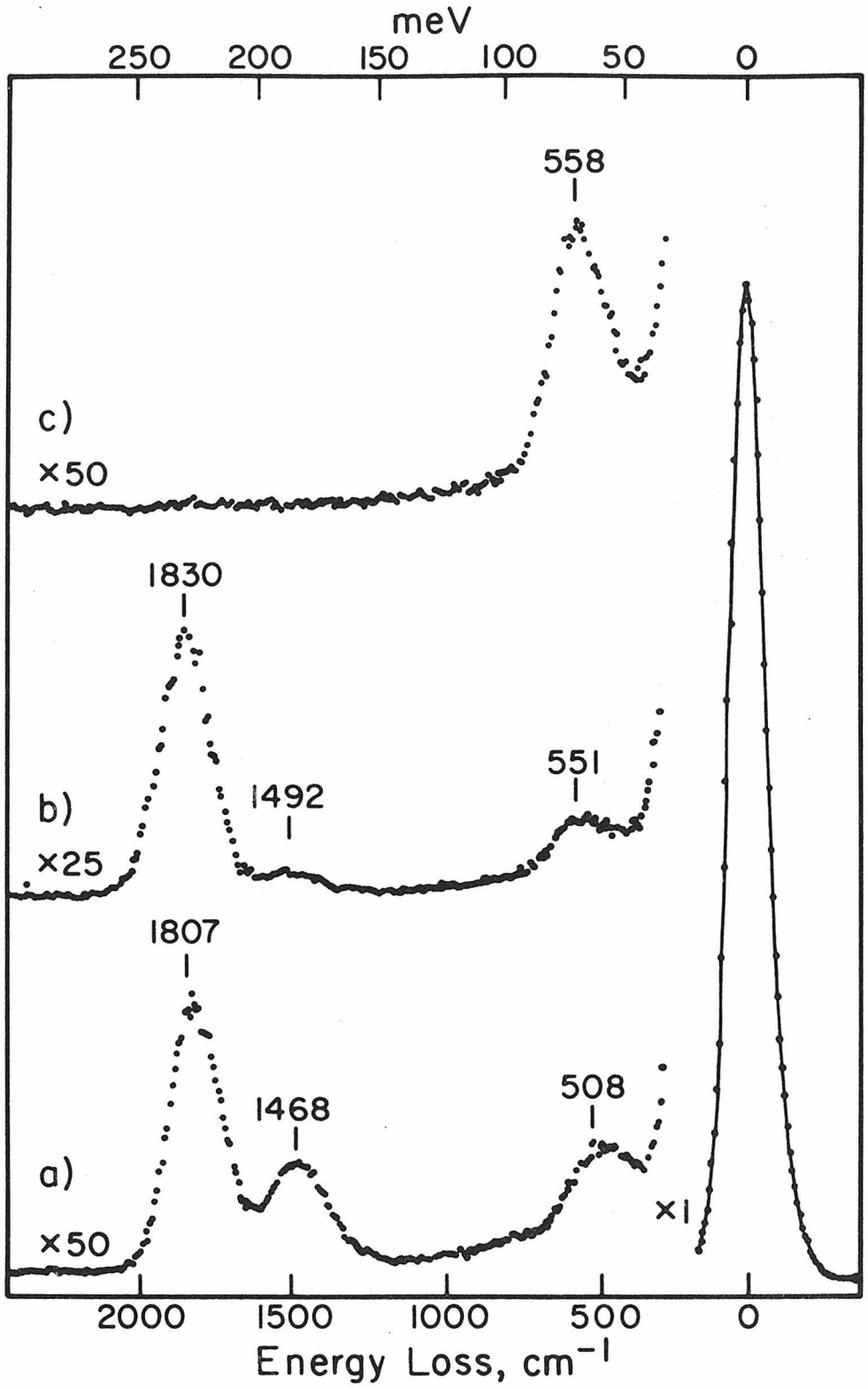
meV
250
200
150
100
50
0
558
c)
×50
1830
1492
551
b)
×25
1807
1468
508
a)
×50
×1
2000
1500
1000
500
0
Energy Loss, cm⁻¹

Fig. 3

Chapter VII

A Theory of Dipole-Forbidden Vibrational Excitation of Molecules Adsorbed on Metal Surfaces in the Born Approximation

ABSTRACT

The probability of vibrational excitation by slow electrons of a periodic array of molecules adsorbed on a metal surface is calculated in the Born approximation. By including both dipole and quadrupole terms, a mechanism is derived for the diffuse scattering of electrons by dipole-forbidden transitions. A comparison of this scattering probability with recent measurements reported for scattering from the β_1 phase of H on W(100) serves to illustrate the magnitude of this effect in terms of the dipole and quadrupole derivatives. Dipole-forbidden scattering by this mechanism is expected to be two to three orders of magnitude weaker than dipole scattering in the specular direction, but may well make a significant contribution when considering scattering out of the specular direction.

1. Introduction

A promising technique in the study of chemisorbed molecules on metal surfaces is the measurement of the surface vibrational energies by inelastic electron scattering. An important consideration in the interpretation of vibrational energy loss data is the assignment of modes to the various energies and the use of the so-called "dipole-normal selection rule" in this interpretation (1). Recent energy loss measurements of hydrogen adsorbed on the W(100) surface show that this "selection rule" may be broken for electrons scattered out of the specular direction (2,3). If dipole-allowed and dipole-forbidden transitions may be identified separately in the angular distribution of inelastically scattered electrons, then the technique will be even more powerful in the interpretation of molecular structures on metal surfaces.

It has been proposed that the excitation of dipole-forbidden transitions may occur through a temporary negative ion resonance (2,4), or through impact or thermal diffuse scattering, in which the electron interacts with the short-range potential of the ion cores (5). In electron scattering from gas molecules, resonance scattering is an important mechanism (6), and calculations have been made of angular distributions expected for resonance scattering from oriented molecules (4). The effect of the metal surface on the temporary negative ion mechanism apparently remains unresolved. In this work, we propose another possible mechanism for the excitation of dipole-forbidden transitions, in which the electron scatters from the periodic potential set up by the surface vibration as it does in dipole scattering. In this picture, vibrations

parallel to the surface appear at higher order in the potential and scatter more weakly than dipole-allowed transitions.

Several authors have calculated the inelastic scattering cross section for scattering from a single dipole on a surface (7 - 9), or for scattering from a dipole array (10,11) in the Born approximation. The effect of metal plasmons in moderating the image potential at high electron energies has been calculated also (12). In general, the assumption of high surface reflectivity and of a perfect imaging plane leads to the result that the electron is scattered only from vibrations which have a component of the dynamic effective charge tensor perpendicular to the surface. The inelastically scattered electrons are peaked sharply in the specular direction. If the quadrupole term in the potential is included, then vibrational modes which are strictly parallel to the surface may be excited also, and the electrons are scattered relatively isotropically. If the approximation of high reflectivity or of a perfect imaging plane is relaxed, then parallel vibrations are allowed also, but the electrons are sharply peaked in the specular direction (8,9).

2. Inelastic Scattering Probability

The periodic potential of an array of dipoles and quadrupoles on a metal surface is calculated as follows (10). First, the potential due to the charge distribution at each lattice site, $\vec{x}_{\parallel}$, together with its image is calculated from

$$\Phi(\vec{r}) = 2 \sum_{\vec{x}_{\parallel}} \left[\frac{P_z r_z}{|\vec{r} - \vec{x}_{\parallel}|^3} + \frac{Q_{xz} r_x r_z + Q_{yz} r_y r_z}{|\vec{r} - \vec{x}_{\parallel}|^5} \right] \qquad (1)$$

Here $\Phi(\vec{r})$ is the potential far from the surface, P_z is the z-component of the dipole moment of the charge distribution, and Q_{xz} and Q_{yz} are the corresponding elements of the quadrupole moment tensor. Since r_z appears in each term, $\Phi = 0$ at the image plane, and Q_{zz} is zero to satisfy the requirement that the quadrupole moment tensor be traceless.

Eq. (1) may be expanded to first order in displacements, which are assigned a phase factor $\exp(i\vec{q}_{\parallel} \cdot \vec{x}_{\parallel})$ for a surface wave of wavevector $\vec{q}_{\parallel}$. Sufficiently far from the surface, the sum in Eq. (1) may be replaced by an integral, and the term which leads to inelastic scattering is

$$V(\vec{r}) = 4\pi n_o \exp(i\vec{q}_{\parallel} \cdot \vec{x}_{\parallel} - q_{\parallel} z) \sum_{\alpha} \left\{ e^*_{z\alpha} + \frac{i}{3}\left[P^*_{xz\alpha} q_x + P^*_{yz\alpha} q_y \right] \right\} e_{\alpha}(\vec{q}_{\parallel}, \omega) \qquad (2)$$

where the sum is over the Cartesian components, and e_{α} is the displacement operator of the normal mode of interest. The z-axis is defined to be perpendicular to the surface. The reciprocal of the unit cell area is n_o. The quantities $e^*_{z\alpha}$, $P^*_{xz\alpha}$ and $P^*_{yz\alpha}$, are defined by

$$e^*_{z\alpha} \equiv \frac{\partial P_z}{\partial u_{\alpha}} \; ; \; P^*_{\beta z\alpha} \equiv \frac{\partial Q_{\beta z}}{\partial u_{\alpha}} \qquad (3)$$

where u_{α} is the displacement vector. This may be generalized to more than one atom per unit cell by summing over each atom.

The scattering probability may be calculated to first order using plane waves reflected from a barrier as the unperturbed wave functions. The Golden Rule may be employed if the wave functions are properly normalized Bloch waves parallel to the surface (8), or the scattered wave function may be calculated directly (10). The resulting scattering

probability per unit solid angle is

$$\frac{dS}{d\Omega} = \frac{2n_o(n_s + 1)e^2m^2}{M\hbar^3\omega(q_\parallel)\cos\alpha}\left\{\left(\sum_\alpha e^*_{z\alpha}\xi_\alpha\right)^2 + \left[\frac{1}{3}\sum_\alpha (P^*_{xz\alpha}q_x + P^*_{yz\alpha}q_y)\xi_\alpha\right]^2\right\}$$

$$\times \left(\frac{k_f}{k_i}\right)|f(q_\parallel, k_{iz}, k_{fz})|^2 \quad , \tag{4}$$

where

$$f(q_\parallel, k_{iz}, k_{fz}) = \frac{1}{q_\parallel + i(k_{iz} + k_{fz})} - \frac{R_f}{q_\parallel + i(k_{iz} - k_{fz})}$$

$$- \frac{R_i}{q_\parallel - i(k_{iz} + k_{fz})} + \frac{R_iR_f}{q_\parallel - i(k_{iz} - k_{fz})} \tag{5}$$

The α-component of the normal coordinate of the vibration is ξ_α. The quantity, n_s, is $[\exp(\hbar\omega/k_BT) - 1]^{-1}$; e is the electronic charge, and m the electronic mass. The surface oscillator has a frequency, $\omega(q_\parallel)$, and a reduced mass, M. The wavevectors of the incident and scattered electrons are $\vec{k}_i$ and $\vec{k}_f$, respectively, and R_i and R_f are the corresponding reflection coefficients. Under the experimental conditions, the approximation $(k_{iz} + k_{fz}) >> q_\parallel$ usually holds, even at large scattering angles. If we assume that $R_i \approx R_f \approx R$, then

$$|f(q_\parallel, k_{iz}, k_{fz})|^2 = \frac{4|R|^2q_\parallel^2}{q_\parallel^2 + (k_{iz} - k_{fz})^2} \tag{6}$$

The shape of $f(q_\parallel, k_{iz}, k_{fz})$ and the role of this approximation has been discussed in detail by Šokčević, et al. (8). Since the full periodic potential was used [Eq. (2)], the requirement of momentum conservation,

$\vec{k}_i - \vec{k}_f = \vec{q}_{\|}$, is obtained also.

The first term of Eq. (4) has been published by a number of authors, and perhaps it is worthwhile summarizing these results. Within the approximation $k_f \approx k_i$, Eq. (6) is consistent with the partially integrated cross section for small-angle scattering reported by Newns (7). It differs from the result of Evans and Mills by a factor of two, which may be due to the definition of reduced mass in Eq. (4) (10). It agrees with the cross section of Šokčević, et al. within a factor $1/\cos\alpha$ (8), and with the result of Persson within a factor of $4\pi^2$ (9). These factors are largely insignificant in a model calculation of this type, but when experimental intensities are interpreted, different values of e^* will be obtained depending on which expression is used. Note that in the derivation of Eq. (4), the potential due to images was included explicitly, and $e^*_{z\alpha}$ and $P^*_{\alpha z\beta}$ are defined so as to be compared (where possible) directly with gas phase values.

The first term of the differential scattering probability depends on the quantity, $\sum_\alpha e^*_{z\alpha}\xi_\alpha$. In many cases, it appears that the dynamic effective charge tensor is diagonal, and only normal modes which involve motion perpendicular to the surface can cause scattering in the dipole approximation (10). The second term in Eq. (4), which depends on the quadrupole derivatives, $P^*_{xz\alpha}$ and $P^*_{yz\alpha}$, is then the first term which, in general, excites modes which are strictly parallel to the surface. Since the product, $q_{\|} f(q_{\|}, k_{iz}, k_{fz})$, is approximately constant with scattering angle when $|q_{\|}| > 0$, the electrons scattered by the parallel vibrations will be scattered through all angles.

To illustrate the influence of the quadrupole potential on the inelastic cross section, we consider recent energy loss measurements by Ho et al. (2) of the β_1 state of H adsorbed on the W(100) surface. In this work, an intense energy loss feature at 130 meV, observed also by previous workers (13 - 15), is ascribed to the dipole-allowed normal vibration (ν_1). Additional features at 80 meV and 160 meV are assigned to the weak (ν_2) and strong (ν_3) parallel modes of atomic hydrogen in a bridged site. Within this picture, the parameters, $e^*_{z\alpha}$ and $P^*_{\alpha z\beta}$, can be estimated, and the importance of the quadrupole term can be assessed.

The plane of incidence is along the [001] direction, and it is the angular dependence of scattering in this plane which is of interest. We assume that ν_2 and ν_3 are strictly parallel to the surface, and that the normal coordinate of each parallel mode is in the [001] direction for half the H atoms on the surface. This is to be expected for H occupying all possible bridged sites as proposed by Estrup and Anderson (16). Then, the term in brackets in Eq. (4) may be simplified. For the ν_1 mode, scattering in the x-z plane depends only on e^*_{zz} and P^*_{xzz}. For the ν_2 and ν_3 modes, the scattering probability depends only on P^*_{xzx}, where the x-axis is in the [001] direction.

The differential scattering probability can be compared directly with experiment after integration over the acceptance aperture of the spectrometer. An analytic expression has been given for the partially integrated dipole scattering probability in the specular direction (17,10), and an expression for the quadrupole term can be developed in the same way. Since we are concerned primarily with scattering out of the specular direction, however, $f(q_{\parallel},k_{iz},k_{fz})$ can be taken as a slowly varying

function over the analyzer aperture, and the scattering probability is well approximated by $\frac{dS}{d\Omega}\Delta\Omega$. This quantity is shown in Fig. 1 as a function of scattering angle for $\Delta\Omega = 1 \times 10^{-4}$ steradian. The dynamic effective charge, e^*, and the quadrupole derivative, P^*_{zxz}, which appear in the scattering probability of ν_1, are 0.17 and 4.5 au, respectively. The quantity, P^*_{xzx}, which determines the intensity of the modes ν_2 and ν_3, is taken as 2.7 au. These values are chosen arbitrarily to match approximately the experimental intensities for scattering close to the specular direction and at 30^o off specular. The angle of incidence, α, is 23^o, and the primary energy is 9.65 eV.

The quadrupole terms, P^*_{xzx} and P^*_{xzz}, seem somewhat large when compared with fixed dipole moments; but the same considerations apply in estimating these quantities as in estimating e^*. Unfortunately, P^*_{xzx} and P^*_{xzz} are not so amenable to independent measurement as e^*. As a point of reference, the quadrupole derivative of H_2 has been estimated from calculations to be 1.13 au (17).

The comparison with the experimental results of Ho et al. (2) certainly does not suggest that the detailed angular intensities are explainable purely in terms of this potential. In addition, this scattering probability is only weakly dependent on energy, and rather sharp features in the scattering probability as a function of energy have been reported recently (3). Nevertheless, this calcuation suggests that an additional mechanism for diffuse scattering may exist and may be detectable at the limit of sensitivity of present instruments.

Evans and Mills (11) have summed the Born series to all orders for electrons scattered near the specular direction. Their result shows that

for a single vibrational loss, terms higher than the first make a negligible correction, so long as the first order scattering probability is small. Nevertheless, the Born approximation must be viewed with caution at higher scattering angles. In addition, the polarization interaction and exchange between the surface molecule and the electron may be important in calculating small scattering probabilities.

3. Conclusions

In this work, we have calculated the probability of inelastic electron scattering from a periodic array of adsorbed molecules on metal surfaces in the Born approximation. Both dipole and quadrupole terms are included in the potential of the surface vibration, and an additional mechanism for the diffuse scattering of electrons by dipole-forbidden transitions is derived. The dipole-forbidden scattering by this mechanism occurs at second order and may be expected to be two or three orders of magnitude less intense than dipole scattering in the specular direction, assuming a quadrupole derivative of 1 - 3 atomic units.

References

1. H. Ibach, H. Froitzheim and B. Sexton, Appl. Surface. Sci. 1, 1 (1977).
2. W. Ho, R. F. Willis and E. W. Plummer, Phys. Rev. Letters 40, 1463 (1978).
3. R. F. Willis, W. Ho and E. W. Plummer, Surface Sci., to be published.
4. J. W. Davenport, W. Ho and J. R. Schrieffer, Phys. Rev. B17, 3115 (1978).
5. V. Roundy and D. L. Mills, Phys. Rev. B5, 1347 (1972).
6. G. J. Schulz, Rev. Modern Phys. 45, 423 (1973).
7. D. M. Newns, Phys. Letters 60A, 461 (1977).
8. D. Šokčević, Z. Lenac and R. Brako, Z. Physik B28, 273 (1977).
9. B. N. J. Persson, Solid State Commun. 24, 573 (1977).
10. E. Evans and D. L. Mills, Phys. Rev. B5, 4126 (1972).
11. E. Evans and D. L. Mills, Phys. Rev. B7, 853 (1973).
12. F. Delanaye, A. Lucas and G. D. Mahan, Surface Sci. 70, 629 (1978).
13. H. Froitzheim, H. Ibach and S. Lehwald, Phys. Rev. Letters 36, 1549 (1976).
14. C. Backx, B. Feuerbacher, B. Fitton and R. F. Willis, Phys. Letters 60A, 145 (1977).
15. A. Adnot and J. D. Carette, Phys. Rev. Letters 39, 209 (1977).
16. P. J. Estrup and J. Anderson, J. Chem. Phys. 45, 2254 (1966).
17. E. L. Breig and C. C. Lin, J. Chem. Phys. 43, 3839 (1965).

Figure Caption

Fig. 1 Scattering probability as a function of scattering angle using assumed values of e^* and $P^*_{\alpha z \beta}$ as given in the text.

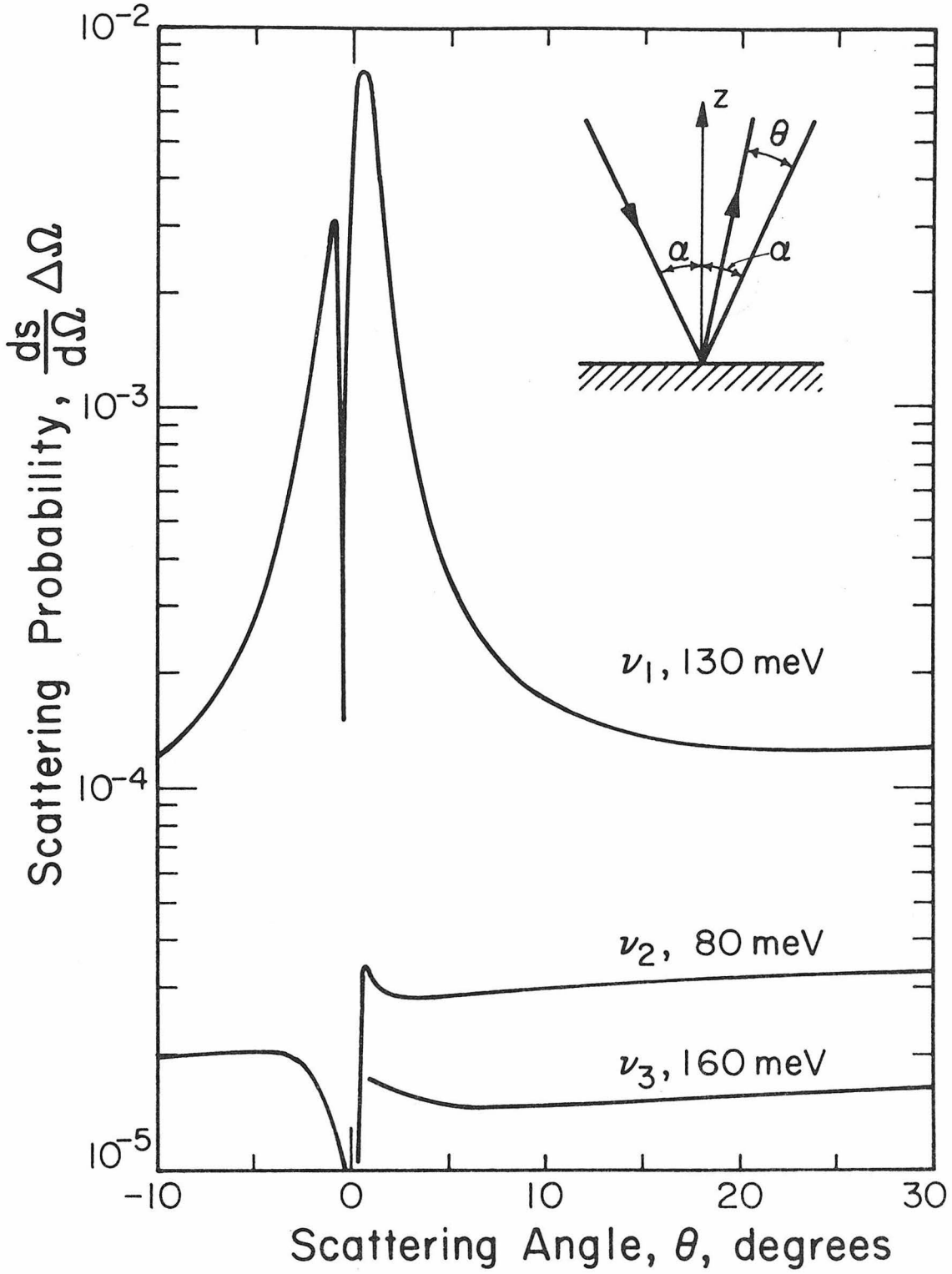
10^{-2}
10^{-3}
10^{-4}
10^{-5}
Scattering Probability, $\frac{ds}{d\Omega}\Delta\Omega$
z
θ
α
α
ν_1, 130 meV
ν_2, 80 meV
ν_3, 160 meV
-10
0
10
20
30
Scattering Angle, θ, degrees

Fig. 1

Conclusions

The structure of chemisorbed CO, O_2 and NO has been studied on the Ru(001) surface. An electron spectrometer capable of measuring the vibrational energies of chemisorbed molecules was designed and constructed. In addition to characterizing the chemisorption of CO, O_2 and NO through the vibrational spectrum, the instrument was shown to be capable of ultraviolet photoemission and Auger electron spectroscopies.

Vibrational energy loss measurements proved to be useful in analyzing the structure of these molecules chemisorbed on the basal plane of ruthenium. Carbon monoxide is bonded upright on the Ru(001) surface with a single carbon-metal bond at all coverages. Comparison with independent LEED studies, however, shows that the linear CO molecule cannot be assigned strictly to an on-top site at saturation coverage. CO occupies a variety of low symmetry sites at saturation.

Oxygen is adsorbed dissociatively on the Ru(001) surface, and the oxygen atoms occupy three-fold or bridged sites. When CO is coadsorbed with oxygen, the carbon-metal bond in the adsorbed CO is weaker, and the carbon-oxygen bond is stronger than on the clean surface.

The carbon-oxygen stretching frequency of adsorbed CO increases by 100 cm^{-1} from low coverage to saturation. This can be modeled in terms of a direct interaction between the chemisorbed molecules.

Nitric oxide is adsorbed on Ru(001) in two states at temperatures below 150 K. The low coverage state shows the nitrogen-oxygen stretching frequency of a nitrosyl group bonded to two or three metal atoms. At coverages above approximately 0.4 (relative to saturation), a second state

appears which has the N-O stretching frequency of a terminally bonded linear nitrosyl. The more highly coordinated state dissociates at room temperature. A mechanism involving the blocking of sites by the nitrogen and oxygen atoms resulting from the dissociation is proposed to explain the temperature behavior of adsorbed NO.

The vibrational energy loss spectra reported here have provided incisive information about the chemisorption of small molecules on the Ru(001) surface. Inelastic electron scattering will continue to make a significant contribution in the study of more complicated adsorbates on metal surfaces.

APPENDIX A

Mechanical Design of the Spectrometer

A photograph of the spectrometer, taken during assembly, is shown in Fig. 1. The cover plates are removed so that the optics and internal wiring are exposed. The four sets of tube lenses are held in optical benches, as can be seen in Fig. 5. The tubes rest on ground alumina rods which are held by a slot milled in the stainless steel bar. The lenses are held in the mounting by screws on ceramic insulators which clamp the tubes to the bench from the bottom. Electrical contact is made through these clamping screws in the cathode optics. In the other lens systems, the electrical leads are attached to the top of the lens elements.

The tube lenses are of the most common variety, in which the spacing: diameter ratio is 0.1. The lens pieces were machined so that if the external spacing between cylinders is 0.020" the internal spacing will be optically correct. As illustrated in Fig. 2 of Chapter 2, the external and internal gaps are staggered so that the electron path is shielded from the ground potential of the support and the unknown potential of insulators.

In general, the 0.020" spacing can be set during assembly of the optics and will be preserved by the clamping screws. However, certain of the optical pieces are too narrow to accommodate clamping screws, and these are spaced from one another with 0.020" thick 0.875" OD ceramic disks. The four assembled sets of tube lenses are shown in Fig. 2 and Fig. 4.

In Fig. 5, the deflector arrangement is illustrated also. This is a

view of the last element before the multiplier, and three deflector plates have been provided rather than two, as is the case in the other optics. The three central pieces are machined from Cu-Be (largely Berylco 10) and gold plated, as are the rest of the optics (see Chapter 2). They are shaped as arcs of a circle and spaced on ceramic standoffs from the main lens block. The ceramic standoffs are also arcs of a circle and are slightly smaller than the deflectors, so as to be obscured from the beam path. Electrical and mechanical contact is through an insulated 0-80 screw to the outside of the lens element.

The optics are positioned by slots milled in the angle support pieces of the spectrometer (Fig. 1). The frame is designed so that as the analyzer rotates, the analyzer optics drift out of the optical plane defined by the monochromator optics by less than 0.002". The axis of rotation of the analyzer is perpendicular to this plane within 0.05^{o}. This alignment can be preserved during disassembly and reassembly by inserting pins in the alignment holes throughout the frame.

The hemispheres are aligned separately on their own mounting plates and then keyed to the spectrometer angle support pieces. The analyzer hemispheres are shown in Fig. 3, and the monochromator hemispheres are quite similar. The inner hemisphere and Herzog plate are shown attached to the mounting plate. The hemispheres are attached to the plate through 0.062"sapphire balls which are held by the 0.042" key holes. The hemispheres are then clamped to the plate with screws on ceramic insulators from the back side.

A key has been provided to Fig. 1 which may prove of some use in the next chapter on spectrometer maintenance.

Figure Captions

Fig. 1. The electron spectrometer during assembly. A - Dispenser Cathode. B - Cathode Optics. C - Monochromator Hemispheres. D - Monochromator Angle Support. E - Optical Bench. F - Gun Focusing Optics. G - Analyzer Entrance Aperture. H - Analyzer Angle Support (right side). O - Electron Multiplier Mounting. J - Flexible Shielded Cables. K - Lower Bearing. L - Spur Gear (6" pitch diameter).

Fig. 2. Monochromator optics. The lenses on the left are the cathode optics. The gun focusing optics are on the right. The stainless steel tabs provide electrical contact to deflector plates inside the optics.

Fig. 3. Analyzer hemispheres. The outer hemisphere is on the left. The inner hemisphere, Herzog plate and hemisphere mounting plate are on the right. The mounting plate is 4.600" across.

Fig. 4. Analyzer optics. The beam-defining and focusing optics are on the right. The optics on the left perform the energy selection and acceleration into the electron multiplier.

Fig. 5. End view of multiplier optics (also shown in Fig. 4). Three deflector plates mounted on ceramic insulators are visible, as is the energy defining aperture. The stainless steel bench (bottom) is 1.124" in width.

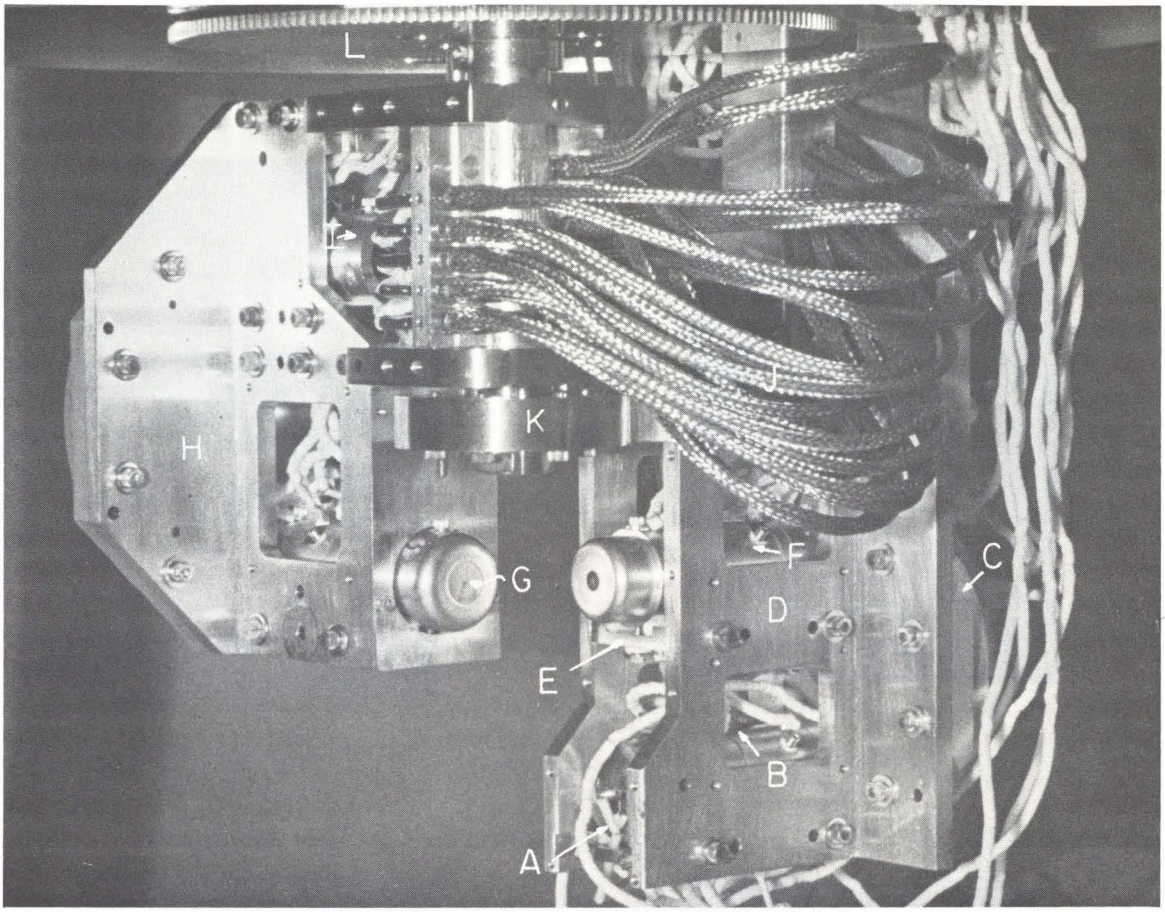

Fig. 1

Fig. 3

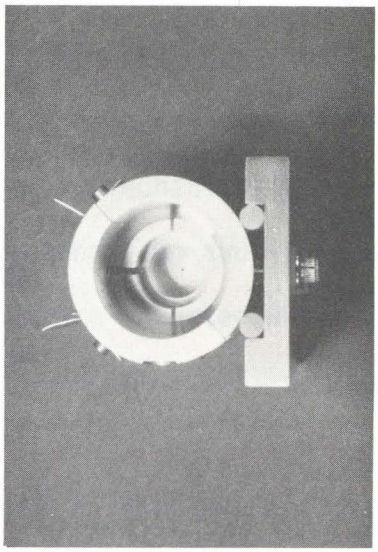

Fig. 5

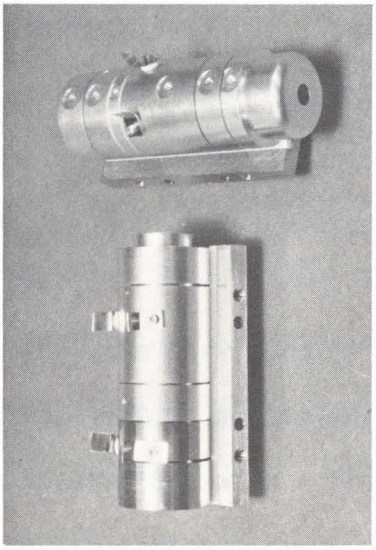

Fig. 2

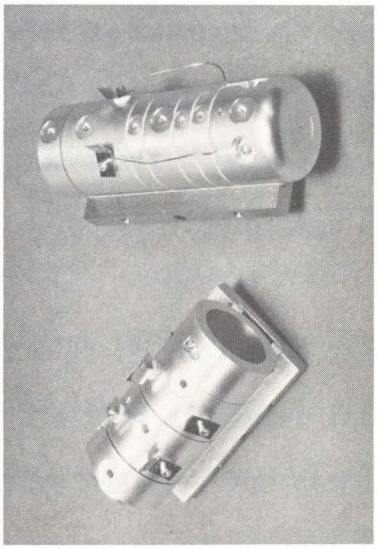

Fig. 4

Appendix B

Operation and Maintenance of the Electron Spectrometer

The electron spectrometer used in this work has been described in Chapter 2. The purpose of this Appendix is to give some details of the spectrometer operation and maintenance which are not contained in Chapter 2.

The spectrometer itself is a simple device mechanically. The stainless steel frame has been aligned in the machine shop and is keyed together with alignment pins. If these pins are inserted while assembling any part of the instrument, then alignment will not be a problem.

The wiring of the spectrometer is also straightforward. The electrode connections are made through two 20-pin feedthroughs on the spectrometer flange. A separate 10-pin feedthrough is used for the leads to the cathode heater. The electrical connections for the analyzer are made through flexible shielded cables provided by Ceramaseal. These cables are fastened in stainless clamps to the monochromator frame and to the analyzer on either side of the analyzer shaft. On the analyzer side, the contacts are accessible through the upper side plates of the analyzer.

The main servicing of the spectrometer will be replacing the cathode and the electron multiplier. The cathode is a #134 dispenser cathode from Spectra Mat with a free-standing tungsten heater. The cathode is mounted in a Pierce-diode configuration in the first element of the

monochromator. The cathode block, a round molybdenum piece, is accessible through the lower access plate at the end of the monochromator tube lenses. The block (and its contact) can be removed by loosening the last screw which penetrates the lower optical bench. The cathode is attached to the block with three 0.01" Ta wires spot-welded to the cathode body and to both ends of the Mo block. Before spot-welding to the block, the cathode should be threaded through the light Mo-foil heat shield.

After the cathode is mounted in its block, the cylindrical Mo piece must be spaced in the optical bench 0.02" ± 0.001" from the Mo anode. This may be accomplished either with a feeler gauge or with one of the 0.875" OD x 0.02" ceramic spacers (see Appendix A).

The free-standing heater must be supported by inserting two short pieces of Ta wire into the light W windings of the heater. The wires should be tacked to the heater and to the contacts which come from the four-hole alumina tubing. This tube is clamped to the back of the optical bench and should stay in place when the cathode is changed.

The electron multiplier is a Spiraltron (SEM 4211) furnished by Galileo. To change the multiplier, the top access plates of the analyzer and the angle support on the right side (facing the scattering center from the analyzer side) must be removed. In order to slide out the angle support, the analyzer hemisphere mounting plate must be loosened and backed away from the angle support. This is to allow the support piece to clear the screws of the analyzer Herzog plate, which are hidden until disassembly.

The multiplier is exposed at this point. The multiplier collector must be removed through the central flange of the spectrometer plate. The leads, which go to the terminals of the multiplier support piece, should be disconnected from the top two connectors on the left side of the analyzer by loosening their set screws. It is important that the Cu-Be connector remain anchored to the lead from the flexible cable so that the lead is not pulled through and lost.

The multiplier support piece can be released by removing one 0-80 screw from the half-cylindrical Cu-Be shield on top of the multiplier entrance. This piece is lifted off a support post on the left side of the multiplier, which can then be removed. A new multiplier can be spot-welded to the support wires after its leads are appropriately trimmed. Remember, the multiplier is made of thin glass and must be handled carefully.

After the multiplier and Cu-Be shield have been replaced in the spectrometer, the multiplier must be positioned so that the last terminal is within 1 mm of the collector. To satisfy this condition, the last terminal should penetrate the hole along the axis of rotation by about 1.5 mm. It should be clearly visible through the open port of the collector feedthrough. The collector may be replaced after the multiplier has been positioned. Check that the collector is not shorted to the last multiplier terminal at all angles of rotation of the analyzer.

The operation of the electron spectrometer requires careful tuning. Since the work function of the cathode and spectrometer surfaces changes with chemical environment and with time, retuning is frequently necessary. The following suggestions should help in this procedure.

The hemispheres and Herzog elements should be at their theoretical values after allowing for a contact potential difference, $\Delta\phi$, between the cathode and hemisphere surfaces. The pass energy of the hemispheres is defined by the potential difference between the inner and outer surfaces. The potential of the passed electrons is

$$V_p = (V_i - V_o)\left(\frac{R_o}{R_i} - \frac{R_i}{R_o}\right)^{-1} \tag{1}$$

where R_i and R_o are the radii of the inner and outer hemispheres, respectively. If the hemispheres are properly adjusted, this potential difference and the voltage applied to the elements can be used to calculate the energy zero relative to the pass energy, and therefore the contact potential difference, with an uncertainty given by the thermal width of the cathode.

$$\Delta\phi = (V_{inner} - V_{cath}) - \frac{R_z}{R_i}\ (V_p) \tag{2}$$

When the contact potential difference has been determined, the cathode voltage should be set to the desired impact energy minus the positive contact potential difference. The Herzog voltage should then be set to the pass energy minus the impact energy. Parameters useful in determining the various hemisphere potentials are given in Table I. These potentials are defined relative to the energy zero normally used in electron optical calculations, and must be added to the quantity, $-V_o$, to determine the applied voltage. V_o is the true impact energy assuming that the work functions of the sample and of the gold spectrometer surface are the same.

If the monochromator parameters are inserted in Eq. (2), it reduces

to

$$\Delta\phi = 0.882\ V_7 - 1.882\ V_6 - V_1$$

where the V_i refer to the electrode voltages, and the electrodes are defined in Figure 2 of Chapter 2.

Table I

	Monochromator	Analyzer
R_i	2.064 cm	3.016 cm
R_o	3.016 cm	4.286 cm
$\frac{V_i - V_o}{V_p}$	0.777	0.508
$\frac{V_i}{V_p}$	1.462	1.286
$\frac{V_o}{V_p}$	0.684	0.778

Appendix C

Spectrometer Electronics and Software

The basic control of the spectrometer for electron energy loss spectroscopy and Auger electron spectroscopy is specified in Figure 2 of Chapter 2.

The spectrometer electrodes are connected through shielded cables to a large switch box where they are connected to the various power supplies. A set of switches can connect the leads to a set of high-resistance potentiometers connected to high voltage supplies, or to a set of low-noise wire-wound potentiometers for low voltage operation. In high voltage operation, the analyzer is retarded by a Kepco APH 1000 supply between 0 and 1000 eV. The gun energy, E_0, is set by a Fluke 412B supply between 0 and 2kV. Since there is no separate cathode supply in the high voltage operation, the hemisphere and anode potentials will have to be altered when the impact energy is changed. The potentiometers are floating at high voltage and should be adjusted only with an insulated tool.

In low voltage operation, the gun energy and analyzer energy may both be adjusted as desired. In the energy loss mode, E_L, the gun energy is fixed, and the analyzer energy is set by a 12-bit digital-to-analog converter (DAC). This is the usual mode of operation, but two other modes may be selected. In order to measure cross sections, S(E), the analyzer supplies are set to pass electrons of energy, $E_0 - \Delta E$, where ΔE is fixed by the cathode supply (in the energy loss mode). The DAC is then used to select the impact energy.

In a third mode of operation, RE, chiefly of use to gas phase spectroscopists in measuring threshholds, the analyzer is set to pass electrons of constant kinetic energy as the impact energy is swept.

Two rotary switches in the control box are used to connect the various elements to a voltmeter. The two switches define a two-digit octal address which corresponds to the various electrode and power supply leads. Addresses beginning with the digit 7 are connected to the voltmeter through a 4000:1 divider. In the high voltage operation, all voltages are connected through the high-impedance divider.

Three DAC's have been provided to allow for the sweeping voltage and for two non-linear corrections to the optics. Any element may be connected to the extra programmable supplies by means of a switch under the associated potentiometer.

As the energy of the electrons counted by the analyzer or produced by the monochromator is changed, the potential ratios between element 13 of the analyzer and ground potential or between element 12 of the gun and ground potential is changed. Ground potential is defined as the kinetic energy of the electrons produced by the monochromator or detected by the analyzer. The lens systems before and after the scattering region were chosen to correct for these changes while remaining for the most part at constant potential. However, additional corrections may be necessary if the analyzer or gun is swept through a wide energy range. This can be verified by varying the gun and analyzer energy together through the energy range of interest.

The three programming voltages are set by the laboratory computer

with the commands, S:Dn;x and I:Dn;x, where n is DAC-number 16, 17 or 18, and x is the absolute value of the desired voltage. Since these voltages are set through adjustable supplies, the software scaling routines must be adjusted accordingly. Two new instructions, S:X; x_{max} and S:En;x_{min}, were defined to set the scale and to provide the display routines with information about the DAC function. The operands, x_{max} and x_{min}, are the maximum and minimum voltages of the programmable supply, scaled by a constant, a, which is used to scale x_{max}, x_{min} to the range 0-10.000, which is the range accepted by the assembly routine. The values of a and n appropriate to various situations are listed in Table I. The odd values of n are intended to allow for an unusual way of programming the Kepco PCX supplies in low-voltage operation.

These supplies can be programmed as rather slow operational amplifiers. The usual programming method is to apply a constant current to the inverting input of the amplifier which generates an output according to the feedback resistance, set by the voltage adjustment knob of the power supply. In order that the full resolution of the DAC can be used in energy loss experiments, a second method of programming has been provided in which the power supply is programmed as a voltage adder. That is, the current supplied by the DAC is summed to the current from the internal reference of the supply. If the DAC in question is to be programmed in this way, the corresponding odd value of n should be employed in the S:En;x_{min} instruction.

During the tuning of the spectrometer, it is frequently necessary

to set manually the retarding voltage more accurately than is possible with the power supply potentiometer. For this reason, the input current of DAC 16 can be varied with a separate 10-turn potentiometer when it is set for voltage adding operation. The retarding voltage can then be set to the nearest mV, as necessary.

Table I

n	Display units	a	Relevant DAC	Function
0	eV	0.1	16	Electron Energy
1	eV	0.1	16	0-100 eV
2	eV	10	16	Electron Energy
3	eV	10	16	0-20 eV
4	eV	0.1	17	Control
5	eV	0.1	17	Offset A
6	mV	1	17	V_{ref} for
7	mV	1	17	temperature controller
8	eV	0.1	17	Control
9	eV	0.1	17	Offset B
10	eV	0.1	17	Set Analyzer
11	eV	0.1	17	Pass Energy, 0-1000 eV

APPENDIX D

The use of various low-energy electron spectroscopies is becoming increasingly common in surface research and analysis. An experimental problem encountered frequently in such measurements is to control the sample temperature without accumulating noise due to magnetic fields, in the case of resistive heating, or due to background electron current in the case of heating by electron bombardment. Either scheme for heating the sample will render the measurements unsatisfactory. In this work, we describe a temperature-controlling scheme in which temperature control and data acquisition take place in alternating time periods.

The demands placed on the temperature controller in such a system are as follows. Temperatures commonly used range from 100 K to 1000 K, with higher temperatures necessary during cleaning. Good thermal contact with a liquid nitrogen reservoir is necessary to reach 100 K. Work with clean surfaces requires that the sample cool as quickly as possible after cleaning, so the sample is placed in the lightest possible mounting. In our work, the metallic crystals are spot welded to two Ta wires and heated resistively. Currents of $\sim$ 20 amps are required to reach 1200 K. However, since the sample is usually quite massive ($\sim$ 0.5 g) and at these temperatures is cooled chiefly by conduction, a rather slow controller is adequate to maintain the sample temperature.

The temperature controller (Fig. 1) is designed to work in conjunction with a pulse counter and a parallel input/output port of a minicomputer. It obviously would work as well with a square-wave source to provide the switching and a multichannel analyzer for data acquisition. A signal from the computer is used to disable the power supply of the temperature controller during periods in which the pulse counter is being read. During

periods in which the heater is on, the spurious signal from the pulse counter is ignored by the computer. If this is used with a multichannel analyzer, the square-wave source must also be used to disable the MCA or to gate the input. In order that the crystal temperature recover quickly during the periods in which the controller is active, a comparator is used for temperature control. The heater current used to control the temperature is set by the constant-current power supply.[1]

The thermocouple EMF is conditioned by an Analog Devices 184K instrumentation amplifier before comparison with a voltage reference. The EMF may be read on a 3½ digit panel meter (AD2010) which is also used by the computer to acquire temperature data. An external input is provided so that the temperature also may be programmed with a ramp generator or digital/analog converter.

The comparator is an LM 301A operational amplifier designed to operate with 1 mV of hysteresis.[2] Using a W-5% Re/W-26% Re thermocouple and a gain of 100 on the input amplifier, a temperature control of $\pm 1^{o}$ should be possible. However, ground currents which occur during the heater operation cause an additional error, so the true accuracy is $\pm 5^{o}$, with heater currents of $\sim$ 10 amps. The analog circuitry must be isolated carefully from the high current source for the controller to function.

This controller has been used successfully in a series of vibrational energy loss measurements of oxygen adsorbed on the Ru(001) surface between 100 K and 1000 K.[3] At 1000 K, the temperature controller required a duty cycle of two-thirds. The switching rate was approximately 0.3 hertz, and the temperature regulation was $\pm$ 15 K. Better control is possible at higher switching rates. The heater supply may be switched

at rates of 0 - 60 hertz.

Acknowledgment:

The support of the National Science Foundation (Grant No. CHE77-16314) is gratefully acknowledged. We also thank John Yehle for his help in the design and construction of this device.

References

1. J. L. Taylor, Ph.D. thesis, California Institute of Technology, 1978.
2. W. C. Jung, IC Op-Amp Cookbook, Howard W. Sams and Co., Inc., Indianapolis, 1976.
3. G. E. Thomas and W. H. Weinberg, J. Chem. Phys. (October 15, 1978).

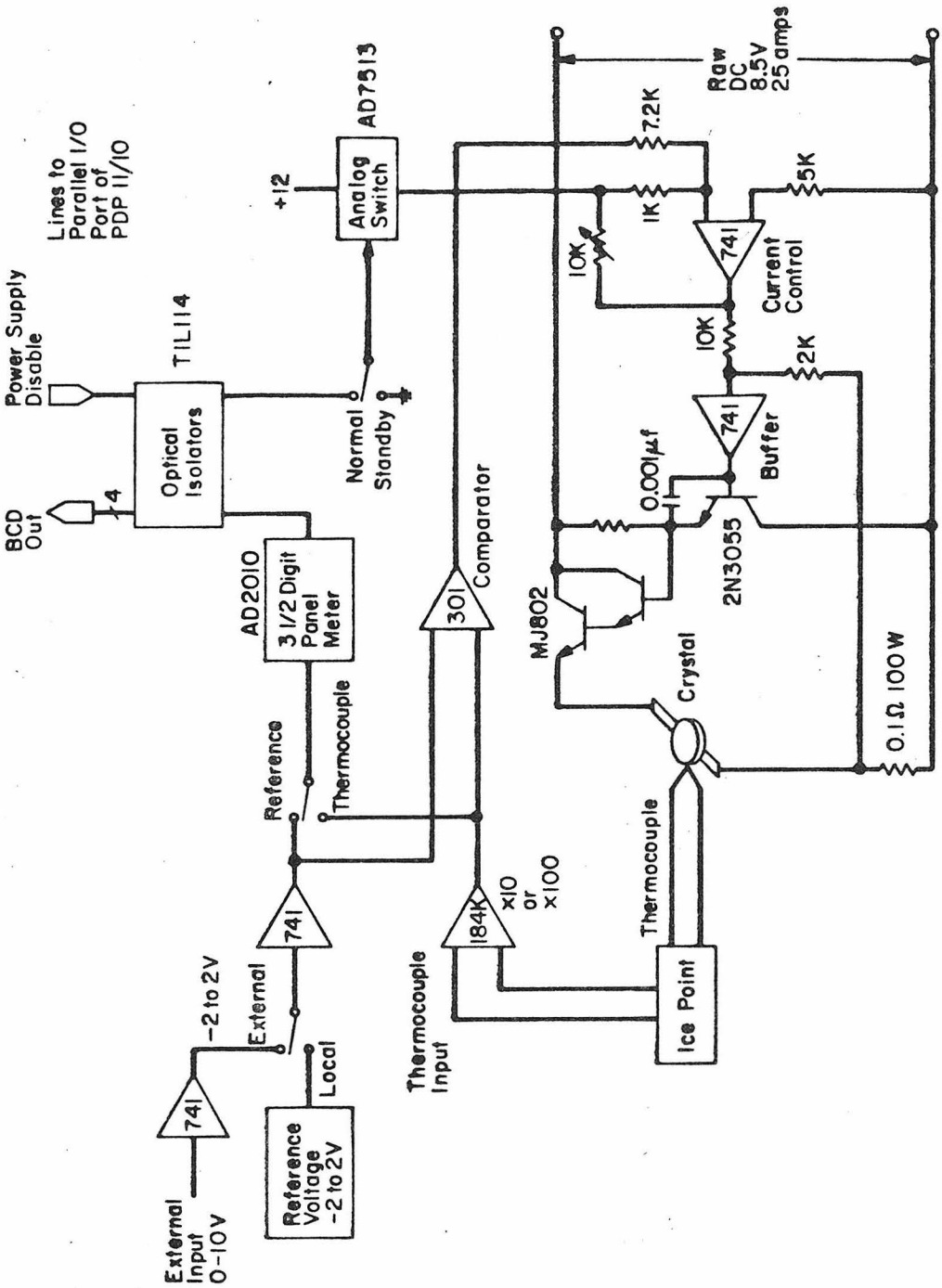
Lines to Parallel I/O Port of PDP 11/10
Power Supply Disable
BCD Out
4
TIL114
Optical Isolators
+12
AD7513
Analog Switch
Normal
Standby
AD2010
3 1/2 Digit Panel Meter
Reference
Thermocouple
301
Comparator
741
External
Local
-2 to 2V
External Input 0-10V
Reference Voltage -2 to 2V
184K
×10 or ×100
Thermocouple Input
MJ802
2N3055
Crystal
Thermocouple
Ice Point
0.1Ω 100W
Raw DC 8.5V 25 amps
7.2K
1K
5K
10K
741
Current Control
10K
2K
741
Buffer
0.001μf

Fig. 1